

# High-Ionization Emission in Metal-Deficient Blue Compact Dwarf Galaxies<sup>1</sup>

Trinh X. Thuan

*Astronomy Department, University of Virginia, Charlottesville, VA 22903*

`txt@virginia.edu`

and

Yuri I. Izotov

*Main Astronomical Observatory, National Academy of Sciences of Ukraine, 03680, Kyiv, Ukraine*

`izotov@mao.kiev.ua`

## ABSTRACT

Primordial stars are expected to be very massive and hot, producing copious amounts of hard ionizing radiation. The best place to study hard ionizing radiation in the local universe is in very metal-deficient Blue Compact Dwarf (BCD) galaxies. We have carried out a MMT spectroscopic search for [Ne v]  $\lambda 3426$  (ionization potential of 7.1 Ryd), [Fe v]  $\lambda 4227$  (ionization potential of 4 Ryd) and He II  $\lambda 4686$  (ionization potential of 4 Ryd) emission in a sample of 18 BCDs. We have added data from previous work and from the Data Release 3 of the Sloan Digital Sky Survey. In total, we have assembled a BCD high-ionization sample with [Ne v] emission in 4 galaxies, [Fe v] emission in 15 galaxies and He II emission in 465 galaxies. With this large sample, we have reached the following conclusions. There is a general trend of higher [Ne v], [Fe v] and He II emission at lower metallicities. However metallicity is not the only factor which controls the hardness of the radiation. High-mass X-ray binaries and main-sequence stars are probably excluded as the main sources of the very hard ionizing radiation responsible for [Ne v] emission. The most likely source of [Ne v] emission is probably fast radiative shocks moving with velocities  $\gtrsim 450 \text{ km s}^{-1}$  through a dense interstellar medium with an electron number density of several hundreds per  $\text{cm}^{-3}$  and associated with supernova explosions of the most massive stars. These have masses of  $\sim 50 - 100 M_{\odot}$  and are formed in very compact super-star clusters. The softer ionizing radiation required for He II emission is likely associated with less massive evolved stars and/or radiative shocks moving through a less dense interstellar medium.

*Subject headings:* galaxies: irregular — galaxies: ISM — galaxies: abundances — galaxies: evolution

---

<sup>1</sup>The observations reported here were obtained at the MMT Observatory, a joint facility of the Smithsonian Institution and the University of Arizona.

## 1. INTRODUCTION

Galaxy formation is one of the most fundamental problems in astrophysics. To understand how galaxies form, we need to unravel how stars form from the primordial gas and how the first stars interact with their surrounding environments. As there are no heavy elements in the early universe, the thermodynamic behaviour of the gas is essentially controlled by  $\text{H}_2$  cooling, and the first Population III stars are expected to be very massive and hot (e.g., Abel et al. 2002; Bromm et al. 2002). Their effective temperatures are around  $10^5$  K, so they emit very hard ionizing radiation with photon energies exceeding 4 Ryd (54.4 eV). These first stars are thus very effective in ionizing hydrogen and helium (twice), and strong He II emission lines are expected to be present in the spectra of primeval galaxies (e.g., Schaerer 2002, 2003). Emission lines of high-ionization ions of heavy elements should be present as well.

While much progress has been made in finding large populations of galaxies at high ( $z \geq 3$ ) redshifts (e.g., Steidel et al. 1996), truly young galaxies in the process of forming remain elusive in the distant universe. The spectra of those far-away galaxies generally indicate the presence of a substantial amount of heavy elements, implying previous star formation and metal enrichment.

Instead of focussing on high-redshift galaxies, another approach is to study the properties of the massive stellar populations and their interaction with the ambient interstellar medium (ISM) in a class of nearby metal-deficient dwarf galaxies called Blue Compact Dwarf (BCD) galaxies, some of which are thought to be undergoing their first episode of star formation (Izotov & Thuan 2004b). These galaxies have a heavy element mass fraction  $Z$  in the range  $1/50 - 1/3 Z_\odot$  (Izotov & Thuan 1999), assuming a solar oxygen abundance  $12 + \log(\text{O}/\text{H})_\odot = 8.91$ . Thus, their massive stellar populations have properties intermediate between those of massive stars in solar-metallicity galaxies such as the Milky Way and those of the first stars. BCDs constitute then excellent nearby laboratories for studying high-ionization emission and the hardness of the ionizing radiation in a very metal-deficient environment.

The hardness of the ionizing radiation in BCDs has long been known to increase with decreasing metallicity (e.g., Campbell et al. 1986). This is supported by the fact that the strong nebular emission line He II  $\lambda 4686$  is often seen in the spectra of BCDs, with a flux which increases with decreasing metallicity of the ionized gas (Guseva et al. 2000). Besides He II emission, high-ionization emission lines of heavy elements ions are also seen in the spectra of some BCDs. Fricke et al. (2001) and Izotov et al. (2001b) first detected the high-ionization emission line  $[\text{Fe v}] \lambda 4227$  in the BCDs Tol 1214–277 and SBS 0335–052. The presence of this line, just as that of the He II  $\lambda 4686$  line, requires ionizing radiation with photon energies in excess of 4 Ryd. More impressively, Izotov et al. (2001b) discovered  $[\text{Fe vi}] - [\text{Fe vii}]$  emission in SBS 0335–052 implying that this BCD contains intense radiation with photon energies above  $\sim 7$  Ryd ( $\sim 100$  eV), i.e. in the range of soft X-rays. Note that the ionization potential of  $\text{Fe}^{5+}$  is 5.5 Ryd and that of  $\text{Fe}^{6+}$  is 7.3 Ryd. Later, Izotov et al. (2004a) discovered  $[\text{Ne v}] \lambda 3346, 3426$  emission lines in the spectrum of Tol 1214–277. The existence of these lines requires the presence of hard radiation with photon energies

above 7.1 Ryd. Such hard ionizing radiation is confirmed by the detection of [Ne IV] (the ionization potential of  $\text{Ne}^{3+}$  is 4.7 Ryd) and [Fe VI] – [Fe VII] emission in a new spectrum of Tol 1214–277 (Izotov et al. 2004c).

While the presence of hard radiation is well established in some BCDs, the origin of this radiation is much less clear, in spite of several attempts to account for it (e.g., Garnett et al. 1991; Schaerer & Vacca 1998).

Several mechanisms for producing hard ionizing radiation have been proposed, such as massive main-sequence stars (Schaerer & de Koter 1997), Wolf-Rayet stars (Schaerer 1996), primordial zero-metallicity stars (Schaerer 2002, 2003), high-mass X-ray binaries (Garnett et al. 1991) and fast radiative shocks (Dopita & Sutherland 1996). However, no mechanism has emerged clearly as the leading candidate, mainly because of the lack of a large data base to confront the models with observations. Despite the importance of understanding the high-ionization phenomenon to interpret the spectra of primordial star-forming galaxies when these are discovered in the future, very few observations of high-ionization emission lines in metal-deficient BCDs exist. The He II  $\lambda 4686$  emission line has been detected in only a few dozens BCDs, and [Ne v] and [Fe v] – [Fe VII] emission has been seen in only two BCDs (Guseva et al. 2000; Fricke et al. 2001; Izotov et al. 2001b, 2004a,c). This scarcity of data is partly due to the faintness of these high-ionization lines (less than 5% of the flux of  $\text{H}\beta$  in the case of He II  $\lambda 4686$ , and less than 2% of  $\text{H}\beta$  in the case of the [Ne v]  $\lambda 3346$ ,  $\lambda 3426$  emission lines) and their detection requires a 4 m-class telescope or larger. To increase the number of known BCDs with high-ionization emission lines, and construct a reasonably large sample with which to study statistical trends of high-ionization emission with metallicity and other parameters, we have embarked in a program to obtain high signal-to-noise spectra in the blue wavelength region of a selected sample of BCDs with the 6.5m MMT. To augment our sample, we have also carried out a systematic search of the Data Release 3 (DR3) of the Sloan Digital Sky survey (SDSS) (Abazajian et al. 2005) for emission line galaxies with detected He II  $\lambda 4686$  and [Fe v]  $\lambda 4227$  emission lines. Finally, for our statistical studies, we have also included several more BCDs with detected He II  $\lambda 4686$  emission and three BCDs with detected [Fe v]  $\lambda 4227$  emission from the sample which Izotov & Thuan (2004a) used to determine the primordial Helium abundance.

We describe the new observational data in Section 2, and how we derive element abundances in Section 3. We describe in Section 4 our sample of galaxies with high-ionization emission lines assembled from present and previous spectroscopic work. We use that sample for statistical studies of the high-ionization emission in Section 5. We discuss possible mechanisms for the hard radiation in Section 6. We explore how the compactness of the star-forming region may play a role in high-ionization emission in Section 7, and summarize our conclusions in Section 8.

## 2. MMT OBSERVATIONS AND DATA REDUCTION

We have obtained new high signal-to-noise ratio spectrophotometric observations for 26 H II regions in 18 BCDs and for one supergiant H II region in the spiral galaxy M101 with the 6.5-meter MMT on the nights of 2004 February 19 – 20 and 2005 February 4. In selecting the observational sample, we have been guided by several considerations. First, we wish the equivalent width of the H $\beta$  emission line in the H II regions to span a reasonably large range. Since EW(H $\beta$ ) is an indicator of the age of the most recent burst of star formation in the BCD, this ensures that our BCD sample spans a large burst age range, and gives us some handle on the time scale of the high-ionization emission phenomenon. Second, since the study of how high-ionization emission depends on metallicity is one of our main scientific objectives, we have chosen H II regions with metallicities spanning the entire metallicity range of BCDs, from  $\sim Z_{\odot}/50$  to  $\sim Z_{\odot}/3$ . Third, we have been careful to include BCDs with and without Wolf-Rayet (WR) stars since we want to study whether high-ionization emission is correlated or not with the presence of WR stars. Fourth, we have included objects known from previous spectroscopic work (our 4m or SDSS spectra) to have high-ionization emission, He II  $\lambda 4686$  or [Fe v]  $\lambda 4227$  lines, to check if the presence of these lines necessarily implies that higher ionization lines are present. Finally, we also include BCDs with different morphologies. Star formation in BCDs appears to occur in two different modes: a relatively quiescent “passive” mode without super-star cluster (SSC) formation, with a low star formation rate (SFR) in a diffuse star-forming region, and a considerably more “active” mode with SSC formation, a high SFR in a very compact star-forming region. This will allow us to check whether the presence of high-ionization emission is related to the compactness of the H II region.

The 18 BCDs and the H II region in the spiral galaxy M101 observed with the MMT are listed in Table 1 in order of increasing right ascension, along with some of their general properties such as coordinates, apparent magnitudes, redshifts and absolute magnitudes. In addition, we have also included in Table 1 BCDs previously observed with other telescopes which show in their spectra the high-ionization [Fe v]  $\lambda 4227$  emission line. Three BCDs were observed by Izotov & Thuan (2004a) with the Kitt Peak 4m telescope and five others were selected from the DR3 of the SDSS (Abazajian et al. 2005).

All observations were made with the Blue Channel of the MMT spectrograph. We used a  $2'' \times 300''$  slit and a 800 grooves/mm grating in first order. The above instrumental set-up gave a spatial scale along the slit of  $0''.6 \text{ pixel}^{-1}$ , a scale perpendicular to the slit of  $0.75 \text{ \AA pixel}^{-1}$ , a spectral range of 3200–5200 $\text{\AA}$  and a spectral resolution of  $\sim 3 \text{ \AA}$  (FWHM). The seeing was in the range  $1''$ – $2''$ . Total exposure times varied between 10 and 105 minutes. Each exposure was broken up into 2–7 subexposures, not exceeding 15 minutes, to allow for removal of cosmic rays. Three Kitt Peak IRS spectroscopic standard stars, G191B2B, Feige 34 and HZ 44 were observed at the beginning, middle and end of each night for flux calibration. Spectra of He–Ar comparison arcs were obtained before and after each observation to calibrate the wavelength scale. The log of the observations is given in Table 2.

The two-dimensional spectra were bias subtracted and flat-field corrected using IRAF<sup>2</sup>. We then use the IRAF software routines IDENTIFY, REIDENTIFY, FITCOORD, TRANSFORM to perform wavelength calibration and correct for distortion and tilt for each frame. Night sky subtraction was performed using the routine BACKGROUND. The level of night sky emission was determined from the closest regions to the galaxy that are free of galaxian stellar and nebular line emission, as well as of emission from foreground and background sources. One-dimensional spectra were then extracted from each two-dimensional frame using the APALL routine. Before extraction, distinct two-dimensional spectra of the same H II region were carefully aligned using the spatial locations of the brightest part in each spectrum, so that spectra were extracted at the same positions in all subexposures. For all objects, we extracted the brightest part of the BCD, using a  $6'' \times 2''$  extraction aperture. In the case of five BCDs, Mrk 71, I Zw 18, Mrk 35, Mrk 178 and Mrk 59, spectra of 2 – 3 different H II regions in the same galaxy were extracted. All extracted spectra from the same object were then co-added. We have summed the individual spectra from each subexposure after manual removal of the cosmic rays hits. The spectra obtained from each subexposure were also checked for cosmic rays hits at the location of strong emission lines, but none was found.

Particular attention was paid to the derivation of the sensitivity curve. It was obtained by fitting with a high-order polynomial the observed spectral energy distribution of the bright hot white dwarf standard stars G191B2B, Feige 34 and HZ 44. Because the spectra of these stars have only a small number of a relatively weak absorption features, their spectral energy distributions are known with very good accuracy (Oke 1990). Moreover, the response function of the CCD detector is smooth, so we could derive a sensitivity curve with a precision better than 1% over the whole optical range.

We show in Figure 1 the spectrum with labeled emission lines of one of the most interesting BCDs in our sample, SBS 0335–052E. This BCD with a metallicity of only  $\sim 2.5\%$  that of the Sun (Izotov et al. 1997c, 1999), is one of the most metal-deficient star-forming galaxies known in the local universe. It has a SFR of  $\sim 0.4 M_{\odot} \text{ yr}^{-1}$  and most of the star formation occurs in six SSCs within a region of  $\sim 500$  pc in size (Thuan et al. 1997). Several high-ionization emission lines are seen in its spectrum. In addition to the [Fe v]  $\lambda 4227$  emission line already discussed by Fricke et al. (2001) and Izotov et al. (2001b), we report here the discovery of the [Ne iv]  $\lambda 4725$  and [Ne v]  $\lambda 3346, 3426$  emission lines. This makes SBS 0335–052E only the second BCD known to have [Ne iv] and [Ne v] emission, after Tol 1214–277 (Izotov et al. 2004a,c). This discovery confirms and strengthens the finding by Izotov et al. (2001b) who discovered [Fe vi] – [Fe vii] emission in SBS 0335–052E and concluded that ionizing radiation above  $\sim 7$  Ryd must be intense in this galaxy. We note that, except for a very few papers from our group (e.g., Izotov et al. 2004a,c), the 3200–3700 Å spectral region has not been explored extensively before for BCDs. Not only does this spectral

---

<sup>2</sup>IRAF is distributed by National Optical Astronomical Observatory, which is operated by the Association of Universities for Research in Astronomy, Inc., under cooperative agreement with the National Science Foundation.

region contain the high-ionization [Ne v] lines discussed before, it also includes the Balmer jump, He I recombination lines, and in the case of SBS 0335–052E which has a higher redshift, the He II  $\lambda 3203$  line.

The spectra for the other 26 H II regions observed with the MMT are shown in Figure 2. The four dotted vertical lines show respectively the locations of the [Ne v]  $\lambda 3346$ ,  $3426$ , [Fe v]  $\lambda 4227$  and He II  $\lambda 4686$  emission lines. All spectra in Figs. 1 and 2 have been reduced to zero redshift. Of note is the detection of [O II]  $\lambda 3727$  and [O III]  $\lambda 5007$  emission lines in the spectrum of the C component of the second-most metal-deficient star-forming galaxy known, I Zw 18, with a metallicity of  $\sim 2\%$  that of the Sun. I Zw 18 C is a star-forming complex located  $\sim 22''$  northwest of the main star-forming region of I Zw 18. Although I Zw 18 C has been studied spectroscopically before (Izotov & Thuan 1998; van Zee et al. 2000; Izotov et al. 2001c), no oxygen lines have been detected. The MMT observations show conclusively that the ionized gas in the C component of I Zw 18 does contain heavy elements, just as its main component. We also point out the detection of the Bowen fluorescent O III  $\lambda 3092$  emission line (Aller 1984) in the spectrum of the highest-redshift BCD in the sample, J 0519+0007 (Table 1). This is the first such detection in the spectra of a low-metallicity BCD. The presence of this line indicates intense Ly $\alpha$  emission in the star-forming region of J 0519+0007.

The observed line fluxes  $F(\lambda)$  normalized to  $F(\text{H}\beta)$  and multiplied by a factor of 100 and their errors, for the 27 H II regions shown in Figs. 1 and 2 are given in Table 3. They were measured using the IRAF SPLIT routine. The line flux errors listed include statistical errors derived with SPLIT from non-flux calibrated spectra, in addition to errors introduced in the standard star absolute flux calibration. Since the differences between the response curves derived for the three standard stars are not greater than 1%, we set the errors in flux calibration to 1% of the line fluxes. The line flux errors will be later propagated into the calculation of abundance errors. The line fluxes were corrected for both reddening (Whitford 1958) and underlying hydrogen stellar absorption derived simultaneously by an iterative procedure as described in Izotov et al. (1994). The corrected line fluxes  $100 \times I(\lambda)/I(\text{H}\beta)$ , equivalent widths  $\text{EW}(\lambda)$ , extinction coefficients  $C(\text{H}\beta)$ , and equivalent widths  $\text{EW}(\text{abs})$  of the hydrogen absorption stellar lines are also given in Table 3, along with the uncorrected H $\beta$  fluxes.

### 3. PHYSICAL CONDITIONS AND DETERMINATION OF HEAVY ELEMENT ABUNDANCES

To determine element abundances, we follow generally the procedures of Izotov et al. (1994, 1997a) and Thuan et al. (1995). We adopt a two-zone photoionized H II region model: a high-ionization zone with temperature  $T_e(\text{O III})$ , where [O III], [Ne III] and [Ar IV] lines originate, and a low-ionization zone with temperature  $T_e(\text{O II})$ , where [N II], [O II], [S II] and [Fe III] lines originate. As for the [S III] and [Ar III] lines, they originate in the intermediate zone between the high and low-ionization regions (Garnett 1992). We have derived the chlorine abundance from [Cl III]

emission lines in 2 H II regions. We assume that these lines also originate in the intermediate zone as the ionization potentials of the  $S^{2+}$ ,  $Ar^{2+}$  and  $Cl^{2+}$  ions are similar. The temperature  $T_e(O\ III)$  is calculated using the  $[O\ III]\ \lambda 4363/(\lambda 4959+\lambda 5007)$  ratio. To take into account the electron temperatures for different ions, we have used the H II photoionization models of Stasińska & Izotov (2003), as fitted by the expressions in Izotov et al. (2005a). These expressions are based on more recent stellar atmosphere models and updated atomic collisional strengths as compared to those of Izotov et al. (1994, 1997a). Since our observations cover only the blue part of the optical spectrum, the  $[S\ II]\ \lambda 6717, 6731$  emission lines usually used to determine the electron number density  $N_e(S\ II)$  were not available. Therefore, we set  $N_e(S\ II) = 10\ \text{cm}^{-3}$ . The low-density limit for abundance determinations should hold as long as  $N_e$  is less than  $10^4\ \text{cm}^{-3}$ . Ionic and total heavy element abundances for the 24 H II regions observed with the MMT are derived in the manner described in Izotov et al. (2005a) and are given in Table 4 along with the adopted ionization correction factors *ICF*. We do not derive element abundances for I Zw 18C, Mrk 35 (#2) and Mrk 178 (#3) as the electron temperature-sensitive  $[O\ III]\ \lambda 4363$  emission line is not detected in the spectra of those H II regions. We have compared the abundances derived here with previous determinations in several objects. There is general good agreement, the differences between independent measurements not exceeding  $\sim 0.05$  dex. We note that in SBS 0335–052W (the star-forming dwarf galaxy which shares the same large H I envelope with SBS 0335–052E, see Pustilnik et al. 2001), the oxygen abundance  $12 + \log O/H = 7.11 \pm 0.05$  derived here is lower than the one derived by Lipovetsky et al. (1999). Remarkably, it is lower than in I Zw 18 (this paper), stealing from the latter the qualification of “most metal-deficient star-forming galaxy known in the local universe” (Izotov et al. 2005b).

#### 4. A SAMPLE OF BLUE COMPACT DWARF GALAXIES WITH HIGH-IONIZATION EMISSION LINES

Using present and previous observations, we now construct a sample which contains as many BCDs with high-ionization emission as possible. Out of the 27 H II regions observed with the MMT, we have detected  $[Fe\ v]\ \lambda 4227$  emission line in 8 H II regions, including SBS 0335–052E, and  $[Ne\ v]\ \lambda 3346, 3426$  in 3 H II regions. We have also searched for  $[Fe\ v]\ \lambda 4227$  emission in spectra obtained earlier for our program on the determination of the primordial helium abundance (Izotov & Thuan 2004a), and in the spectra of the SDSS DR3. The search yielded 3 BCDs from the Izotov & Thuan (2004a) sample and 5 BCDs from the SDSS. To these data we have added Tol 1214–277, known to possess both  $[Ne\ v]\ \lambda 3346, 3426$  and  $[Fe\ v]\ \lambda 4227$  emission (Fricke et al. 2001; Izotov et al. 2004a,c). The emission line fluxes and their equivalent widths of the objects selected from Izotov & Thuan (2004a) and from the SDSS DR3 are shown in Table 5. The element abundances in these H II regions are derived in the same manner as for the objects observed with the MMT and are given in Table 6. In total, our sample contains 15 BCDs with detected  $[Fe\ v]\ \lambda 4227$  emission (ionization potential of 4 Ryd). Out of those 15, only 4 show the higher ionization  $[Ne\ v]\ \lambda 3346, 3426$  emission line (ionization potential of 7.1 Ryd). This represents a substantial increase of the

total number of known star-forming galaxies with high-ionization emission lines in their spectra. The spectra of galaxies with [Fe v]  $\lambda 4227$  emission (indicated by a dotted vertical line) are shown in the wavelength range  $\lambda 4150 - 4770$  in Fig. 3. Those with [Ne v]  $\lambda 3346, 3426$  emission (indicated by two dotted vertical lines) are shown in the wavelength range  $\lambda 3150 - 3650$  in Fig. 4.

We have also conducted a search for galaxies with He II  $\lambda 4686$  emission (ionization potential of 4 Ryd). The resulting sample is considerably larger: 465 star-forming galaxies, of which 396 galaxies came from the SDSS DR3 and the remaining 69 galaxies from our previous observations and the present MMT ones. We have also measured line fluxes and derived heavy element abundances for all of these galaxies in the manner described above. However, because of the large data set, we do not tabulate them but will simply plot them in various figures to detect and study statistical trends.

## 5. STATISTICAL PROPERTIES OF THE HIGH-IONIZATION SAMPLE

### 5.1. Metallicity dependence

As mentioned in the Introduction, previous spectroscopic studies (e.g., Campbell et al. 1986) have revealed that the hardness of the stellar ionizing radiation in BCDs increases with decreasing metallicity. This trend implies that nebular emission lines of ions with high ionization potentials are stronger in galaxies with lower metallicity. We can check this trend with our large He II sample. Fig. 5 shows the He II  $\lambda 4686$  to  $H\beta$  flux ratio as a function of the oxygen abundance in the ionized gas. The dots show individual data points while the open circles show the means of the data points in the 7.1 - 7.6, 7.6 - 8.1 and 8.1 - 8.6 intervals of  $12 + \log O/H$ . The error bars show the mean error in each interval. There is an evident trend with metallicity. At low oxygen abundance,  $12 + \log O/H < 7.6$ , the mean He II  $\lambda 4686$  flux is  $0.018 \pm 0.011$  that of the  $H\beta$  emission line. However at high oxygen abundance,  $12 + \log O/H \gtrsim 7.9$ , the He II  $\lambda 4686$  emission is weaker on average, with the mean flux being only  $0.010 \pm 0.006$  of the  $H\beta$  emission line flux. There is however not a well-defined relation between He II  $\lambda 4686$  emission and metallicity. The data show a large scatter with an upper envelope. This implies that metallicity is not the only parameter which governs He II  $\lambda 4686$  emission. We can also check the dependence of other high-ionization line fluxes on metallicity, albeit with smaller samples. Figs. 6 and 7 show respectively [Fe v]  $\lambda 4227$  and [Ne v]  $\lambda 3346, 3426$  emission as a function of ionized gas oxygen abundance. There appears also to be a trend of higher [Fe v]  $\lambda 4227$  emission toward lower metallicities, with [Fe v]  $\lambda 4227/H\beta = 0.0066 \pm 0.0038$  for  $12 + \log O/H < 7.6$  and [Fe v]  $\lambda 4227/H\beta = 0.0036 \pm 0.0021$  for  $12 + \log O/H \gtrsim 7.6$ . As for [Ne v] emission, the sample is too small to make definite conclusions. However, Fig. 7 does show that the two lowest-metallicity BCDs have systematically higher [Ne v]  $\lambda 3426$  fluxes than the two highest-metallicity galaxies. Of note is the considerably larger [Ne v] flux (nearly a factor of 4) of the BCD Tol 1214–277 (second point from the left) as compared to that of SBS 0335–052E which is more metal-deficient.



## 5.2. Hardness ratios

To quantify the hardness of ionizing radiation for low-ionization ions, Vilchez & Pagel (1988) have introduced the parameter  $\eta$  for the oxygen and sulfur ionic fractions defined as  $\eta = \frac{O^+/O^{2+}}{S^+/S^{2+}}$ . We cannot do the same for our high-ionization ions as we have no observational constraints on the electron temperatures in the  $He^{2+}$ ,  $Ne^{4+}$  and  $Fe^{4+}$  zones of the H II regions. Therefore, we simply compare the flux ratios of emission lines for different ions of the same element. In Table 7 we show these flux ratios for each galaxy with detected heavy element high-ionization emission lines, with the means and dispersions of these ratios for two subsamples, a low-metallicity subsample with  $12 + \log O/H \leq 7.6$ , and a higher-metallicity subsample with  $12 + \log O/H > 7.6$ . Again, there is clear indication from comparison of these mean values that the hardness of the ionizing radiation is higher for the lower-metallicity subsample. We do not compute the mean values for the  $I([Ne\ v] \lambda 3426)/I([Ne\ III] \lambda 3868)$  flux ratio because of poor statistics, but it is clear from Table 7 that this ratio for the two more metal-deficient galaxies SBS 0335–052 and Tol 1214–277 is significantly greater than that for the two more metal-rich galaxies, HS 0837+4717 and Mrk 209. Thus these hardness flux ratios support the conclusion reached in section 5.1, that the ionizing radiation becomes harder in lower-metallicity BCDs.

## 5.3. Dependence on the age of the starburst

While it is clear that the hardness of the ionizing radiation in BCDs decreases with increasing metallicity, the large scatter of the He II  $\lambda 4686$  fluxes in Fig. 5, of the [Fe v]  $\lambda 4227$  fluxes in Fig. 6 and of the [Ne v]  $\lambda 3426$  fluxes in Fig. 7, tells us that metallicity is not the only factor which controls their fluxes. We explore here another factor which may influence the hardness of the ionizing radiation in BCDs, the age of the current starburst.

The age of the starburst may play a role as stars go through different evolutionary phases which may modify their ionizing fluxes. The equivalent width of the  $H\beta$  emission line  $EW(H\beta)$  is a good indicator of the starburst age (see, e.g., Schaerer & Vacca 1998). The greater  $EW(H\beta)$  is, the younger is the starburst. Stellar evolution models predict (Schaerer & Vacca 1998) that  $EW(H\beta)$  is  $\sim 600\text{\AA}$  for a zero-age starburst. The origin of nebular He II  $\lambda 4686$  emission in photoionized supergiant H II regions has been a subject of debate for many years, ever since it was realized that the flux of this line is several times larger than model predictions for H II regions photoionized by main-sequence stars (e.g., Garnett et al. 1991; Schaerer 1996). In Fig. 8 we show the dependence on  $EW(H\beta)$  of the He II  $\lambda 4686$  emission line flux relative to the  $H\beta$  flux. The dots show individual data points while the open circles show the means of the data points in the 0 - 100  $\text{\AA}$ , 100 - 200  $\text{\AA}$  and 200 - 300  $\text{\AA}$  intervals of  $EW(H\beta)$ . The error bars show the mean error in each interval. There is no clear general trend. The ratio He II  $\lambda 4686/H\beta$  is the same, equal to  $0.011 \pm 0.007$ , for either the sample of objects with  $EW(H\beta) < 100\text{\AA}$  or the one containing objects with  $EW(H\beta) \gtrsim 100\text{\AA}$ . Thus, the hardness of the ionizing radiation with photon energy above 4 Ryd does not appear to

depend on starburst age.

There are however two features to notice in Fig. 8 which constrain the nature of the source of ionizing radiation. First, in very young bursts with  $EW(H\beta) \gtrsim 300\text{\AA}$  corresponding to a starburst age of  $\sim 3 - 4$  Myr, there is a clear absence of strong He II emission. Such ages correspond to lifetimes of very massive stars, with masses  $\sim 100 M_{\odot}$ . This implies that the ionizing radiation responsible for He II  $\lambda 4686$  emission probably does not come from massive stars in their main-sequence phase, but rather in their post-main-sequence phase. Second, strong He II  $\lambda 4686$  emission is detected in many starbursts with  $EW(H\beta) \sim 50 - 300\text{\AA}$ , corresponding to starburst ages in the range  $\sim 3 - 10$  Myr. Such ages correspond to lifetimes of main sequence stars in the mass range from 50 to  $15 M_{\odot}$ . Thus, it appears that, not only the most massive evolved stars are responsible for the hard ionizing radiation, but also less massive stars and/or their descendants and remnants.

Next, we explore other possible sources of hard ionizing radiation in low-metallicity BCDs.

## 6. SOURCES OF HARD IONIZING RADIATION

### 6.1. Wolf-Rayet stars

If present photoionization models of main-sequence stars cannot account for the intensity of nebular He II  $\lambda 4686$  emission, models for post-main sequence Wolf-Rayet stars also fail. Schaerer (1996) has synthesized the nebular and Wolf-Rayet He II  $\lambda 4686$  emission in young starbursts. For heavy element mass fractions  $Z_{\odot}/5 \leq Z \leq Z_{\odot}$ , he predicts strong nebular He II emission due to a significant fraction of WC stars in the early WR phases of the burst. However, Guseva et al. (2000) have found that the strength of the He II  $\lambda 4686$  does not correlate with the WR stellar population in the galaxy, so that WR stars cannot be the main contributor to He II  $\lambda 4686$  emission.

### 6.2. The hottest normal main-sequence stars and primordial stars

Izotov et al. (2004a,c) have modeled the physical conditions in the BCD Tol 1214–277 to reproduce the observed fluxes of the He II  $\lambda 4686$ , [Ne v]  $\lambda 3426$  and [Fe v]  $\lambda 4227$  emission lines. This BCD is characterized by a metallicity of about 4% that of the Sun and by the strongest [Ne v]  $\lambda 3426\text{\AA}$  emission line known. To produce strong [Ne v]  $\lambda 3426\text{\AA}$ , the ionizing radiation must be intense at  $\lambda \lesssim 128\text{\AA}$  because the ionization potential of the  $\text{Ne}^{4+}$  ion is 7.1 Rydberg. Using Kurucz and CoStar stellar atmosphere models, Izotov et al. (2004a,c) have calculated several spherically symmetric ionization-bounded H II region models which reproduce reasonably well the observed emission line fluxes of the  $\text{O}^+$ ,  $\text{O}^{2+}$ ,  $\text{Ne}^{2+}$ ,  $\text{S}^{2+}$ ,  $\text{Ar}^{2+}$  and  $\text{Ar}^{3+}$  ions. However, the models fail to reproduce the observed [Ne v]  $\lambda 3426$ /[Ne III]  $\lambda 3868$  and He II  $\lambda 4686$ / $H\beta$  flux ratios in Tol 1214–277, the predicted values being respectively some  $10^4$  and 50 times smaller respectively, even with the CoStar atmosphere models of the hottest main-sequence stars from Schaerer & de Koter (1997)

(their F1 model with  $T_{\text{eff}} \approx 54000$  K). The models also fail to reproduce the high-ionization line ratios in less extreme objects such as Mrk 209. The F1 model predicts  $[\text{Ne v}] \lambda 3426/[\text{Ne III}] \lambda 3868$  and  $\text{He II } \lambda 4686/\text{H}\beta$  line flux ratios that are smaller than the observed ones by factors of  $10^3$  and 10 respectively. The difference between the observations and model predictions is even larger when Kurucz (1979) stellar atmosphere models are used.

While the gas in our BCDs is not as metal-deficient as the primordial gas, we have also compared our observations with high-ionization line fluxes predicted for primordial stars (Schaerer 2002, 2003). We found that it is possible, in principle, to reproduce the observed  $\text{He II } \lambda 4686$ ,  $[\text{Fe v}] \lambda 4227$  and  $[\text{Ne v}] \lambda 3426$  emission line fluxes by models of very low metallicity ( $Z \lesssim 10^{-7}$ ) massive ionizing stars. However, such models of Population III stars would predict equivalent widths of  $\text{H}\beta$  and  $\text{Ly}\alpha$  emission lines that are several times larger than those observed (Tables 3 and 5). Thus neither models of normal stars, of Wolf-Rayet stars nor of primordial stars are able to reproduce the observed high-ionization line fluxes.

### 6.3. High-mass X-ray binaries

The energy of the photons that can produce  $\text{Ne}^{4+}$  ions are in the soft X-ray range. Thus high-mass X-ray binaries (HMXBs) may also be an important source of ionizing radiation. If stellar atmosphere models of normal hot stars fail to provide the necessary ionizing radiation, can HMXBs do better? Izotov et al. (2004a,c) have estimated that the X-ray luminosity required to reproduce the large observed flux of the  $[\text{Ne v}]$  emission in Tol 1214–277 at wavelengths shorter  $\sim 100\text{\AA}$  (corresponding to a photon energy of 0.14 keV) should be as high as  $L_X = 10^{39} - 10^{40}$  erg  $\text{s}^{-1}$ . Tol 1214–277 has not been observed in the X-ray range. In fact, of the four BCDs known to possess  $[\text{Ne v}] \lambda 3426$  emission (Fig. 4), only SBS 0335–052E has *Chandra* X-ray observations (Thuan et al. 2004). It is found that more than 90% of its 0.5 – 10 keV (or 1 – 25 $\text{\AA}$ ) flux comes from a point-source with a luminosity of  $3.5 \times 10^{39}$  erg  $\text{s}^{-1}$ . If that point source is composed of a single object, then its luminosity would place it in the range of the so-called ultraluminous X-ray sources (ULXs).

Thuan et al. (2004) have suggested that the high X-ray luminosities of these sources may be due to a metallicity effect. The X-ray heating of the gas as it falls toward a compact object depends strongly on the atomic number  $Z$ , since the photoelectric cross-section varies as  $Z^4$ . Thus in low-metallicity systems, the X-ray heating is less, resulting in a larger accretion rate and X-ray luminosity (van Paradijs & McClintock 1995). It is also plausible that a lower gaseous metallicity may also result in higher mass accreting black holes, first by allowing the formation of more massive progenitor stars because of reduced cooling, and second by helping the formation of a more massive compact object from a normal progenitor OB star. A lower metallicity results in the reduction of the mass-loss rate in the radiatively driven winds, leading to a more massive stellar core, which may then collapse into a more massive black hole.

The X-ray spectrum of the point source in SBS 0335–052E is well fitted by a moderately soft power law (Thuan et al. 2004), typical of X-ray emission from HMXBs. The observed  $[\text{Ne v}] \lambda 3426/[\text{Ne III}] \lambda 3868$  flux ratio in SBS 0335–052E is  $\sim 2.7$  times smaller than that in Tol1214–277 (Table 7), so that the X-ray luminosity of the ULX observed in it (Thuan et al. 2004), can in principle account for the  $[\text{Ne v}]$  emission. However, based on the very scarce X-ray data on low-metallicity BCDs, there does not appear to be a one-to-one correlation between the presence of a ULX and  $[\text{Ne v}]$  emission. Thus the  $[\text{Ne v}] \lambda 3426$  emission line is not seen in the MMT spectra (Fig. 2) of the BCDs I Zw 18 with a metallicity of about 2% that of the Sun, and Mrk 59 with a metallicity of about 12% that of the Sun, although a X-ray point-source has been detected in I Zw 18 (Thuan et al. 2004), and two in Mrk 59 (Thuan et al. 2005, in preparation), with X-ray luminosities comparable to the one in SBS 0335–052E (Thuan et al. 2004). This lack of correlation appears to rule out HMXBs as mainly responsible for the high-ionization  $[\text{Ne v}] \lambda 3426$  emission.

#### 6.4. Fast radiative shocks

Garnett et al. (1991) have suggested that fast radiative shocks in giant H II regions can produce relatively strong He II emission under certain conditions. Hydrodynamical models by Dopita & Sutherland (1996) have indeed shown that fast shocks are an efficient means to generate a strong local UV photon field in the ISM of a galaxy. The total optical and UV emission from the shock and the precursor region scales as the mechanical energy flux through the shock. The  $\text{H}\beta$  luminosity generated in the shock region which measures the number of recombinations that occur in the ionized gas column behind the shock provides a convenient way for estimating the total mechanical energy dissipation rate through the shock structure. With shock velocities of  $\sim 400 - 500 \text{ km s}^{-1}$ , examination of the Dopita & Sutherland (1996) models shows that if the  $\text{H}\beta$  luminosity generated in the shock region is several percent of the  $\text{H}\beta$  luminosity produced by massive stars, such shocks can be responsible for the observed fluxes of both the He II  $\lambda 4686\text{\AA}$  and  $[\text{Ne v}] \lambda 3346, 3426\text{\AA}$  emission lines for all four BCDs with  $[\text{Ne v}] \lambda 3346, 3426$  emission, the spectra of which are shown in Fig. 4.

There is an observational check for the presence of such fast radiative shocks. Their large velocities should produce broad components in the line profiles of the strong emission lines. Indeed, broad wings of the  $\text{H}\beta$  and  $[\text{O III}] \lambda 4959, 5007$  emission lines are seen in the spectra of all four BCDs with detected  $[\text{Ne v}] \lambda 3426$  emission: SBS 0335–052 (Fig. 1), HS 0837+4717 and Mrk 209 (Fig. 2) and Tol 1214–277 (Fig. 2 in Izotov et al. 2004c), and the broad component fluxes are  $\sim 1\% - 2\%$  of the narrow component fluxes. The full widths at half maximum FWHM  $\gtrsim 15 \text{\AA}$  of the broad components correspond to gas velocities in expanding shells of  $\gtrsim 900/2 \text{ km s}^{-1} = 450 \text{ km s}^{-1}$ . The  $[\text{Ne v}]$  emission and the broad components in the 4 BCDs appear to be related to the evolution of the most massive stars. This is because their  $\text{H}\beta$  equivalent widths are high,  $\text{EW}(\text{H}\beta) \gtrsim 190\text{\AA}$  (Table 3), corresponding to a starburst age  $\lesssim 3 - 4 \text{ Myr}$ , the main-sequence lifetime of a  $\gtrsim 50 - 100 M_{\odot}$  star. Thus, on the basis of a meager sample of four objects,  $[\text{Ne v}] \lambda 3426$  emission

does appear to be accompanied by fast gas velocities of  $\sim 450 \text{ km s}^{-1}$ , in the range of velocities expected to be produced by fast shocks. However, the reverse is not true: the presence of broad components is not necessarily accompanied by high-ionization emission. For example, broad wings of the strong emission lines are also seen in the spectra of II Zw 40, Mrk 71 and Mrk 59 (Fig. 2). However, their spectra which have a comparable signal-to-noise ratio, do not show [Ne v]  $\lambda 3426$  emission. Metallicity probably plays a role here. The latter three galaxies with broad wings of the strong emission lines but without [Ne v] emission are all more metal-rich (their  $12 + \log \text{O/H}$  are respectively 8.1, 7.9 and 8.0) than the four BCDs with broad wings and [Ne v] emission (their  $12 + \log \text{O/H}$  are respectively 7.3, 7.6, 7.8 and 7.5). It is probable that in higher-metallicity BCDs, for a given shock velocity, the shock-heated ionized gas cools more efficiently and hence the high-ionization postshock region is narrower, so that the fraction of highly ionized ions is lower than that in lower-metallicity BCDs. Unfortunately, we cannot check this metallicity dependence directly with hydrodynamical calculations as Dopita & Sutherland (1996) computed only models with solar metallicity.

In summary, existing models of massive main-sequence stars and of post-main-sequence Wolf-Rayet stars are unable to account for the hard radiation responsible for He II  $\lambda 4686$  emission, let alone for the considerably harder radiation responsible for [Ne v]  $\lambda 3426$  emission. HMXBs may play a role although the scarce X-ray data on high-ionization BCDs show that there is not a one-to-one relationship between X-ray and [Ne v]  $\lambda 3426$  emission. Fast radiative shocks with velocities  $\sim 450 \text{ km s}^{-1}$  associated with the evolution of massive ( $M \sim 50 - 100 M_{\odot}$ ) stars appear to be the best candidate in town. The presence of such fast motions is supported by the broad components observed in the line profiles of the strong emission lines. Fast radiative shocks are also able to account for the general trend of more intense high-ionization emission at lower metallicities, since the high-ionization postshock region should become wider with decreasing heavy element abundances and less cooling.

## 7. HIGH-IONIZATION EMISSION AND SUPER-STAR CLUSTERS IN BLUE COMPACT DWARF GALAXIES

We discuss in this section how the compactness of the star-forming regions in BCDs may play an important role in the high-ionization phenomenon.

### 7.1. Imaging data and super-star clusters

One striking common feature which links the BCDs with detected [Ne v]  $\lambda 3426$  emission in Fig. 4 is the presence of luminous, compact and high-surface-brightness Super-Star Clusters (SSCs). This can be seen in Fig. 9 which shows the *HST* images of SBS 0335–052E, Tol 1214–277 and Mrk 209, and the SDSS image of HS 0837+4717. We will use broad-band images to discuss the sizes

and luminosities of the SSCs.

The Tol 1214–277 image was obtained by us using the WFPC2 camera aboard *HST*<sup>3</sup> on 1996 June 29 (PI: T. X. Thuan, proposal ID No. 6678). In addition to the *V* (F555W filter, 1600 s exposure time) image shown in Fig. 9, we have also obtained an *I* (F814W filter, 3200 s exposure time) image. Tol 1214–277 was centered on the WF3 chip, giving an angular resolution of  $0''.101$  per pixel. A pixel corresponds to a spatial extent of 50 pc at the distance of 103 Mpc of the BCD. Fig. 9 shows that star formation in Tol 1214–277 occurs primarily in a bright compact stellar cluster. There is a low-surface-brightness component to the south-west of the cluster. The compact cluster has a FWHM of 3.8 pixels, corresponding to a spatial extent of 190 pc. Its *V*, *I* magnitudes and *V* – *I* color are respectively equal to  $18.62 \pm 0.01$  mag,  $19.42 \pm 0.01$  mag and  $-1.20 \pm 0.02$  mag. At the distance of Tol 1214–277, this corresponds to  $M(V) = -16.44$  mag. If this luminosity comes from a single object, then the brightness of the SSC in Tol 1214–277 would be more than 5 times brighter than the brightest SSC in SBS 0335–052E (Thuan et al. 1997). However, because Tol 1214–277 is nearly 2 times more distant than SBS 0335–052E, the linear resolution is poor and we cannot exclude the possibility that the star-forming region is composed of several SSCs. We have checked its surface brightness profile and find it to be symmetric. Thus either the star-forming region in Tol 1214–277 contains a single SSC, or if it contains several SSCs, these must be very close to each other. We note finally that the star-forming region of Tol 1214–277 is extremely blue in *V* – *I*, not only because of the young OB stars contained in it, but also because of the strong [O III]  $\lambda 5007$  nebular emission line which, at the redshift  $z = 0.0260$  of Tol 1214–277, falls into the *V* band.

Images of the three other BCDs were extracted from the *HST* and SDSS archives. The UV image of SBS 0335–052E was obtained by Kunth et al. (2003) with the *HST*/ACS camera in the F140LP filter (PI: D. Kunth, proposal ID No. 9470). The angular resolution is  $0''.032$  per pixel which corresponds to a spatial scale of 8.9 pc per pixel at the distance of 54.3 Mpc. We measured the FWHMs of SSCs 1, 4 and 5 (using the notation of Thuan et al. 1997) to be respectively 5.7, 4.8 and 4.3 pixels, corresponding to linear sizes of 51, 43 and 38 pc. The *J* image of Mrk 209 in the F110W filter was obtained by Schulte-Ladbeck et al. (2001) with the *HST*/NICMOS camera (PI: R. E. Schulte-Ladbeck, proposal ID No. 7859). The angular resolution is  $0''.076$  per pixel, corresponding to a spatial scale of 2.2 pc per pixel at the distance of 5.8 Mpc. Four bright compact clusters are seen which each have a FWHM  $\sim$  of 2.2 pixels, corresponding to a linear size 4.8 pc. Their apparent *J* magnitudes are in the range 18.5 – 18.7 mag, corresponding to absolute magnitudes  $M(J) = -10.3$  -  $-10.1$  mag. Since  $V - J = -0.06$  (Thuan 1983),  $M(V) = -10.4$  -  $-10.2$ . Both these linear sizes and luminosities put the star clusters in Mrk 209 in the category of SSCs. Finally, because HS 0837+4717 has not been imaged by *HST*, we show in Fig. 9 its *g*-band SDSS image. Here, the angular resolution is  $0''.398$  per pixel which at the distance of 168

---

<sup>3</sup>Based on observations obtained with the NASA/ESA *Hubble Space Telescope* through the Space Telescope Science Institute, which is operated by AURA, Inc. under NASA contract NAS5-26555.

Mpc corresponds to a spatial scale of 325 pc per pixel. The star-forming region has a size FWHM = 3.9 pixels, corresponding to a linear size of 1267 pc. Its apparent  $g$  magnitude measured in a 3'' aperture is 17.9 mag, corresponding to an absolute magnitude  $-18.2$  mag. There are probably several compact clusters in the star-forming region of HS 0837+4717 which are not resolved because of the large distance of the BCD and the poor angular resolution of the SDSS images.

Our size and luminosity estimates of SSCs above should be considered as upper limits because of the presence of the nebular emission which is more extended than the ionizing star clusters. In principle, both continuum and line nebular emission ought to be subtracted from the broad-band images. However, this cannot be done as we do not have high spatial resolution narrow-filter images of the BCDs centered on the emission lines. At least for SBS 0335–052E, the overestimate in the SSC sizes is small as the contribution of the nebular emission in the UV range at  $\sim 1400\text{\AA}$  is minimal.

## 7.2. Active vs. passive star formation

The previous discussion shows that of the four galaxies with detected [Ne v]  $\lambda 3346$ , 3426 emission, at least three, SBS 0335–052E, Tol 1214–277 and Mrk 209, have star formation occurring in very luminous and compact SSCs. We cannot tell for HS 0837+4717 because it has not been imaged by *HST*. The compactness of the star-forming region thus appears to play a key role in the production of high-ionization radiation with photon energy above 7.1 Ryd.

Based on the detailed study of two of the most metal-deficient BCDs known, I Zw 18 and SBS 0335–052E, star formation in BCDs appears to occur in two quite different modes: SBS 0335–052E makes stars in an “active” mode characterized by SSC formation, a high star formation rate (SFR) of  $\sim 0.4 M_{\odot} \text{ yr}^{-1}$  (Thuan et al. 1997), a compact size, hot dust, and significant amounts of  $\text{H}_2$ , while I Zw 18 is characterized by a more quiescent “passive” mode with an absence of SSCs, a low SFR [some 8 times less than in SBS 0335–052E, Kennicutt et al. (1994)], a larger size with cooler dust and no significant amount of  $\text{H}_2$ . For the purpose of our discussion, we will call “active” BCDs those with SSCs, and “passive” BCDs those without. Clearly, metallicity is not the distinguishing factor between SBS 0335–052E and I Zw 18 since both BCDs have similar heavy element abundance. Theoretical models (Hirashita & Hunt 2004) suggest that the difference between the two modes can be understood through a difference in size and density of the star-forming regions. The active mode occurs in regions which are compact (with radius  $\lesssim 50$  pc) and dense (with gas number density  $\gtrsim 500 \text{ cm}^{-3}$ ) as in SBS 0335–052E. On the other hand, the passive mode occurs in regions that are diffuse (with radius  $\gtrsim 100$  pc) and less dense (with gas number density  $\lesssim 100 \text{ cm}^{-3}$ ) as in I Zw 18.

Our preferred mechanism for the source of hard ionizing radiation, fast radiative shocks, would work best in dense environments with electron number densities of several hundreds per  $\text{cm}^{-3}$ , similar to those in “active” low-metallicity BCDs with SSC formation. The luminosities in emission

lines scale as the square of the electron number density. Therefore, shocks moving through a dense ISM can radiate more and produce high [Ne v] emission-line luminosities. The electron number densities  $N_e(\text{S II})$  are indeed high in at least three BCDs with [Ne v] emission:  $N_e(\text{S II}) = 390 \text{ cm}^{-3}$  for SBS 0335–052 (Izotov et al. 1997c),  $400 \text{ cm}^{-3}$  for Tol 1214–277 (Izotov et al. 2001a) and  $300 - 400 \text{ cm}^{-3}$  for HS 0837+4717 (Pustilnik et al. 2004). As for Mrk 209 where [Ne v] emission is tentatively detected, its electron number density is lower,  $N_e(\text{S II}) \lesssim 100 \text{ cm}^{-3}$  (Izotov et al. 1997a). On the other hand, the emission-line luminosities of postshock regions in the low-density ISM of “passive” BCDs without SSC formation are expected to be considerably lower, and any [Ne v] emission would go undetected.

However, if the presence of fast shocks and dense stellar clusters is a necessary condition for [Ne v] emission, it is not a sufficient condition. [Ne v] emission is absent in higher-metallicity BCDs, such as II Zw 40, Mrk 59 and Mrk 71, despite the presence of compact stellar clusters (as examination of archival *HST* images shows), and of broad components of the strong emission lines (Fig. 2). A low-metallicity ISM is also needed. Thus, the presence of [Ne v] emission requires the following three conditions to be fulfilled simultaneously: 1) a low gaseous metallicity; 2) the presence of fast shocks and 3) a dense ISM and compact stellar clusters.

### 7.3. The decoupling of the very hard and moderate ionizing radiations

It thus appears that the very high-ionization radiation with photon energy greater than 7.1 Ryd is associated with very dense star-forming regions. To check for the compactness of the [Ne v]  $\lambda 3426$  emission, we have plotted in Fig. 10 its spatial distribution in the BCD SBS 0335–052E along the slit, with a position angle of  $-30$  degrees. For comparison, we have also plotted the spatial distributions of other emission lines, [Fe v]  $\lambda 4227$ , He II  $\lambda 4686$ ,  $\text{H}\beta$   $\lambda 4861$ , [O III]  $\lambda 4363$  and [O III]  $\lambda 5007$ . These distributions are similar to those obtained by Izotov et al. (2001b). In particular, we confirm the excess of He II  $\lambda 4686$  emission in the shell at an angular distance of  $5''.5$  to the northwest of SSC 1 [see Fig. 10 of Thuan et al. (1997)]. This excess emission at a location where there is no visible star cluster supports the hypothesis that He II emission in SBS 0335–052E is due mainly to radiative shocks. It is seen from Fig. 10 that the spatial distribution of [Ne v]  $\lambda 3426$  emission is more compact than those of other high-ionization ions. Thus, although the maxima of both [Ne v]  $\lambda 3426$  and He II  $\lambda 4686$  emissions are between SSCs 1,2 and SSCs 4,5 [the SSC notation of Thuan et al. (1997) is used], the spatial distribution of the [Ne v] emission is not as extended as that of the He II emission. This observation has two consequences. First, it supports our previous conclusion that very hard ionizing radiation is associated with the active mode of star formation in BCDs with very compact star-forming regions. Second, it implies that the source of very hard radiation (with photon energy  $\gtrsim 7$  Ryd) responsible for the [Ne v] emission is distinct spatially from the source of moderate ionizing radiation (with photon energy between 4 and 7 Ryd) responsible for the He II and [Fe v] emission (Fig. 10a). Comparison of the high-ionization emission of two of the most-metal deficient BCDs known in the local universe, I Zw 18 and SBS 0335–052E, supports



that contention. Despite very similar strengths of the He II  $\lambda 4686$  emission line relative to  $H\beta$  in the two BCDs, strong [Ne v]  $\lambda 3346,3426$  emission is seen only in SBS 0335–052E but not in I Zw 18. Their nearly equal metallicities suggest once again that metallicity is not the only factor which controls the amount of hard ionizing radiation relative to moderate ionizing radiation.

Fig. 10b also shows that He II  $\lambda 4686$  emission does not follow [O III]  $\lambda 5007$  emission. While the latter is strongest at the location of SSC 1, the former is offset in the direction of SSCs 4 and 5. This feature has been noted before by Izotov et al. (1997c, 2001b). This is consistent with the idea that the extended He II  $\lambda 4686$  emission is due mainly to the ionizing radiation from radiative shocks, in contrast to the [O III]  $\lambda 5007$  emission which originates mainly from the ionizing radiation of main-sequence stars.

## 8. SUMMARY AND CONCLUSIONS

The first Population III stars are expected to be very massive and hot, producing copious amounts of hard ionizing radiation. The best place to study hard ionizing radiation in the local universe is in metal-deficient blue compact dwarf (BCD) galaxies as the hardness of the ionizing radiation in BCDs has long been known to increase with decreasing metallicity. We have carried out with the 6.5m MMT a spectroscopic search for the high-ionization [Ne v]  $\lambda 3426$  emission line (ionization potential of 7.1 Ryd) in 18 BCDs. We have detected [Ne v] emission in 2 BCDs, SBS 0335–052E and HS 0837+4717 and tentatively in Mrk 209. With the previous detection of that line in Tol 1214–277 (Izotov et al. 2004a), there are now 4 BCDs known to possess [Ne v] emission. We have also examined the BCD spectra for other high ionization lines such as [Fe v]  $\lambda 4227$  (ionization potential of 4 Ryd) and He II  $\lambda 4686$  (ionization potential of 4 Ryd). In order to construct a large sample of BCDs with high-ionization lines to study statistical trends, we have combined the present MMT observations of BCDs with previous ones obtained for our primordial helium program (Izotov & Thuan 2004a) and those available in the Data Release 3 of the Sloan Digital Sky Survey. We have thus assembled 15 BCDs with [Fe v]  $\lambda 4227$  emission and 465 BCDs with He II  $\lambda 4686$  emission. Studies of statistical trends in the resulting sample yield the following main results:

1) There is a general tendency for higher He II, [Fe v] and [Ne v] emission at lower metallicities. The hardness of the radiation as measured by the flux ratios of emission lines for different ions of the same element also increases with decreasing metallicity. However the scatter is large indicating that metallicity is not the only parameter which controls the hardness of the ionizing radiation.

2) The hardness of the ionizing radiation with photon energy greater than 4 Ryd does not depend on the burst age as measured by the equivalent width of  $H\beta$ ,  $EW(H\beta)$ . There is a clear absence of He II emission in very young 3 – 4 Myr starbursts with  $EW(H\beta) \gtrsim 300 \text{ \AA}$ , implying that the source of ionization is not massive stars in their main-sequence phase, but in their post-main-sequence phase. Strong He II emission is seen in starbursts with  $EW(H\beta) \sim 50 - 300 \text{ \AA}$ , suggesting that less massive stars and their descendants also contribute radiation to ionize helium. Present

photoionization models of main-sequence and of Wolf-Rayet stars cannot account for the observed He II emission.

3) The X-ray luminosity in luminous high-mass X-ray binaries (HMXBs) observed in a few very metal-deficient BCDs can account for their [Ne v] emission. However, the scarce X-ray data does not show a one-to-one correlation between the presence of a HMXB and [Ne v] emission, so that HMXBs are probably ruled out as the main source of hard ionizing radiation with energy above 7.1 Ryd.

4) The most likely source of [Ne v] emission is probably fast radiative shocks moving with velocities  $\sim 450 \text{ km s}^{-1}$  through a dense ISM with electron number densities of several hundreds  $\text{cm}^{-3}$ . These shocks are probably produced via the evolution of massive stars with masses of  $\sim 50 - 100 M_{\odot}$ , formed in very compact and dense super-star clusters (SSCs). These fast radiative shocks are evidenced by broad components in the line profiles of the strong emission lines. However the presence of compact SSCs and broad components is not necessarily accompanied by high-ionization emission. Metallicity appears to play an important role. [Ne v] emission is detected only in low-metallicity galaxies with  $12 + \log \text{O}/\text{H} \lesssim 7.8$ . In higher-metallicity galaxies with higher metallicity the postshock regions are cooled more efficiently. Therefore, their high-ionization regions are smaller and their emission lower.

5) The spatial distribution of [Ne v] emission is more compact than that of He II emission, suggesting spatially distinct sources of ionizing radiation for the two. While [Ne v] emission requires hard radiation produced by fast radiative shocks moving through a dense interstellar medium, and probably associated with the evolution of the most massive stars, softer ionizing radiation, likely associated with the evolution of less massive stars and/or radiative shocks moving through a lower density ISM, is required for He II emission.

The MMT time was available thanks to a grant from the Frank Levinson Fund of the Peninsula Community Foundation to the Astronomy Department of the University of Virginia . The research described in this publication was made possible in part by Award No. UP1-2551-KV-03 of the U.S. Civilian Research & Development Foundation for the Independent States of the Former Soviet Union (CRDF). It has also been supported by NSF grant AST-02-05785. Y.I.I. thanks the hospitality of the Astronomy Department of the University of Virginia. All the authors acknowledge the work of the Sloan Digital Sky Survey (SDSS) team. Funding for the Sloan Digital Sky Survey (SDSS) has been provided by the Alfred P. Sloan Foundation, the Participating Institutions, the National Aeronautics and Space Administration, the National Science Foundation, the U.S. Department of Energy, the Japanese Monbukagakusho, and the Max Planck Society. The SDSS Web site is <http://www.sdss.org/>. The SDSS is managed by the Astrophysical Research Consortium (ARC) for the Participating Institutions. The Participating Institutions are The University of Chicago, Fermilab, the Institute for Advanced Study, the Japan Participation Group, The Johns Hopkins University, the Korean Scientist Group, Los Alamos National Laboratory, the Max-Planck-Institute for Astronomy (MPIA), the Max-Planck-Institute for Astrophysics (MPA), New

Mexico State University, University of Pittsburgh, University of Portsmouth, Princeton University, the United States Naval Observatory, and the University of Washington.

## REFERENCES

- Abazajian, K., et al. 2005, *AJ*, 129, 1755
- Abel, T., Bryan, G. L., & Norman, M. L. 2002, *Science*, 295, 93
- Aller, L. H. 1984, *Physics of Thermal Gaseous Nebulae* (Dordrecht: Reidel)
- Bromm, V., Coppi, P. S., & Larson, R. B. 2002, *ApJ*, 564, 23
- Campbell, A., Terlevich, R., & Melnick, J. 1986, *MNRAS*, 223, 811
- Dopita, M. A., & Sutherland, R. S. 1996, *ApJS*, 102, 161
- Feibelman, W. A., Hyung, S., & Aller, L. H. 1996, *MNRAS*, 278, 625
- Ferland, G. J., Korista, K. T., Verner, D. A., Ferguson, J. W., Kingdon, J. B., & Verner, E. M. 1998, *PASP*, 110, 761
- Fricke, K. J., Izotov, Y. I., Papaderos, P., Guseva, N. G., & Thuan, T. X. 2001, *AJ*, 121, 169
- Garnett, D. R. 1992, *AJ*, 103, 1330
- Garnett, D. R., Kennicutt, R. C., Chu, Y.-H., & Skillman, E. D. 1991, *ApJ*, 373, 458
- Guseva, N. G., Izotov, Y. I., & Thuan, T. X. 2000, *ApJ*, 531, 776
- Hirashita, H., & Hunt, L.K. 2004, *A&A*, 421, 555
- Izotov, Y. I., & Thuan, T. X. 1998, *ApJ*, 497, 227
- Izotov, Y. I., & Thuan, T. X. 1999, *ApJ*, 511, 639
- Izotov, Y. I., & Thuan, T. X. 2004a, *ApJ*, 602, 200
- Izotov, Y. I., & Thuan, T. X. 2004b, *ApJ*, 616, 768
- Izotov, Y. I., Chaffee, F. H., & Green, R. F. 2001a, *ApJ*, 562, 727
- Izotov, Y. I., Chaffee, F. H., & Schaerer, D. 2001b, *A&A*, 378, L45
- Izotov, Y. I., Chaffee, F. H., Foltz, C. B., et al. 2001c, *ApJ*, 560, 222
- Izotov, Y. I., Thuan, T. X., & Lipovetsky, V. A. 1994, *ApJ*, 435, 647
- Izotov, Y. I., Thuan, T. X., & Lipovetsky, V. A. 1997a, *ApJS*, 108, 1

- Izotov, Y. I., Foltz, C. B., Green, R. F., Guseva, N. G., & Thuan, T. X. 1997b, *ApJ*, 487, L37
- Izotov, Y. I., Lipovetsky, V. A., Chaffee, F. H., Foltz, C. B., Guseva, N. G., & Kniazev, A. Y. 1997c, *ApJ*, 476, 698
- Izotov, Y. I., Chaffee, F. H., Foltz, C. B., Green, R. F., Guseva, N. G., & Thuan, T. X. 1999, *ApJ*, 527, 757
- Izotov, Y. I., Noeske, K. G., Guseva, N. G., Papaderos, P., Thuan, T. X., & Fricke, K. J. 2004a, *A&A*, 415, L27
- Izotov, Y. I., Stasińska, G., Guseva, N. G., & Thuan, T. X. 2004b, *A&A*, 415, 87
- Izotov, Y. I., Papaderos, P., Guseva, N. G., Fricke, K. J., & Thuan, T. X. 2004c, *A&A*, 421, 539
- Izotov, Y. I., Stasińska, G., Meynet, G., Guseva, N. G., & Thuan, T. X. 2005a, *A&A*, submitted
- Izotov, Y. I., Thuan, T. X., & Guseva, N. G. 2005b, *ApJ*, in press; preprint astro-ph/0506498
- Kennicutt, R.C., Tamblyn, O., & Congdon, C.E. 1994, *ApJ*, 435, 22
- Kunth, D., Leitherer, C., Mas-Hesse, J. M., Östlin, G., & Petrosian, A. 2003, *ApJ*, 597, 263
- Kurucz, R. L. 1979, *ApJS*, 40, 1
- Lipovetsky, V. A., Chaffee, F. H., Izotov, Y. I., et al. 1999, *ApJ*, 519, 177
- Masegosa, J., Moles, M., & Campos-Aguilar, A. 1994, *ApJ*, 420, 576
- Oke, J. B. 1990, *AJ*, 99, 1621
- Pustilnik, S., Brinks, E., Thuan, T. X., Lipovetsky, V. A., & Izotov, Y. I. 2001, *AJ*, 121, 1413
- Pustilnik, S., Kniazev, A., Pramskij, A., Izotov, Y., Foltz, C., Brosch, N., Martin, J.-M., & Ugryumov, A. 2004, *A&A*, 419, 469
- Schaerer, D. 1996, *ApJ*, 467, L17
- Schaerer, D. 2002, *A&A*, 382, 28
- Schaerer, D. 2003, *A&A*, 397, 527
- Schaerer, D., & de Koter, A. 1997, *A&A*, 322, 598
- Schaerer, D., & Vacca, W. D. W. 1998, *ApJ*, 497, 618
- Schulte-Ladbeck, R. E., Hopp, U., Greggio, L., Crone, M. M., & Drozdovsky, I. O. 2001, *AJ*, 121, 3007
- Steidel, C. C., Giavalisco, M., Pettini, M., Dickinson, M., & Adelberger, K. L. 1996, *ApJ*, 462, 17

- Stasińska G. 1990, A&AS, 83, 501
- Stasińska, G., & Izotov, Y. I. 2003, A&A, 397, 71
- Terlevich, R., Melnick, J., Masegosa, J., Moles, M., & Copetti, M. V. F. 1991, A&AS, 91, 285
- Thuan, T.X. 1983, ApJ, 268, 667
- Thuan, T. X., Izotov, Y. I. 1997, ApJ, 489, 623
- Thuan, T. X., Izotov, Y. I., & Lipovetsky, V. A. 1995, ApJ, 445, 108
- Thuan, T. X., Izotov, Y. I., & Lipovetsky, V. A. 1997, ApJ, 477, 661
- Thuan, T. X., Izotov, Y. I., & Foltz, C. B. 1999, ApJ, 525, 105
- Thuan, T. X., Bauer, F. E., Papaderos, P., & Izotov, Y. I. 2004, ApJ, 606, 213
- van Paradijs, J., & McClintock, J.E. 1995, in X-ray Binaries, ed. W.H. Lewin, J. van Paradijs, & E.P.J. van den Heuvel (Cambridge: Cambridge Univ. Press), 58
- van Zee, L., Westpfahl, D., Haynes, M. P., & Salzer, J. J. 1998, AJ, 115, 1000
- Vílchez, J. M., & Pagel, B. E. J. 1988, MNRAS, 231, 257
- Whitford, A. E. 1958, AJ, 63, 201

Table 1. General Parameters of Galaxies

Name	Coordinates (2000.0)		$m_{pg}$	$z$	$M_{pg}$	Other names
	$\alpha$	$\delta$				
a) Galaxies observed with the MMT						
SBS 0335 – 052W	03 <sup>h</sup> 37 <sup>m</sup> 38 <sup>s</sup> .4	–05°02′37″	19.0	0.01367	–14.7	
SBS 0335 – 052E	03 37 44.0	–05 02 39	16.3	0.01347	–17.4	
J 0519 + 0007	05 19 02.7	+00 07 29	18.2	0.04460	–18.1	
II Zw 40	05 55 42.6	+03 23 32	15.0	0.00265	–15.1	UGCA 116
Mrk 71	07 28 42.5	+69 11 21	11.0	0.00031	–14.5	NGC 2363
HS 0822 + 3542	08 25 55.4	+35 32 32	18.0	0.00244	–11.9	J 0825 + 3532
Mrk 94	08 37 43.5	+51 38 31	16.0	0.00249	–14.0	SBS 0834 + 518
HS 0837 + 4717	08 40 29.9	+47 07 09	18.0	0.04212	–18.1	J 0840 + 4707
SBS 0911 + 472	09 14 34.9	+47 02 07	16.0	0.02729	–19.2	
SBS 0926 + 606A	09 30 06.4	+60 26 53	17.0	0.01370	–16.7	
I Zw 18	09 34 02.1	+55 14 25	16.0	0.00243	–13.9	Mrk 116
SBS 0940 + 544	09 44 16.6	+54 11 33	18.0	0.00541	–13.7	
SBS 1030 + 583	10 34 10.2	+58 03 49	16.0	0.00753	–16.4	Mrk 1434
Mrk 35	10 45 22.4	+55 57 37	13.0	0.00331	–17.6	Haro3
Mrk 178	11 33 28.9	+49 14 13	15.0	0.00076	–12.4	UGC 4561
SBS 1152 + 579	11 55 28.3	+57 39 52	16.0	0.01732	–18.2	Mrk 193
Mrk 209	12 26 16.1	+48 29 31	15.0	0.00101	–13.0	I Zw 36
Mrk 59	12 59 00.3	+34 50 40	13.0	0.00258	–17.1	NGC 4861
J 1404 + 5423	14 04 29.5	+54 23 47	14.0	0.00095	–13.9	
b) Galaxies observed with the 4m KPNO telescope with detected [Fe v] $\lambda$ 4227 emission						
J 0519 + 0007	05 19 02.7	+00 07 29	18.2	0.04460	–18.1	
HS 1028 + 3843	10 31 51.8	+38 28 07	19.4	0.02945	–16.0	
HS 2236 + 1344	22 38 31.1	+14 00 29	18.2	0.02115	–16.4	
c) SDSS galaxies with detected [Fe v] $\lambda$ 4227 emission						
J 0240 – 0828	02 40 52.2	–08 28 27	19.8	0.08231	–18.1	
J 0840 + 4707	08 40 29.9	+47 07 09	18.0	0.04212	–18.1	HS 0837 + 4717
J 0944 – 0038	09 44 01.9	–00 38 32	17.5	0.00483	–13.9	CGCG 007–025
J 1253 – 0312	12 53 06.0	–03 12 59	16.2	0.02280	–18.6	
J 1323 – 0132	13 23 47.5	–01 32 52	19.1	0.02254	–15.7	

Table 2. Journal of the MMT Observations

Name	Date of Obs.	Exposure	Airmass
SBS 0335 – 052W	2005, Feb 4	2700s	1.27 - 1.31
SBS 0335 – 052E	2004, Feb 19 - 20	6300s	1.32 - 1.47
J 0519 + 0007	2004, Feb 19	3600s	1.20 - 1.28
II Zw 40	2005, Feb 4	1200s	1.32 - 1.37
Mrk 71	2004, Feb 19 - 20	1320s	1.26 - 1.37
HS 0822 + 3542	2005, Feb 4	2700s	1.12 - 1.19
Mrk 94	2005, Feb 4	1800s	1.32 - 1.36
HS 0837 + 4717	2004, Feb 20	2700s	1.13 - 1.19
SBS 0911 + 472	2005, Feb 4	1800s	1.04 - 1.05
SBS 0926 + 606A	2005, Feb 4	1800s	1.18 - 1.20
I Zw 18	2005, Feb 4	3600s	1.19 - 1.28
SBS 0940 + 544	2005, Feb 4	2700s	1.08 - 1.09
SBS 1030 + 583	2005, Feb 4	1800s	1.12 - 1.13
Mrk 35	2004, Feb 20	1575s	1.10 - 1.12
Mrk 178	2005, Feb 4	1800s	1.06 - 1.07
SBS 1152 + 579	2005, Feb 4	1178s	1.12 - 1.13
Mrk 209	2004, Feb 19	2400s	1.14 - 1.20
Mrk 59	2004, Feb 20	1200s	1.06 - 1.09
J 1404 + 5423	2005, Feb 4	600s	1.09

TABLE 3  
EMISSION LINE INTENSITIES AND EQUIVALENT WIDTHS

Ion	GALAXY											
	SBS 0335-052W			SBS 0335-052E			J 0519+0007			II Zw 40		
	$F(\lambda)/F(H\beta)$	$I(\lambda)/I(H\beta)$	EW <sup>a</sup>	$F(\lambda)/F(H\beta)$	$I(\lambda)/I(H\beta)$	EW <sup>a</sup>	$F(\lambda)/F(H\beta)$	$I(\lambda)/I(H\beta)$	EW <sup>a</sup>	$F(\lambda)/F(H\beta)$	$I(\lambda)/I(H\beta)$	EW <sup>a</sup>
3092 O III	...	...	...	...	...	...	1.84 ± 0.70	2.12 ± 0.82	1.5	...	...	...
3188 He I	...	...	...	3.36 ± 0.17	3.91 ± 0.21	3.0	2.44 ± 0.41	2.79 ± 0.47	2.2	...	...	...
3203 He II	...	...	...	0.96 ± 0.14	1.11 ± 0.17	0.9	0.59 ± 0.26	0.67 ± 0.30	0.5	...	...	...
3346 [Ne V]	...	...	...	0.43 ± 0.07	0.49 ± 0.09	0.4	...	...	...	...	...	...
3425 [Ne V]	...	...	...	0.63 ± 0.06	0.72 ± 0.06	0.6	...	...	...	...	...	...
3499 He I	...	...	...	0.13 ± 0.04	0.15 ± 0.04	0.1	...	...	...	...	...	...
3554 He I	...	...	...	0.13 ± 0.03	0.14 ± 0.04	0.1	...	...	...	...	...	...
3587 He I	...	...	...	0.21 ± 0.03	0.24 ± 0.03	0.2	...	...	...	...	...	...
3614 He I	...	...	...	0.32 ± 0.04	0.35 ± 0.05	0.3	...	...	...	...	...	...
3634 He I	...	...	...	0.15 ± 0.03	2.28 ± 1.25	0.2	...	...	...	0.21 ± 0.10	0.45 ± 0.20	0.4
3687 H19	...	...	...	0.33 ± 0.03	2.42 ± 0.60	0.4	0.78 ± 0.16	3.14 ± 1.15	1.1	0.35 ± 0.09	1.45 ± 1.42	1.0
3692 H18	...	...	...	0.62 ± 0.03	2.62 ± 0.32	0.7	1.01 ± 0.18	3.29 ± 1.00	1.6	0.28 ± 0.09	1.35 ± 1.78	0.7
3697 H17	...	...	...	1.17 ± 0.03	3.23 ± 0.22	1.4	1.56 ± 0.18	3.87 ± 0.74	2.4	0.69 ± 0.10	2.13 ± 0.91	1.8
3704 H16	...	...	...	1.18 ± 0.04	3.15 ± 0.23	1.5	1.32 ± 0.17	3.61 ± 0.79	2.0	0.60 ± 0.10	1.92 ± 0.97	1.6
3712 H15	...	...	...	1.08 ± 0.04	3.04 ± 0.23	1.3	1.34 ± 0.17	3.63 ± 0.79	2.1	0.76 ± 0.11	2.17 ± 0.85	2.3
3722 H14	...	...	...	22.44 ± 0.32	24.59 ± 0.38	27.9	28.01 ± 0.49	30.31 ± 0.56	43.1	34.56 ± 0.53	67.99 ± 1.10	96.4
3727 [O II]	64.59 ± 1.47	69.43 ± 1.65	41.0	2.25 ± 0.05	4.32 ± 0.11	2.8	2.78 ± 0.18	5.19 ± 0.41	4.2	1.48 ± 0.11	3.55 ± 0.33	4.2
3750 H12	...	...	...	2.94 ± 0.05	5.07 ± 0.11	3.6	3.27 ± 0.18	5.59 ± 0.37	5.3	1.78 ± 0.10	4.09 ± 0.31	5.0
3771 H11	...	...	...	4.22 ± 0.07	6.49 ± 0.12	5.1	4.42 ± 0.17	6.91 ± 0.34	6.8	2.66 ± 0.11	5.68 ± 0.30	7.2
3798 H10	...	...	...	0.75 ± 0.03	0.81 ± 0.04	0.9	0.94 ± 0.19	1.01 ± 0.20	1.5	0.74 ± 0.09	1.36 ± 0.16	2.0
3820 He I	...	...	...	5.94 ± 0.09	8.30 ± 0.14	7.3	6.39 ± 0.20	8.84 ± 0.33	10.7	3.75 ± 0.12	7.53 ± 0.32	10.2
3835 H9	5.80 ± 0.56	7.53 ± 1.13	3.4	21.75 ± 0.31	23.50 ± 0.36	25.4	31.34 ± 0.50	33.49 ± 0.56	48.3	32.02 ± 0.48	57.27 ± 0.90	85.7
3868 [Ne III]	10.24 ± 0.62	10.88 ± 0.67	5.1	15.54 ± 0.22	18.55 ± 0.28	19.7	15.62 ± 0.28	18.79 ± 0.40	24.3	10.00 ± 0.18	18.29 ± 0.39	27.3
3889 He I + H8	18.43 ± 0.71	20.71 ± 1.08	12.7	20.78 ± 0.30	24.00 ± 0.36	26.4	24.07 ± 0.39	27.47 ± 0.50	39.9	19.35 ± 0.30	33.03 ± 0.56	53.5
3968 [Ne III] + H7	16.37 ± 0.55	18.22 ± 0.87	13.5	1.34 ± 0.04	1.43 ± 0.04	1.7	1.55 ± 0.14	1.64 ± 0.15	2.5	1.22 ± 0.08	1.97 ± 0.12	3.3
4026 He I	...	...	...	0.34 ± 0.02	0.36 ± 0.03	0.4	0.65 ± 0.12	0.68 ± 0.13	1.1	0.65 ± 0.07	1.02 ± 0.11	1.8
4068 [S II]	...	...	...	0.11 ± 0.02	0.12 ± 0.02	0.1	...	...	...	0.24 ± 0.06	0.38 ± 0.10	0.7
4076 [S II]	...	...	...	23.15 ± 0.33	26.09 ± 0.39	31.4	22.98 ± 0.37	25.94 ± 0.46	39.6	16.31 ± 0.26	25.68 ± 0.45	44.2
4101 Hδ	24.13 ± 0.73	26.40 ± 1.12	15.6	0.23 ± 0.03	0.25 ± 0.03	0.3	...	...	...	...	...	...
4121 He I	...	...	...	0.20 ± 0.02	0.21 ± 0.02	0.3	0.36 ± 0.11	0.38 ± 0.11	0.6	...	...	...
4143 He I	...	...	...	0.25 ± 0.02	0.26 ± 0.02	0.3	0.45 ± 0.08	0.46 ± 0.09	0.8	0.14 ± 0.00	0.20 ± 0.00	0.4
4227 [Fe V]	...	...	...	0.14 ± 0.02	0.14 ± 0.02	0.2	...	...	...	...	...	...
4287 [Fe II]	...	...	...	44.64 ± 0.63	47.58 ± 0.69	66.9	44.74 ± 0.67	47.57 ± 0.75	87.1	34.60 ± 0.51	46.55 ± 0.71	94.1
4340 Hγ	45.32 ± 0.94	47.52 ± 1.19	34.0	10.39 ± 0.15	10.71 ± 0.16	15.7	13.30 ± 0.24	13.63 ± 0.26	25.7	8.05 ± 0.14	10.57 ± 0.19	21.9
4363 [O III]	3.99 ± 0.44	4.08 ± 0.45	2.7	0.29 ± 0.02	0.30 ± 0.02	0.4	0.42 ± 0.14	0.43 ± 0.15	0.8	0.37 ± 0.05	0.48 ± 0.07	1.0
4387 He I	...	...	...	3.30 ± 0.05	3.37 ± 0.06	5.2	3.72 ± 0.15	3.78 ± 0.15	7.7	3.23 ± 0.09	3.98 ± 0.11	8.6
4471 He I	3.31 ± 0.42	3.36 ± 0.43	2.2	0.38 ± 0.02	0.38 ± 0.02	0.7	0.52 ± 0.14	0.53 ± 0.14	1.2	0.43 ± 0.07	0.48 ± 0.08	1.1
4658 [Fe III]	...	...	...	2.51 ± 0.04	2.52 ± 0.04	4.5	1.81 ± 0.13	1.81 ± 0.13	4.1	0.52 ± 0.05	0.57 ± 0.06	1.2
4686 He II	...	...	...	0.11 ± 0.02	0.11 ± 0.02	0.2	...	...	...	...	...	...
4702 [Fe III]	...	...	...	1.66 ± 0.03	1.66 ± 0.04	3.0	2.24 ± 0.13	2.23 ± 0.13	5.0	2.21 ± 0.07	2.39 ± 0.08	5.7
4711 [Ar IV] + He I	...	...	...	0.08 ± 0.02	0.08 ± 0.02	0.1	...	...	...	...	...	...
4725 [Ne IV]	...	...	...	0.95 ± 0.03	0.95 ± 0.03	1.7	1.29 ± 0.11	1.28 ± 0.11	2.9	1.41 ± 0.07	1.50 ± 0.07	3.8
4740 [Ar IV]	...	...	...	100.00 ± 1.42	100.00 ± 1.44	189.7	100.00 ± 1.46	100.00 ± 1.49	235.6	100.00 ± 1.43	100.00 ± 1.47	258.7
4861 Hβ	100.00 ± 1.75	100.00 ± 1.86	80.1	0.17 ± 0.02	0.17 ± 0.02	0.3	...	...	...	...	...	...
4881 [Fe II]	...	...	...	0.18 ± 0.02	0.17 ± 0.02	0.3	...	...	...	...	...	...
4907 [Fe IV]	...	...	...	0.94 ± 0.03	0.92 ± 0.03	1.8	0.95 ± 0.12	0.94 ± 0.12	2.3	1.32 ± 0.08	1.27 ± 0.07	3.4
4921 He I	...	...	...	108.95 ± 1.54	106.94 ± 1.54	214.4	147.22 ± 2.14	144.32 ± 2.13	342.7	267.35 ± 3.82	253.21 ± 3.69	652.7
4959 [O III]	42.48 ± 0.94	41.83 ± 0.94	35.7	0.65 ± 0.02	0.63 ± 0.02	1.2	...	...	...	...	...	...
4988 [Fe III]	...	...	...	324.81 ± 4.60	317.64 ± 4.56	648.7	441.67 ± 5.23	431.54 ± 5.19	1028.1	832.86 ± 11.87	769.80 ± 11.20	2051.0
5007 [O III]	125.42 ± 2.17	123.15 ± 2.15	109.7	0.29 ± 0.02	0.28 ± 0.02	0.6	...	...	...	...	...	...
5041 Si III	...	...	...	0.17 ± 0.02	0.17 ± 0.02	0.4	...	...	...	...	...	...
5047 He I	...	...	...	...	...	...	...	...	...	...	...	...
C(Hβ)	...	0.115	...	...	0.145	...	...	0.130	...	...	0.960	...
F(Hβ) <sup>b</sup>	...	0.28	...	...	7.31	...	...	1.39	...	...	8.47	...
EW(abs) Å	...	0.75	...	...	2.10	...	...	3.10	...	...	1.00	...



TABLE 3—Continued

GALAXY												
Ion	Mrk 71A			Mrk 71B			Mrk 71C			HS 0822+3542		
	$F(\lambda)/F(H\beta)$	$I(\lambda)/I(H\beta)$	EW <sup>a</sup>	$F(\lambda)/F(H\beta)$	$I(\lambda)/I(H\beta)$	EW <sup>a</sup>	$F(\lambda)/F(H\beta)$	$I(\lambda)/I(H\beta)$	EW <sup>a</sup>	$F(\lambda)/F(H\beta)$	$I(\lambda)/I(H\beta)$	EW <sup>a</sup>
3448 He I	0.17 ± 0.05	0.20 ± 0.06	0.2	...	...	...	...	...	...	...	...	...
3531 He I	0.13 ± 0.04	0.15 ± 0.05	0.2	...	...	...	...	...	...	...	...	...
3554 He I	0.10 ± 0.03	0.11 ± 0.03	0.2	...	...	...	...	...	...	...	...	...
3587 He I	0.29 ± 0.05	0.32 ± 0.06	0.4	...	...	...	...	...	...	...	...	...
3614 He I	0.29 ± 0.05	0.33 ± 0.05	0.4	0.25 ± 0.07	0.30 ± 0.08	0.2	...	...	...	...	...	...
3634 He I	0.27 ± 0.04	0.30 ± 0.05	0.4	0.23 ± 0.04	0.27 ± 0.05	0.2	...	...	...	...	...	...
3692 H18	0.56 ± 0.04	2.25 ± 0.25	1.3	0.91 ± 0.06	1.91 ± 0.53	0.9	...	...	...	0.94 ± 0.12	3.09 ± 0.71	1.4
3697 H17	0.48 ± 0.04	2.29 ± 0.30	1.0	0.76 ± 0.06	1.77 ± 0.62	0.7	...	...	...	0.81 ± 0.12	2.89 ± 0.77	1.2
3704 H16	1.30 ± 0.04	3.07 ± 0.15	3.1	1.33 ± 0.07	2.39 ± 0.43	1.3	1.10 ± 0.19	2.12 ± 2.21	0.7	1.96 ± 0.15	3.97 ± 0.48	3.0
3712 H15	1.17 ± 0.04	2.86 ± 0.15	2.9	1.37 ± 0.07	2.43 ± 0.42	1.4	1.39 ± 0.19	2.45 ± 1.79	0.8	1.59 ± 0.15	3.61 ± 0.57	2.5
3722 H14	1.42 ± 0.04	3.07 ± 0.14	3.6	1.33 ± 0.07	2.38 ± 0.42	1.4	1.47 ± 0.19	2.53 ± 1.72	0.9	...	...	...
3727 [O II]	38.27 ± 0.55	42.34 ± 0.64	96.7	62.31 ± 0.90	71.25 ± 1.09	62.2	114.96 ± 1.72	131.07 ± 2.07	65.6	37.13 ± 0.60	36.63 ± 0.63	57.0
3750 H12	2.37 ± 0.05	4.10 ± 0.11	6.1	2.37 ± 0.07	3.55 ± 0.13	2.4	1.85 ± 0.19	2.98 ± 0.41	1.1	2.35 ± 0.14	4.47 ± 0.34	3.5
3771 H11	3.06 ± 0.06	4.85 ± 0.11	7.9	2.70 ± 0.07	3.90 ± 0.13	2.8	2.16 ± 0.21	3.29 ± 0.41	1.3	3.11 ± 0.15	5.24 ± 0.31	4.5
3798 H10	4.22 ± 0.07	6.10 ± 0.12	10.9	4.30 ± 0.09	5.67 ± 0.14	4.5	3.49 ± 0.20	4.76 ± 0.37	2.2	4.32 ± 0.15	6.47 ± 0.29	6.2
3820 He I	0.85 ± 0.04	0.94 ± 0.04	2.2	0.95 ± 0.06	1.08 ± 0.07	1.0	...	...	...	1.15 ± 0.15	1.14 ± 0.15	1.6
3835 H9	6.01 ± 0.09	8.03 ± 0.14	15.6	5.82 ± 0.11	7.38 ± 0.16	6.0	5.09 ± 0.25	6.55 ± 0.40	3.1	5.97 ± 0.17	8.11 ± 0.28	8.5
3868 [Ne III]	49.31 ± 0.70	53.73 ± 0.80	128.1	42.20 ± 0.61	47.33 ± 0.71	43.3	33.55 ± 0.55	37.54 ± 0.64	19.9	27.37 ± 0.44	27.00 ± 0.46	36.7
3889 He I + H8	16.96 ± 0.24	19.87 ± 0.30	44.5	16.89 ± 0.25	19.67 ± 0.31	18.3	16.99 ± 0.33	19.68 ± 0.45	11.8	18.63 ± 0.32	20.55 ± 0.40	27.0
3968 [Ne III] + H7	27.20 ± 0.39	30.70 ± 0.46	73.8	25.70 ± 0.38	29.18 ± 0.45	29.0	22.30 ± 0.42	25.38 ± 0.54	14.8	22.85 ± 0.38	24.66 ± 0.45	33.9
4026 He I	1.57 ± 0.04	1.68 ± 0.04	4.4	1.39 ± 0.05	1.53 ± 0.06	1.6	1.07 ± 0.16	1.17 ± 0.18	0.8	1.98 ± 0.12	1.96 ± 0.12	3.0
4068 [S II]	0.47 ± 0.02	0.50 ± 0.03	1.3	0.83 ± 0.05	0.91 ± 0.06	1.0	1.36 ± 0.17	1.49 ± 0.19	1.0	...	...	...
4076 [S II]	0.11 ± 0.02	0.12 ± 0.02	0.3	...	...	...	...	...	...	...	...	...
4101 Hδ	23.17 ± 0.33	25.91 ± 0.38	67.1	23.40 ± 0.34	26.12 ± 0.40	29.0	23.78 ± 0.41	26.44 ± 0.49	19.2	24.40 ± 0.39	26.04 ± 0.45	39.2
4121 He I	0.25 ± 0.03	0.26 ± 0.03	0.7	0.32 ± 0.05	0.35 ± 0.06	0.4	...	...	...	0.48 ± 0.11	0.47 ± 0.11	0.8
4143 He I	0.25 ± 0.03	0.27 ± 0.03	0.7	0.32 ± 0.05	0.35 ± 0.05	0.4	...	...	...	0.47 ± 0.08	0.47 ± 0.08	0.8
4227 [Fe V]	0.06 ± 0.02	0.06 ± 0.02	0.2	0.27 ± 0.06	0.29 ± 0.07	0.4	...	...	...	...	...	...
4340 Hγ	44.40 ± 0.63	47.28 ± 0.69	137.5	44.06 ± 0.63	47.13 ± 0.69	59.8	44.01 ± 0.67	46.97 ± 0.74	39.8	46.49 ± 0.69	47.57 ± 0.74	86.0
4363 [O III]	14.55 ± 0.21	15.08 ± 0.22	45.8	11.05 ± 0.17	11.64 ± 0.18	15.2	7.16 ± 0.18	7.54 ± 0.19	6.6	10.51 ± 0.20	10.37 ± 0.20	18.9
4387 He I	0.45 ± 0.03	0.47 ± 0.03	1.5	0.42 ± 0.04	0.44 ± 0.04	0.6	...	...	...	0.44 ± 0.01	0.43 ± 0.01	0.8
4471 He I	3.63 ± 0.06	3.73 ± 0.06	12.4	3.43 ± 0.07	3.57 ± 0.07	5.1	3.09 ± 0.14	3.21 ± 0.15	3.1	3.57 ± 0.12	3.52 ± 0.12	6.6
4563 Si II	0.07 ± 0.02	0.07 ± 0.02	0.2	0.22 ± 0.04	0.22 ± 0.04	0.3	...	...	...	...	...	...
4571 Si II	0.06 ± 0.02	0.06 ± 0.02	0.2	0.08 ± 0.03	0.09 ± 0.03	0.1	...	...	...	...	...	...
4658 [Fe III]	0.15 ± 0.02	0.15 ± 0.02	0.6	0.22 ± 0.03	0.22 ± 0.03	0.3	0.39 ± 0.01	0.40 ± 0.01	0.5	0.41 ± 0.07	0.40 ± 0.07	0.8
4686 He II	0.32 ± 0.02	0.32 ± 0.02	1.2	2.22 ± 0.05	2.26 ± 0.06	3.5	1.59 ± 0.12	1.61 ± 0.12	1.9	...	...	...
4702 [Fe III]	0.07 ± 0.01	0.07 ± 0.01	0.3	...	...	...	...	...	...	...	...	...
4711 [Ar IV] + He I	2.89 ± 0.05	2.91 ± 0.05	10.9	1.89 ± 0.05	1.91 ± 0.06	3.2	0.94 ± 0.12	0.95 ± 0.12	1.1	1.53 ± 0.10	1.51 ± 0.10	3.1
4740 [Ar IV]	1.84 ± 0.04	1.85 ± 0.04	7.1	0.94 ± 0.04	0.95 ± 0.04	1.7	...	...	...	0.84 ± 0.09	0.83 ± 0.09	1.8
4861 Hβ	100.00 ± 1.42	100.00 ± 1.43	396.7	100.00 ± 1.42	100.00 ± 1.44	180.8	100.00 ± 1.47	100.00 ± 1.48	127.3	100.00 ± 1.46	100.00 ± 1.48	232.1
4921 He I	1.15 ± 0.03	1.14 ± 0.03	4.6	1.21 ± 0.05	1.19 ± 0.05	2.2	1.07 ± 0.09	1.06 ± 0.09	1.4	1.16 ± 0.10	1.15 ± 0.10	2.7
4959 [O III]	248.26 ± 3.52	244.12 ± 3.50	1007.0	211.26 ± 3.00	208.24 ± 2.98	389.8	156.07 ± 2.27	153.97 ± 2.26	190.2	123.21 ± 1.79	121.54 ± 1.79	273.8
5007 [O III]	714.99 ± 9.80	700.31 ± 9.71	2588.0	640.56 ± 9.10	628.28 ± 8.99	1172.0	474.83 ± 6.87	466.19 ± 6.79	599.9	368.99 ± 5.32	363.97 ± 5.32	854.3
5015 He I	...	...	...	...	...	...	...	...	...	2.38 ± 0.09	2.34 ± 0.09	5.4
C(Hβ)	...	0.155	...	...	0.195	...	...	0.190	...	...	0.000	...
F(Hβ) <sup>b</sup>	...	36.22	...	...	12.97	...	...	2.76	...	...	1.68	...
EW(abs) Å	...	3.45	...	...	0.75	...	...	0.45	...	...	3.20	...

TABLE 3—Continued

Ion	GALAXY											
	Mrk 94			HS 0837+4717			SBS 0911+472			SBS 0926+606A		
	$F(\lambda)/F(H\beta)$	$I(\lambda)/I(H\beta)$	EW <sup>a</sup>	$F(\lambda)/F(H\beta)$	$I(\lambda)/I(H\beta)$	EW <sup>a</sup>	$F(\lambda)/F(H\beta)$	$I(\lambda)/I(H\beta)$	EW <sup>a</sup>	$F(\lambda)/F(H\beta)$	$I(\lambda)/I(H\beta)$	EW <sup>a</sup>
3188 He I	...	...	...	3.37 ± 0.23	3.99 ± 0.27	2.4	3.14 ± 0.32	3.90 ± 0.40	1.4	...	...	...
3203 He II	...	...	...	0.59 ± 0.16	0.70 ± 0.20	0.4	...	...	...	...	...	...
3346 [Ne V]	...	...	...	0.26 ± 0.08	0.30 ± 0.10	0.2	...	...	...	...	...	...
3425 [Ne V]	...	...	...	0.41 ± 0.11	0.47 ± 0.13	0.3	...	...	...	...	...	...
3554 He I	0.33 ± 0.14	0.36 ± 0.15	0.4	0.26 ± 0.10	0.29 ± 0.12	0.2	...	...	...	...	...	...
3587 He I	0.32 ± 0.16	0.35 ± 0.17	0.4	0.26 ± 0.08	0.30 ± 0.09	0.2	...	...	...	...	...	...
3614 He I	...	...	...	0.42 ± 0.09	0.47 ± 0.10	0.4	...	...	...	...	...	...
3634 He I	...	...	...	0.37 ± 0.10	0.42 ± 0.11	0.4	...	...	...	...	...	...
3687 H19	...	...	...	...	...	...	...	...	...	...	...	...
3692 H18	0.65 ± 0.09	2.13 ± 0.67	1.1	0.65 ± 0.05	1.68 ± 0.52	0.8	0.63 ± 0.10	2.26 ± 1.81	0.4	0.62 ± 0.13	1.65 ± 1.94	0.5
3697 H17	0.62 ± 0.09	2.14 ± 0.71	1.1	0.84 ± 0.06	1.87 ± 0.44	1.0	0.70 ± 0.10	2.33 ± 1.65	0.5	0.76 ± 0.13	1.79 ± 1.62	0.6
3704 H16	1.50 ± 0.10	3.01 ± 0.37	2.7	1.84 ± 0.08	2.98 ± 0.33	2.3	1.27 ± 0.13	2.96 ± 1.19	0.9	1.27 ± 0.13	2.31 ± 1.01	1.0
3712 H15	1.27 ± 0.10	2.75 ± 0.43	2.3	1.38 ± 0.07	2.48 ± 0.36	1.7	1.27 ± 0.13	2.96 ± 1.19	0.9	1.20 ± 0.14	2.22 ± 1.11	0.9
3722 H14	1.22 ± 0.10	2.62 ± 0.40	2.3	1.43 ± 0.07	2.52 ± 0.36	1.8	1.40 ± 0.13	3.11 ± 1.11	0.9	1.48 ± 0.13	2.50 ± 0.86	1.1
3727 [O III]	119.82 ± 1.74	128.06 ± 1.97	218.8	46.44 ± 0.68	51.60 ± 0.80	58.8	170.87 ± 2.48	195.10 ± 3.02	115.1	155.08 ± 2.26	162.57 ± 2.51	117.2
3750 H12	2.81 ± 0.11	4.27 ± 0.22	5.5	2.50 ± 0.08	3.67 ± 0.15	3.2	2.17 ± 0.12	4.02 ± 0.28	1.5	2.68 ± 0.15	3.77 ± 0.26	2.0
3771 H11	3.39 ± 0.12	4.90 ± 0.21	6.6	3.29 ± 0.10	4.51 ± 0.17	4.4	2.86 ± 0.14	4.75 ± 0.29	1.9	3.15 ± 0.16	4.26 ± 0.26	2.4
3798 H10	4.65 ± 0.13	6.28 ± 0.22	8.7	4.63 ± 0.11	5.96 ± 0.17	6.2	3.82 ± 0.14	5.83 ± 0.27	2.6	4.23 ± 0.16	5.40 ± 0.25	3.2
3820 He I	0.78 ± 0.09	0.83 ± 0.09	1.5	0.98 ± 0.07	1.08 ± 0.08	1.3	...	...	...	0.79 ± 0.14	0.82 ± 0.14	0.6
3835 H9	6.47 ± 0.15	8.14 ± 0.22	12.6	6.00 ± 0.12	7.44 ± 0.18	8.2	5.70 ± 0.16	7.88 ± 0.27	3.9	5.97 ± 0.16	7.18 ± 0.24	4.6
3868 [Ne III]	42.62 ± 0.63	45.08 ± 0.70	80.7	46.09 ± 0.67	50.43 ± 0.77	65.6	39.39 ± 0.60	44.09 ± 0.70	24.0	38.81 ± 0.59	40.39 ± 0.65	26.9
3889 He I + H8	17.82 ± 0.29	20.09 ± 0.35	35.0	17.05 ± 0.27	19.43 ± 0.33	24.1	16.94 ± 0.29	20.34 ± 0.39	11.9	18.23 ± 0.31	19.88 ± 0.37	14.2
3968 [Ne III] + H7	27.60 ± 0.42	30.23 ± 0.49	55.0	28.65 ± 0.43	31.80 ± 0.50	42.0	24.89 ± 0.40	28.92 ± 0.50	17.3	26.58 ± 0.42	28.43 ± 0.48	21.3
4026 He I	1.72 ± 0.08	1.80 ± 0.08	3.5	1.76 ± 0.07	1.90 ± 0.08	2.6	1.18 ± 0.10	1.30 ± 0.12	0.8	1.14 ± 0.10	1.18 ± 0.10	0.9
4068 [S II]	1.01 ± 0.06	1.06 ± 0.07	2.1	1.06 ± 0.06	1.14 ± 0.06	1.6	1.76 ± 0.12	1.92 ± 0.13	1.2	1.69 ± 0.11	1.74 ± 0.12	1.3
4076 [S II]	0.48 ± 0.06	0.50 ± 0.06	1.0	...	...	...	0.42 ± 0.10	0.46 ± 0.11	0.3	0.58 ± 0.10	0.60 ± 0.10	0.4
4101 Hδ	23.57 ± 0.36	25.69 ± 0.41	49.4	23.93 ± 0.36	26.28 ± 0.41	37.4	22.56 ± 0.35	25.81 ± 0.44	16.5	24.50 ± 0.39	26.04 ± 0.44	20.8
4121 He I	...	...	...	0.27 ± 0.04	0.29 ± 0.05	0.4	...	...	...	...	...	...
4143 He I	...	...	...	0.40 ± 0.04	0.42 ± 0.05	0.6	...	...	...	...	...	...
4227 [Fe V]	...	...	...	0.58 ± 0.06	0.61 ± 0.07	1.0	...	...	...	...	...	...
4287 [Fe II]	...	...	...	0.28 ± 0.05	0.30 ± 0.05	0.5	...	...	...	...	...	...
4340 Hγ	44.96 ± 0.66	47.05 ± 0.71	108.0	44.92 ± 0.65	47.46 ± 0.70	82.3	43.53 ± 0.65	46.97 ± 0.72	35.8	45.54 ± 0.68	47.05 ± 0.72	43.0
4363 [O III]	7.61 ± 0.14	7.78 ± 0.15	18.5	16.70 ± 0.26	17.39 ± 0.27	30.7	6.66 ± 0.15	6.99 ± 0.16	5.3	6.80 ± 0.15	6.90 ± 0.16	6.1
4387 He I	0.41 ± 0.08	0.42 ± 0.08	1.0	0.57 ± 0.08	0.60 ± 0.09	1.1	...	...	...	...	...	...
4415 [Fe II]	...	...	...	0.34 ± 0.05	0.35 ± 0.05	0.6	...	...	...	...	...	...
4471 He I	3.92 ± 0.09	3.99 ± 0.09	10.2	4.08 ± 0.09	4.21 ± 0.10	8.1	3.44 ± 0.12	3.56 ± 0.12	2.8	3.95 ± 0.13	3.99 ± 0.13	3.9
4563 Si II	0.25 ± 0.05	0.25 ± 0.05	0.7	...	...	...	0.45 ± 0.07	0.46 ± 0.07	0.4	0.54 ± 0.08	0.54 ± 0.08	0.5
4571 Si II	0.29 ± 0.06	0.30 ± 0.06	0.8	...	...	...	0.26 ± 0.06	0.27 ± 0.06	0.2	0.25 ± 0.07	0.25 ± 0.07	0.2
4658 [Fe III]	0.40 ± 0.06	0.40 ± 0.06	1.1	0.72 ± 0.05	0.73 ± 0.05	1.6	1.10 ± 0.09	1.11 ± 0.09	0.9	1.32 ± 0.09	1.32 ± 0.09	1.3
4686 He II	0.84 ± 0.06	0.84 ± 0.06	2.2	1.97 ± 0.07	1.99 ± 0.07	4.3	1.19 ± 0.09	1.20 ± 0.09	1.0	1.18 ± 0.09	1.18 ± 0.09	1.2
4702 [Fe III]	...	...	...	0.19 ± 0.04	0.19 ± 0.04	0.4	...	...	...	...	...	...
4711 [Ar IV] + He I	1.16 ± 0.06	1.16 ± 0.06	3.2	2.17 ± 0.07	2.19 ± 0.07	4.8	0.98 ± 0.08	0.99 ± 0.08	0.9	0.75 ± 0.08	0.75 ± 0.08	0.8
4740 [Ar IV]	0.70 ± 0.06	0.70 ± 0.06	2.0	1.28 ± 0.06	1.29 ± 0.06	2.9	0.53 ± 0.08	0.53 ± 0.08	0.5	0.50 ± 0.09	0.50 ± 0.09	0.5
4861 Hβ	100.00 ± 1.44	100.00 ± 1.46	296.3	100.00 ± 1.43	100.00 ± 1.45	235.0	100.00 ± 1.45	100.00 ± 1.48	98.0	100.00 ± 1.45	100.00 ± 1.47	115.6
4881 [Fe II]	...	...	...	0.46 ± 0.04	0.45 ± 0.04	1.1	0.49 ± 0.08	0.49 ± 0.08	0.5	0.43 ± 0.09	0.43 ± 0.09	0.5
4907 [Fe IV]	...	...	...	0.44 ± 0.05	0.43 ± 0.05	1.0	...	...	...	...	...	...
4921 He I	1.11 ± 0.07	1.09 ± 0.07	3.3	1.15 ± 0.06	1.14 ± 0.06	2.7	1.13 ± 0.10	1.11 ± 0.10	1.1	0.64 ± 0.08	0.63 ± 0.08	0.7
4959 [O III]	203.98 ± 2.92	201.26 ± 2.91	605.4	189.08 ± 2.70	186.71 ± 2.69	442.7	180.09 ± 2.60	176.58 ± 2.58	173.6	165.36 ± 2.37	163.71 ± 2.36	190.3
4988 [Fe III]	0.65 ± 0.07	0.64 ± 0.07	1.9	...	...	...	1.52 ± 0.13	1.48 ± 0.12	1.5	1.98 ± 0.10	1.96 ± 0.10	2.3
5007 [O III]	618.09 ± 8.83	608.22 ± 8.78	1869.0	567.25 ± 6.60	557.94 ± 6.54	1328.1	546.25 ± 7.86	532.90 ± 7.76	531.9	496.04 ± 7.13	490.17 ± 7.10	582.0
C(Hβ)	...	0.105	...	...	0.155	...	...	0.200	...	...	0.075	...
F(Hβ) <sup>b</sup>	...	4.27	...	...	3.68	...	...	2.97	...	...	2.90	...
EW(abs) Å	...	2.35	...	...	1.05	...	...	0.90	...	...	0.70	...

TABLE 3—Continued

Ion	GALAXY											
	I Zw 18NW			I Zw 18SE			I Zw 18C			SBS 0940+544		
	$F(\lambda)/F(H\beta)$	$I(\lambda)/I(H\beta)$	EW <sup>a</sup>	$F(\lambda)/F(H\beta)$	$I(\lambda)/I(H\beta)$	EW <sup>a</sup>	$F(\lambda)/F(H\beta)$	$I(\lambda)/I(H\beta)$	EW <sup>a</sup>	$F(\lambda)/F(H\beta)$	$I(\lambda)/I(H\beta)$	EW <sup>a</sup>
3692 H18	0.52 ± 0.11	1.75 ± 2.88	0.2	...	...	...	...	...	...	1.62 ± 0.24	1.87 ± 1.04	2.3
3697 H17	0.56 ± 0.09	1.78 ± 2.27	0.3	...	...	...	...	...	...	1.66 ± 0.24	1.91 ± 1.03	2.4
3704 H16	0.89 ± 0.10	2.12 ± 1.50	0.4	1.21 ± 0.19	2.55 ± 1.46	1.1	...	...	...	1.63 ± 0.24	1.88 ± 1.04	2.3
3712 H15	0.90 ± 0.09	2.12 ± 1.38	0.4	0.91 ± 0.16	2.20 ± 1.60	0.8	...	...	...	1.51 ± 0.24	1.74 ± 1.09	2.2
3722 H14	0.92 ± 0.10	2.14 ± 1.45	0.4	1.04 ± 0.17	2.35 ± 1.49	0.9	...	...	...	1.66 ± 0.24	1.91 ± 1.01	2.4
3727 [O II]	36.20 ± 0.55	37.66 ± 0.61	17.5	45.39 ± 0.72	53.63 ± 0.90	41.0	113.81 ± 31.99	113.81 ± 32.70	5.6	47.05 ± 0.83	54.02 ± 0.99	64.8
3750 H12	2.26 ± 0.12	3.51 ± 0.22	1.1	2.17 ± 0.20	3.67 ± 0.40	1.9	...	...	...	2.72 ± 0.24	3.12 ± 0.40	3.7
3771 H11	2.69 ± 0.11	3.95 ± 0.20	1.3	2.69 ± 0.15	4.26 ± 0.31	2.4	...	...	...	3.16 ± 0.25	3.61 ± 0.41	4.3
3798 H10	3.71 ± 0.12	5.02 ± 0.20	1.8	3.61 ± 0.16	5.33 ± 0.31	3.2	...	...	...	4.61 ± 0.25	5.24 ± 0.40	6.5
3820 He I	...	...	...	...	...	...	...	...	...	1.09 ± 0.20	1.23 ± 0.23	1.5
3835 H9	5.75 ± 0.14	7.11 ± 0.20	2.8	5.36 ± 0.18	7.34 ± 0.32	4.7	...	...	...	6.72 ± 0.27	7.60 ± 0.42	9.1
3868 [Ne III]	16.62 ± 0.27	17.18 ± 0.29	7.4	11.98 ± 0.25	13.82 ± 0.30	9.2	...	...	...	31.55 ± 0.56	35.54 ± 0.66	42.5
3889 He I + H8	18.28 ± 0.29	20.02 ± 0.35	9.0	16.24 ± 0.30	19.79 ± 0.42	14.1	...	...	...	18.50 ± 0.38	20.78 ± 0.51	27.0
3968 [Ne III] + H7	18.94 ± 0.30	20.63 ± 0.36	9.4	16.87 ± 0.30	20.21 ± 0.42	15.1	...	...	...	24.87 ± 0.48	27.64 ± 0.60	36.2
4026 He I	1.01 ± 0.09	1.03 ± 0.09	0.5	1.43 ± 0.13	1.60 ± 0.14	1.2	...	...	...	1.31 ± 0.18	1.45 ± 0.19	1.9
4068 [S II]	0.37 ± 0.08	0.38 ± 0.08	0.2	0.63 ± 0.12	0.70 ± 0.14	0.5	...	...	...	...	...	...
4076 [S II]	...	...	...	0.37 ± 0.14	0.41 ± 0.16	0.3	...	...	...	...	...	...
4101 Hδ	24.94 ± 0.37	26.52 ± 0.42	13.9	22.78 ± 0.37	26.26 ± 0.47	21.9	...	...	...	24.47 ± 0.43	26.73 ± 0.53	39.2
4227 [Fe V]	0.18 ± 0.07	0.18 ± 0.07	0.1	...	...	...	...	...	...	...	...	...
4340 Hγ	46.04 ± 0.67	47.53 ± 0.71	28.8	43.42 ± 0.65	47.33 ± 0.74	44.2	...	...	...	44.62 ± 0.70	47.32 ± 0.78	76.9
4363 [O III]	6.66 ± 0.13	6.74 ± 0.14	4.0	4.47 ± 0.13	4.77 ± 0.14	4.2	...	...	...	11.61 ± 0.28	12.28 ± 0.30	19.9
4471 He I	2.73 ± 0.08	2.76 ± 0.08	1.8	2.80 ± 0.11	2.94 ± 0.11	2.8	...	...	...	3.45 ± 0.17	3.60 ± 0.18	6.3
4658 [Fe III]	0.45 ± 0.07	0.45 ± 0.07	0.3	0.62 ± 0.12	0.64 ± 0.13	0.7	...	...	...	0.33 ± 0.13	0.34 ± 0.13	0.6
4686 He II	3.44 ± 0.09	3.44 ± 0.09	2.5	0.58 ± 0.13	0.59 ± 0.13	0.6	...	...	...	0.21 ± 0.09	0.21 ± 0.09	0.4
4711 [Ar IV] + He I	0.76 ± 0.07	0.76 ± 0.07	0.6	0.62 ± 0.12	0.63 ± 0.12	0.7	...	...	...	2.00 ± 0.16	2.03 ± 0.16	3.9
4740 [Ar IV]	0.38 ± 0.06	0.38 ± 0.06	0.3	...	...	...	...	...	...	1.14 ± 0.17	1.16 ± 0.17	2.3
4861 Hβ	100.00 ± 1.43	100.00 ± 1.45	81.2	100.00 ± 1.45	100.00 ± 1.47	123.6	100.00 ± 17.71	100.00 ± 17.71	6.7	100.00 ± 1.49	100.00 ± 1.51	206.8
4921 He I	0.67 ± 0.06	0.67 ± 0.06	0.6	1.05 ± 0.10	1.03 ± 0.10	1.3	...	...	...	0.81 ± 0.15	0.80 ± 0.15	1.7
4959 [O III]	67.84 ± 0.98	67.15 ± 0.97	56.7	57.99 ± 0.86	56.85 ± 0.85	70.7	...	...	...	135.67 ± 2.01	134.29 ± 1.99	274.1
4988 [Fe III]	0.75 ± 0.08	0.74 ± 0.08	0.6	1.08 ± 0.10	1.06 ± 0.10	1.4	...	...	...	0.67 ± 0.16	0.66 ± 0.16	1.3
5007 [O III]	203.01 ± 2.90	200.62 ± 2.89	175.4	173.23 ± 2.50	168.79 ± 2.47	212.5	36.80 ± 11.88	36.80 ± 11.88	2.5	404.31 ± 5.91	398.20 ± 5.84	863.4
5015 He I	1.88 ± 0.07	1.86 ± 0.07	1.6	2.11 ± 0.10	2.05 ± 0.10	2.6	...	...	...	1.45 ± 0.19	1.43 ± 0.19	2.4
C(Hβ)	...	0.065	...	...	0.245	...	...	...	...	0.000	0.195	...
F(Hβ) <sup>b</sup>	...	3.19	...	...	1.51	...	...	...	...	0.01	1.07	...
EW(abs) Å	...	0.55	...	...	0.85	...	...	...	...	0.00	0.00	...

TABLE 3—Continued

Ion	GALAXY											
	SBS 1030+583			Mrk 35 (#1)			Mrk 35 (#2)			Mrk 178 (#1)		
	$F(\lambda)/F(H\beta)$	$I(\lambda)/I(H\beta)$	EW <sup>a</sup>	$F(\lambda)/F(H\beta)$	$I(\lambda)/I(H\beta)$	EW <sup>a</sup>	$F(\lambda)/F(H\beta)$	$I(\lambda)/I(H\beta)$	EW <sup>a</sup>	$F(\lambda)/F(H\beta)$	$I(\lambda)/I(H\beta)$	EW <sup>a</sup>
3634 He I	...	...	...	0.33 ± 0.09	0.36 ± 0.10	0.2	...	...	...	...	...	...
3692 H18	...	...	...	0.38 ± 0.04	2.00 ± 0.87	0.3	...	...	...	...	...	...
3697 H17	0.78 ± 0.18	3.19 ± 3.16	0.4	0.46 ± 0.04	2.07 ± 0.73	0.4	...	...	...	...	...	...
3704 H16	0.90 ± 0.19	3.26 ± 2.86	0.4	1.40 ± 0.09	3.00 ± 0.59	1.3	...	...	...	...	...	...
3712 H15	1.36 ± 0.20	3.67 ± 2.06	0.7	1.46 ± 0.09	3.06 ± 0.53	1.4	...	...	...	...	...	...
3722 H14	1.68 ± 0.19	4.00 ± 1.63	0.9	...	...	...	...	...	...	...	...	...
3727 [O II]	92.12 ± 1.39	93.81 ± 1.51	47.1	170.54 ± 2.45	187.39 ± 2.86	160.2	319.92 ± 5.16	307.18 ± 5.47	88.2	113.98 ± 1.98	114.48 ± 2.14	16.4
3750 H12	1.98 ± 0.21	4.31 ± 0.56	1.0	2.30 ± 0.10	3.95 ± 0.21	2.2	...	...	...	...	...	...
3771 H11	2.59 ± 0.20	4.95 ± 0.47	1.3	2.53 ± 0.10	4.24 ± 0.20	2.4	...	...	...	...	...	...
3798 H10	4.07 ± 0.22	6.45 ± 0.42	2.0	3.47 ± 0.10	5.23 ± 0.19	3.3	...	...	...	...	...	...
3820 He I	0.88 ± 0.19	0.89 ± 0.20	0.4	1.21 ± 0.09	1.32 ± 0.10	1.1	...	...	...	...	...	...
3835 H9	5.70 ± 0.21	8.05 ± 0.37	2.9	5.51 ± 0.13	7.40 ± 0.20	5.3	3.91 ± 0.52	8.10 ± 1.33	1.1	...	...	...
3868 [Ne III]	39.76 ± 0.63	40.30 ± 0.67	18.8	24.34 ± 0.38	26.36 ± 0.43	22.8	19.56 ± 0.69	18.78 ± 0.69	3.8	45.18 ± 0.95	45.18 ± 1.00	6.1
3889 He I + H8	18.04 ± 0.34	20.51 ± 0.44	9.4	16.10 ± 0.26	18.81 ± 0.33	15.5	15.92 ± 0.60	19.84 ± 0.95	4.2	14.83 ± 0.59	19.70 ± 1.03	2.3
3968 [Ne III] + H7	25.40 ± 0.43	27.87 ± 0.53	13.4	19.80 ± 0.31	22.57 ± 0.37	19.8	13.51 ± 0.59	17.45 ± 0.96	3.6	23.52 ± 0.71	28.07 ± 1.06	3.8
4026 He I	1.02 ± 0.18	1.03 ± 0.18	0.5	1.73 ± 0.09	1.84 ± 0.10	1.7	...	...	...	...	...	...
4068 [S II]	0.98 ± 0.14	0.99 ± 0.15	0.5	1.26 ± 0.08	1.33 ± 0.09	1.2	3.46 ± 0.47	3.32 ± 0.47	0.7	1.50 ± 0.40	1.49 ± 0.41	0.2
4076 [S II]	...	...	...	0.34 ± 0.06	0.36 ± 0.06	0.3	...	...	...	...	...	...
4101 Hδ	23.81 ± 0.40	25.97 ± 0.48	13.8	23.15 ± 0.35	25.78 ± 0.41	24.2	21.32 ± 0.61	25.15 ± 0.94	5.5	21.15 ± 0.59	25.23 ± 0.91	3.7
4340 Hγ	45.56 ± 0.69	47.34 ± 0.75	29.3	44.00 ± 0.64	46.70 ± 0.70	50.8	44.30 ± 0.88	47.02 ± 1.11	11.9	44.10 ± 0.82	47.21 ± 1.02	8.8
4363 [O III]	10.60 ± 0.24	10.59 ± 0.25	6.8	2.57 ± 0.09	2.65 ± 0.09	3.0	...	...	...	10.66 ± 0.40	10.51 ± 0.41	2.0
4387 He I	...	...	...	0.48 ± 0.06	0.49 ± 0.06	0.6	...	...	...	...	...	...
4471 He I	3.21 ± 0.16	3.19 ± 0.17	2.2	3.85 ± 0.09	3.94 ± 0.10	4.8	2.96 ± 0.38	2.84 ± 0.38	0.7	1.75 ± 0.28	1.72 ± 0.28	0.4
4563 Si II	0.33 ± 0.10	0.33 ± 0.10	0.2	...	...	...	...	...	...	...	...	...
4571 Si II	0.20 ± 0.12	0.20 ± 0.12	0.1	...	...	...	...	...	...	...	...	...
4658 [Fe III]	0.94 ± 0.14	0.93 ± 0.14	0.7	1.09 ± 0.07	1.10 ± 0.07	1.4	...	...	...	...	...	...
4686 He II	2.74 ± 0.16	2.71 ± 0.16	2.0	...	...	...	...	...	...	6.09 ± 0.44	5.95 ± 0.44	1.3
4711 [Ar IV] + He I	1.18 ± 0.13	1.17 ± 0.13	0.9	0.68 ± 0.06	0.68 ± 0.06	0.9	...	...	...	1.68 ± 0.41	1.64 ± 0.41	0.4
4740 [Ar IV]	...	...	...	...	...	...	...	...	...	0.76 ± 0.29	0.74 ± 0.29	0.2
4861 Hβ	100.00 ± 1.46	100.00 ± 1.49	82.8	100.00 ± 1.44	100.00 ± 1.45	145.8	100.00 ± 1.68	100.00 ± 1.81	30.1	100.00 ± 1.63	100.00 ± 1.71	26.9
4881 [Fe II]	0.44 ± 0.13	0.43 ± 0.13	0.4	0.35 ± 0.05	0.35 ± 0.05	0.5	...	...	...	...	...	...
4921 He I	0.59 ± 0.14	0.58 ± 0.14	0.5	1.04 ± 0.06	1.03 ± 0.06	1.5	...	...	...	...	...	...
4959 [O III]	175.54 ± 2.55	172.73 ± 2.55	143.2	136.92 ± 1.96	134.72 ± 1.95	201.4	90.03 ± 1.55	86.44 ± 1.55	24.2	195.53 ± 3.07	189.77 ± 3.06	51.6
4988 [Fe III]	1.68 ± 0.20	1.65 ± 0.20	1.4	1.07 ± 0.06	1.05 ± 0.06	1.5	2.72 ± 0.37	2.61 ± 0.37	0.7	...	...	...
5007 [O III]	526.08 ± 7.59	517.05 ± 7.57	437.8	414.21 ± 5.91	406.07 ± 5.86	632.8	266.63 ± 4.24	256.01 ± 4.24	72.4	585.05 ± 8.99	567.17 ± 8.97	157.3
C(Hβ)	...	0.045	...	...	0.145	...	...	0.000	...	...	0.045	...
F(Hβ) <sup>b</sup>	...	2.90	...	...	5.19	...	...	0.58	...	...	1.03	...
EW(abs) Å	...	1.15	...	...	1.25	...	...	1.25	...	...	0.75	...

TABLE 3—Continued

Ion	GALAXY											
	Mrk 178 (#2)			Mrk 178 (#3)			SBS 1152+579			Mrk 209		
	$F(\lambda)/F(H\beta)$	$I(\lambda)/I(H\beta)$	EW <sup>a</sup>	$F(\lambda)/F(H\beta)$	$I(\lambda)/I(H\beta)$	EW <sup>a</sup>	$F(\lambda)/F(H\beta)$	$I(\lambda)/I(H\beta)$	EW <sup>a</sup>	$F(\lambda)/F(H\beta)$	$I(\lambda)/I(H\beta)$	EW <sup>a</sup>
3188 He I	...	...	...	...	...	...	4.46 ± 0.51	5.41 ± 0.63	3.1	...	...	...
3425 [Ne V]	...	...	...	...	...	...	...	...	...	0.25 ± 0.06	0.27 ± 0.06	0.2
3587 He I	...	...	...	...	...	...	...	...	...	0.24 ± 0.05	0.25 ± 0.05	0.2
3614 He I	...	...	...	...	...	...	...	...	...	0.46 ± 0.08	0.49 ± 0.08	0.5
3634 He I	...	...	...	...	...	...	...	...	...	0.24 ± 0.05	0.25 ± 0.05	0.2
3687 H19	...	...	...	...	...	...	...	...	...	0.34 ± 0.04	2.35 ± 0.66	0.5
3692 H18	...	...	...	...	...	...	0.58 ± 0.13	2.08 ± 1.52	0.7	0.41 ± 0.04	2.42 ± 0.59	0.6
3697 H17	...	...	...	...	...	...	0.79 ± 0.14	2.33 ± 1.21	0.9	0.39 ± 0.04	2.42 ± 0.61	0.5
3704 H16	...	...	...	...	...	...	1.30 ± 0.15	2.86 ± 0.88	1.5	1.05 ± 0.05	3.03 ± 0.28	1.4
3712 H15	...	...	...	...	...	...	1.38 ± 0.16	2.95 ± 0.89	1.6	1.04 ± 0.05	2.95 ± 0.29	1.5
3722 H14	...	...	...	...	...	...	1.65 ± 0.16	3.27 ± 0.76	1.9	1.44 ± 0.05	3.30 ± 0.23	2.1
3727 [O II]	99.16 ± 2.26	96.43 ± 2.35	15.5	329.65 ± 17.03	329.65 ± 18.39	16.0	75.29 ± 1.13	84.81 ± 1.35	87.2	58.15 ± 0.83	61.26 ± 0.94	85.4
3750 H12	...	...	...	...	...	...	2.38 ± 0.14	4.07 ± 0.29	2.8	2.59 ± 0.07	4.43 ± 0.14	4.0
3771 H11	...	...	...	...	...	...	3.04 ± 0.14	4.82 ± 0.27	3.5	3.02 ± 0.07	4.90 ± 0.13	4.6
3798 H10	...	...	...	...	...	...	4.29 ± 0.14	6.18 ± 0.26	5.0	4.25 ± 0.08	6.21 ± 0.14	6.3
3820 He I	...	...	...	...	...	...	1.07 ± 0.15	1.19 ± 0.17	1.2	0.94 ± 0.06	0.98 ± 0.06	1.4
3835 H9	...	...	...	...	...	...	6.08 ± 0.16	8.09 ± 0.26	7.4	6.10 ± 0.11	8.11 ± 0.16	9.2
3868 [Ne III]	54.94 ± 1.49	53.42 ± 1.52	6.6	56.49 ± 6.37	56.49 ± 6.45	1.6	45.64 ± 0.69	50.50 ± 0.80	48.2	42.83 ± 0.61	44.72 ± 0.68	59.6
3889 He I + H8	21.43 ± 1.06	23.44 ± 1.40	3.2	...	...	...	15.81 ± 0.28	18.80 ± 0.37	18.6	17.64 ± 0.26	20.19 ± 0.32	25.6
3968 [Ne III] + H7	25.55 ± 1.06	27.23 ± 1.34	4.2	...	...	...	28.53 ± 0.45	32.46 ± 0.55	35.6	27.28 ± 0.40	30.02 ± 0.46	41.5
4026 He I	...	...	...	...	...	...	1.56 ± 0.11	1.69 ± 0.12	1.8	1.48 ± 0.05	1.53 ± 0.05	2.2
4068 [S II]	...	...	...	...	...	...	1.10 ± 0.10	1.19 ± 0.11	1.3	0.65 ± 0.04	0.67 ± 0.04	1.0
4076 [S II]	...	...	...	...	...	...	...	...	...	0.16 ± 0.03	0.16 ± 0.03	0.2
4101 Hδ	24.51 ± 0.87	26.78 ± 1.28	3.2	...	...	...	22.96 ± 0.36	25.94 ± 0.44	29.0	23.65 ± 0.34	25.97 ± 0.39	37.5
4121 He I	...	...	...	...	...	...	...	...	...	0.18 ± 0.04	0.19 ± 0.04	0.3
4143 He I	...	...	...	...	...	...	...	...	...	0.25 ± 0.04	0.25 ± 0.04	0.4
4227 [Fe V]	...	...	...	...	...	...	...	...	...	0.11 ± 0.03	0.12 ± 0.03	0.2
4340 Hγ	45.70 ± 1.11	47.38 ± 1.44	6.1	...	...	...	44.11 ± 0.66	47.22 ± 0.73	64.6	45.12 ± 0.64	47.30 ± 0.69	77.6
4363 [O III]	15.76 ± 0.79	15.33 ± 0.79	1.9	...	...	...	12.92 ± 0.23	13.49 ± 0.24	18.4	12.39 ± 0.19	12.56 ± 0.19	21.5
4387 He I	...	...	...	...	...	...	0.42 ± 0.09	0.44 ± 0.10	0.6	0.40 ± 0.04	0.40 ± 0.05	0.7
4471 He I	4.69 ± 0.70	4.56 ± 0.70	0.6	...	...	...	3.72 ± 0.12	3.84 ± 0.12	5.4	3.50 ± 0.07	3.53 ± 0.07	6.4
4563 Si II	...	...	...	...	...	...	...	...	...	0.30 ± 0.04	0.30 ± 0.04	0.6
4571 Si II	...	...	...	...	...	...	...	...	...	0.11 ± 0.03	0.11 ± 0.03	0.2
4658 [Fe III]	...	...	...	...	...	...	0.64 ± 0.09	0.64 ± 0.09	1.0	0.23 ± 0.03	0.23 ± 0.03	0.4
4686 He II	7.59 ± 0.73	7.38 ± 0.73	0.9	...	...	...	0.97 ± 0.10	0.98 ± 0.10	1.5	1.12 ± 0.04	1.12 ± 0.04	2.1
4711 [Ar IV] + He I	2.45 ± 0.60	2.38 ± 0.60	0.3	...	...	...	2.49 ± 0.11	2.51 ± 0.11	4.0	1.95 ± 0.05	1.94 ± 0.05	3.9
4740 [Ar IV]	...	...	...	...	...	...	1.71 ± 0.11	1.72 ± 0.11	2.9	1.21 ± 0.04	1.20 ± 0.04	2.5
4861 Hβ	100.00 ± 1.88	100.00 ± 2.08	14.1	100.00 ± 6.28	100.00 ± 6.28	4.9	100.00 ± 1.46	100.00 ± 1.48	169.0	100.00 ± 1.42	100.00 ± 1.44	212.0
4921 He I	...	...	...	...	...	...	0.77 ± 0.10	0.76 ± 0.10	1.3	0.94 ± 0.03	0.93 ± 0.03	2.0
4959 [O III]	222.96 ± 3.89	216.81 ± 3.89	27.9	139.78 ± 7.77	139.78 ± 7.77	5.8	223.23 ± 3.23	219.24 ± 3.20	385.0	200.85 ± 2.85	197.57 ± 2.84	429.7
4988 [Fe III]	...	...	...	...	...	...	1.15 ± 0.10	1.13 ± 0.10	1.9	0.57 ± 0.02	0.56 ± 0.02	1.2
5007 [O III]	661.25 ± 11.14	643.01 ± 11.15	82.1	395.67 ± 18.92	395.67 ± 18.94	17.1	676.22 ± 9.73	661.12 ± 9.62	1192.0	608.88 ± 8.64	597.57 ± 8.59	1466.0
5015 He I	...	...	...	...	...	...	...	...	...	1.46 ± 0.04	1.43 ± 0.04	2.1
C(Hβ)	...	0.000	...	...	0.000	...	...	...	...	...	0.090	...
F(Hβ) <sup>b</sup>	...	0.41	...	...	0.05	...	...	...	...	...	9.17	...
EW(abs) Å	...	0.40	...	...	0.00	...	...	...	...	...	2.50	...

TABLE 3—*Continued*

Ion	GALAXY								
	Mrk 59 (#1)			Mrk 59 (#2)			J 1404+5423		
	$F(\lambda)/F(H\beta)$	$I(\lambda)/I(H\beta)$	EW <sup>a</sup>	$F(\lambda)/F(H\beta)$	$I(\lambda)/I(H\beta)$	EW <sup>a</sup>	$F(\lambda)/F(H\beta)$	$I(\lambda)/I(H\beta)$	EW <sup>a</sup>
3531 He I	0.19 ± 0.04	0.19 ± 0.04	0.1	...	...	...	...	...	...
3587 He I	0.21 ± 0.05	0.21 ± 0.05	0.1	...	...	...	...	...	...
3614 He I	0.37 ± 0.05	0.38 ± 0.05	0.2	...	...	...	0.37 ± 0.08	0.39 ± 0.08	0.3
3634 He I	0.26 ± 0.04	0.26 ± 0.04	0.2	...	...	...	0.39 ± 0.06	0.41 ± 0.07	0.3
3683 H20	0.46 ± 0.04	1.88 ± 0.80	0.3	...	...	...	...	...	...
3687 H19	0.48 ± 0.04	1.89 ± 0.78	0.3	...	...	...	...	...	...
3692 H18	0.61 ± 0.04	2.02 ± 0.64	0.4	...	...	...	0.24 ± 0.05	1.13 ± 1.18	0.3
3697 H17	0.67 ± 0.04	2.07 ± 0.60	0.5	...	...	...	0.50 ± 0.05	1.36 ± 0.56	0.6
3704 H16	1.37 ± 0.05	2.75 ± 0.38	1.0	...	...	...	1.35 ± 0.06	2.21 ± 0.32	1.6
3712 H15	1.16 ± 0.05	2.54 ± 0.40	0.8	...	...	...	1.25 ± 0.06	2.09 ± 0.31	1.5
3722 H14	1.35 ± 0.05	2.72 ± 0.37	0.9	...	...	...	1.02 ± 0.05	1.82 ± 0.32	1.3
3727 [O II]	101.82 ± 1.45	102.86 ± 1.55	71.3	124.76 ± 2.38	124.76 ± 2.50	14.2	108.86 ± 1.55	114.35 ± 1.73	136.6
3750 H12	2.20 ± 0.05	3.56 ± 0.11	1.6	...	...	...	2.59 ± 0.07	3.44 ± 0.12	3.4
3771 H11	2.78 ± 0.06	4.14 ± 0.11	2.0	...	...	...	3.27 ± 0.08	4.16 ± 0.12	4.2
3798 H10	3.98 ± 0.07	5.34 ± 0.11	2.9	...	...	...	4.64 ± 0.09	5.59 ± 0.13	6.0
3820 He I	0.62 ± 0.04	0.63 ± 0.04	0.4	...	...	...	0.88 ± 0.05	0.92 ± 0.06	1.1
3835 H9	6.04 ± 0.10	7.42 ± 0.13	4.4	...	...	...	6.42 ± 0.11	7.44 ± 0.14	8.3
3868 [Ne III]	47.48 ± 0.68	47.85 ± 0.72	32.1	47.36 ± 1.18	47.36 ± 1.21	4.7	50.80 ± 0.73	52.96 ± 0.79	64.7
3889 He I + H8	18.42 ± 0.27	19.86 ± 0.30	13.6	14.76 ± 0.73	14.76 ± 1.11	1.8	18.38 ± 0.27	19.85 ± 0.31	24.5
3968 [Ne III] + H7	28.04 ± 0.40	29.47 ± 0.44	21.2	22.21 ± 0.89	22.21 ± 1.20	2.8	30.94 ± 0.45	32.76 ± 0.49	43.6
4026 He I	1.37 ± 0.04	1.37 ± 0.04	1.0	...	...	...	1.56 ± 0.05	1.61 ± 0.05	2.2
4068 [S II]	0.97 ± 0.04	0.97 ± 0.04	0.7	...	...	...	1.34 ± 0.05	1.38 ± 0.05	2.0
4076 [S II]	0.20 ± 0.03	0.20 ± 0.03	0.2	...	...	...	0.46 ± 0.04	0.47 ± 0.04	0.7
4101 Hδ	24.84 ± 0.36	26.09 ± 0.39	20.6	23.71 ± 0.77	23.71 ± 1.08	3.1	24.68 ± 0.36	26.03 ± 0.39	37.9
4121 He I	...	...	...	...	...	...	0.22 ± 0.04	0.23 ± 0.04	0.3
4143 He I	...	...	...	...	...	...	0.18 ± 0.03	0.18 ± 0.04	0.3
4340 Hγ	46.12 ± 0.66	47.12 ± 0.68	43.6	47.22 ± 1.02	47.22 ± 1.23	6.9	45.68 ± 0.65	47.07 ± 0.69	79.2
4363 [O III]	9.11 ± 0.14	9.11 ± 0.14	8.6	10.40 ± 0.57	10.40 ± 0.57	1.4	9.53 ± 0.15	9.70 ± 0.15	16.7
4387 He I	0.33 ± 0.03	0.33 ± 0.03	0.3	...	...	...	0.42 ± 0.04	0.43 ± 0.04	0.8
4471 He I	3.52 ± 0.06	3.52 ± 0.06	3.6	...	...	...	3.73 ± 0.07	3.78 ± 0.07	7.1
4563 Si II	0.28 ± 0.03	0.27 ± 0.03	0.3	...	...	...	0.25 ± 0.04	0.25 ± 0.04	0.5
4571 Si II	0.19 ± 0.03	0.19 ± 0.03	0.2	...	...	...	0.20 ± 0.03	0.20 ± 0.03	0.4
4658 [Fe III]	0.62 ± 0.03	0.62 ± 0.03	0.7	1.07 ± 0.31	1.07 ± 0.31	0.2	0.70 ± 0.04	0.70 ± 0.04	1.4
4686 He II	0.84 ± 0.03	0.83 ± 0.03	0.9	1.39 ± 0.41	1.39 ± 0.41	0.2	0.71 ± 0.04	0.71 ± 0.04	1.5
4702 [Fe III]	...	...	...	...	...	...	0.23 ± 0.03	0.23 ± 0.03	0.5
4711 [Ar IV] + He I	1.15 ± 0.04	1.14 ± 0.04	1.3	...	...	...	1.38 ± 0.04	1.39 ± 0.04	2.9
4740 [Ar IV]	0.59 ± 0.03	0.59 ± 0.03	0.7	...	...	...	0.82 ± 0.04	0.82 ± 0.04	1.8
4755 [Fe III]	...	...	...	...	...	...	0.26 ± 0.05	0.26 ± 0.05	0.6
4861 Hβ	100.00 ± 1.42	100.00 ± 1.43	125.3	100.00 ± 1.79	100.00 ± 1.87	18.5	100.00 ± 1.42	100.00 ± 1.43	227.6
4881 [Fe II]	0.29 ± 0.03	0.29 ± 0.03	0.4	...	...	...	0.30 ± 0.03	0.30 ± 0.03	0.7
4921 He I	0.82 ± 0.03	0.82 ± 0.03	1.1	...	...	...	0.96 ± 0.04	0.96 ± 0.04	2.2
4959 [O III]	207.99 ± 2.95	206.16 ± 2.95	265.0	212.28 ± 3.57	212.28 ± 3.57	38.9	219.06 ± 3.11	217.34 ± 3.10	483.8
4988 [Fe III]	0.82 ± 0.03	0.82 ± 0.03	1.0	...	...	...	0.69 ± 0.03	0.68 ± 0.03	1.5
5007 [O III]	599.02 ± 7.33	593.36 ± 7.33	568.2	665.63 ± 10.85	665.63 ± 10.86	134.0	660.37 ± 9.37	653.93 ± 9.33	1678.0
5199 [N II]	...	...	...	...	...	...	0.28 ± 0.03	0.28 ± 0.03	0.8
C(Hβ)	0.025	...	...	0.000	...	...	0.075	...	...
F(Hβ) <sup>b</sup>	35.15	...	...	0.71	...	...	23.82	...	...
EW(abs) Å	0.95	...	...	0.00	...	...	0.90	...	...

TABLE 4  
IONIC AND TOTAL HEAVY ELEMENT ABUNDANCES

PROPERTY	GALAXY							
	SBS 0335-052W	SBS 0335-052E	J 0519+0007	II Zw 40	Mrk 71A	Mrk 71B	Mrk 71C	HS 0822+3542
$T_e(\text{O III})$ (K)	$19770 \pm 1330$	$20000 \pm 230$	$19260 \pm 240$	$13020 \pm 110$	$15680 \pm 140$	$14730 \pm 130$	$13900 \pm 160$	$18170 \pm 220$
$T_e(\text{O II})$ (K)	$15590 \pm 970$	$15610 \pm 170$	$15530 \pm 180$	$12670 \pm 100$	$14370 \pm 120$	$13840 \pm 110$	$13310 \pm 150$	$15310 \pm 180$
$\text{O}^+/\text{H}^+$ ( $\times 10^4$ )	$0.056 \pm 0.009$	$0.020 \pm 0.001$	$0.025 \pm 0.001$	$0.108 \pm 0.003$	$0.044 \pm 0.001$	$0.083 \pm 0.002$	$0.175 \pm 0.006$	$0.031 \pm 0.001$
$\text{O}^{++}/\text{H}^+$ ( $\times 10^4$ )	$0.072 \pm 0.011$	$0.182 \pm 0.005$	$0.267 \pm 0.008$	$1.229 \pm 0.033$	$0.697 \pm 0.017$	$0.722 \pm 0.018$	$0.623 \pm 0.021$	$0.255 \pm 0.008$
$\text{O}^{+++}/\text{H}^+$ ( $\times 10^6$ )	...	$0.284 \pm 0.020$	$0.264 \pm 0.045$	$0.375 \pm 0.083$	$0.123 \pm 0.019$	$0.992 \pm 0.077$	$0.783 \pm 0.144$	...
$\text{O}/\text{H}$ ( $\times 10^4$ )	$0.128 \pm 0.014$	$0.204 \pm 0.005$	$0.294 \pm 0.008$	$1.340 \pm 0.033$	$0.742 \pm 0.017$	$0.816 \pm 0.018$	$0.805 \pm 0.022$	$0.286 \pm 0.008$
$12 + \log(\text{O}/\text{H})$	$7.109 \pm 0.048$	$7.311 \pm 0.011$	$7.469 \pm 0.012$	$8.127 \pm 0.011$	$7.871 \pm 0.010$	$7.911 \pm 0.010$	$7.906 \pm 0.012$	$7.457 \pm 0.012$
$\text{Ne}^{++}/\text{H}^+$ ( $\times 10^5$ )	$0.142 \pm 0.022$	$0.298 \pm 0.008$	$0.464 \pm 0.015$	$2.375 \pm 0.072$	$1.265 \pm 0.034$	$1.335 \pm 0.037$	$1.262 \pm 0.047$	$0.430 \pm 0.014$
ICF	1.187	1.047	1.039	0.992	1.003	1.038	1.124	1.046
$\log(\text{Ne}/\text{O})$	$-0.883 \pm 0.111$	$-0.817 \pm 0.017$	$-0.786 \pm 0.019$	$-0.755 \pm 0.018$	$-0.767 \pm 0.016$	$-0.770 \pm 0.016$	$-0.754 \pm 0.022$	$-0.803 \pm 0.020$
$\text{Fe}^{++}/\text{H}^+$ ( $\times 10^6$ )(4658)	...	$0.066 \pm 0.004$	$0.092 \pm 0.025$	$0.142 \pm 0.025$	$0.033 \pm 0.004$	$0.051 \pm 0.008$	$0.103 \pm 0.003$	$0.072 \pm 0.013$
$\text{Fe}^{++}/\text{H}^+$ ( $\times 10^6$ )(4988)	...	$0.109 \pm 0.005$	...	...	...	...	...	...
ICF	...	14.157	16.175	14.972	21.781	12.616	6.105	12.438
$\log(\text{Fe}/\text{O})$ (4658)	...	$-1.340 \pm 0.030$	$-1.298 \pm 0.121$	$-1.799 \pm 0.078$	$-2.018 \pm 0.059$	$-2.101 \pm 0.065$	$-2.110 \pm 0.017$	$-1.502 \pm 0.077$
$\log(\text{Fe}/\text{O})$ (4988)	...	$-1.121 \pm 0.022$	...	...	...	...	...	...

TABLE 4—*Continued*

PROPERTY	GALAXY							
	Mrk 94	HS 0837+4717	SBS 0911+472	SBS 0926+606A	I Zw 18NW	I Zw 18SE	SBS 0940+544	SBS 1030+583
$T_e(\text{O III})$ (K)	$12670 \pm 110$	$19110 \pm 200$	$12780 \pm 130$	$13130 \pm 130$	$19970 \pm 280$	$18070 \pm 320$	$18970 \pm 290$	$15400 \pm 190$
$T_e(\text{O II})$ (K)	$12400 \pm 100$	$15510 \pm 150$	$12490 \pm 120$	$12760 \pm 120$	$15610 \pm 200$	$15280 \pm 250$	$15480 \pm 220$	$14220 \pm 160$
$\text{O}^+/\text{H}^+$ ( $\times 10^4$ )	$0.220 \pm 0.006$	$0.042 \pm 0.001$	$0.326 \pm 0.011$	$0.251 \pm 0.008$	$0.030 \pm 0.001$	$0.046 \pm 0.002$	$0.044 \pm 0.002$	$0.101 \pm 0.004$
$\text{O}^{++}/\text{H}^+$ ( $\times 10^4$ )	$1.051 \pm 0.028$	$0.351 \pm 0.009$	$0.897 \pm 0.027$	$0.767 \pm 0.023$	$0.115 \pm 0.004$	$0.120 \pm 0.005$	$0.255 \pm 0.010$	$0.532 \pm 0.018$
$\text{O}^{+++}/\text{H}^+$ ( $\times 10^6$ )	$0.529 \pm 0.081$	$0.352 \pm 0.034$	$0.815 \pm 0.142$	$0.591 \pm 0.100$	$0.342 \pm 0.033$	$0.063 \pm 0.029$	$0.034 \pm 0.030$	$1.041 \pm 0.175$
$\text{O}/\text{H}$ ( $\times 10^4$ )	$1.276 \pm 0.029$	$0.397 \pm 0.009$	$1.231 \pm 0.029$	$1.024 \pm 0.025$	$0.149 \pm 0.004$	$0.167 \pm 0.006$	$0.300 \pm 0.010$	$0.644 \pm 0.018$
$12 + \log(\text{O}/\text{H})$	$8.106 \pm 0.010$	$7.599 \pm 0.010$	$8.090 \pm 0.010$	$8.010 \pm 0.011$	$7.172 \pm 0.012$	$7.222 \pm 0.015$	$7.477 \pm 0.014$	$7.808 \pm 0.012$
$\text{Ne}^{++}/\text{H}^+$ ( $\times 10^5$ )	$2.048 \pm 0.063$	$0.711 \pm 0.020$	$1.942 \pm 0.066$	$1.628 \pm 0.056$	$0.218 \pm 0.007$	$0.223 \pm 0.010$	$0.510 \pm 0.020$	$0.999 \pm 0.036$
ICF	1.095	1.048	1.207	1.163	1.096	1.118	1.063	1.078
$\log(\text{Ne}/\text{O})$	$-0.755 \pm 0.018$	$-0.726 \pm 0.016$	$-0.720 \pm 0.020$	$-0.733 \pm 0.020$	$-0.794 \pm 0.021$	$-0.824 \pm 0.029$	$-0.743 \pm 0.023$	$-0.777 \pm 0.021$
$\text{Fe}^{++}/\text{H}^+$ ( $\times 10^6$ )(4658)	$0.126 \pm 0.020$	$0.128 \pm 0.010$	$0.344 \pm 0.030$	$0.385 \pm 0.028$	$0.078 \pm 0.012$	$0.116 \pm 0.023$	$0.059 \pm 0.024$	$0.202 \pm 0.030$
$\text{Fe}^{++}/\text{H}^+$ ( $\times 10^6$ )(4988)	$0.204 \pm 0.024$	...	$0.460 \pm 0.040$	$0.571 \pm 0.031$	$0.128 \pm 0.014$	$0.192 \pm 0.019$	$0.116 \pm 0.028$	$0.359 \pm 0.044$
ICF	7.520	12.602	5.133	5.458	6.677	4.889	9.079	8.435
$\log(\text{Fe}/\text{O})$ (4658)	$-2.130 \pm 0.069$	$-1.391 \pm 0.034$	$-1.843 \pm 0.040$	$-1.688 \pm 0.034$	$-1.454 \pm 0.065$	$-1.469 \pm 0.089$	$-1.748 \pm 0.174$	$-1.578 \pm 0.066$
$\log(\text{Fe}/\text{O})$ (4988)	$-1.921 \pm 0.051$	...	$-1.718 \pm 0.039$	$-1.516 \pm 0.026$	$-1.240 \pm 0.050$	$-1.250 \pm 0.046$	$-1.452 \pm 0.104$	$-1.328 \pm 0.054$



TABLE 4—*Continued*

PROPERTY	GALAXY							
	Mrk 35 (#1)	Mrk 178 (#1)	Mrk 178 (#2)	SBS 1152+579	Mrk 209	Mrk 59 (#1)	Mrk 59 (#2)	J 1404+5423
$T_e(\text{O III})$ (K)	$10090 \pm 110$	$14710 \pm 270$	$16540 \pm 440$	$15390 \pm 150$	$15610 \pm 140$	$13540 \pm 100$	$13760 \pm 320$	$13410 \pm 100$
$T_e(\text{O II})$ (K)	$10050 \pm 110$	$13830 \pm 240$	$14760 \pm 370$	$14210 \pm 130$	$14330 \pm 120$	$13060 \pm 90$	$13210 \pm 290$	$12970 \pm 100$
$\text{O}^+/\text{H}^+$ ( $\times 10^4$ )	$0.736 \pm 0.032$	$0.134 \pm 0.007$	$0.092 \pm 0.006$	$0.091 \pm 0.003$	$0.064 \pm 0.002$	$0.147 \pm 0.004$	$0.171 \pm 0.012$	$0.167 \pm 0.004$
$\text{O}^{++}/\text{H}^+$ ( $\times 10^4$ )	$1.433 \pm 0.055$	$0.655 \pm 0.032$	$0.559 \pm 0.038$	$0.681 \pm 0.019$	$0.594 \pm 0.015$	$0.863 \pm 0.020$	$0.907 \pm 0.059$	$0.964 \pm 0.023$
$\text{O}^{+++}/\text{H}^+$ ( $\times 10^6$ )	$0.000 \pm 0.000$	$5.314 \pm 1.975$	$2.025 \pm 0.779$	$0.383 \pm 0.083$	$0.403 \pm 0.037$	$0.470 \pm 0.044$	$0.000 \pm 0.000$	$0.418 \pm 0.054$
$\text{O}/\text{H}$ ( $\times 10^4$ )	$2.169 \pm 0.063$	$0.843 \pm 0.039$	$0.671 \pm 0.039$	$0.776 \pm 0.019$	$0.662 \pm 0.015$	$1.014 \pm 0.020$	$1.078 \pm 0.060$	$1.135 \pm 0.024$
$12 + \log(\text{O}/\text{H})$	$8.336 \pm 0.013$	$7.926 \pm 0.020$	$7.827 \pm 0.025$	$7.890 \pm 0.011$	$7.821 \pm 0.010$	$8.006 \pm 0.009$	$8.032 \pm 0.024$	$8.055 \pm 0.009$
$\text{Ne}^{++}/\text{H}^+$ ( $\times 10^5$ )	$2.790 \pm 0.124$	$1.278 \pm 0.069$	$1.086 \pm 0.077$	$1.255 \pm 0.038$	$1.067 \pm 0.030$	$1.750 \pm 0.046$	$1.646 \pm 0.118$	$1.994 \pm 0.054$
ICF	1.363	1.122	1.075	1.044	1.034	1.064	1.073	1.066
$\log(\text{Ne}/\text{O})$	$-0.756 \pm 0.025$	$-0.769 \pm 0.034$	$-0.760 \pm 0.043$	$-0.773 \pm 0.018$	$-0.778 \pm 0.016$	$-0.736 \pm 0.015$	$-0.785 \pm 0.042$	$-0.727 \pm 0.016$
$\text{Fe}^{++}/\text{H}^+$ ( $\times 10^6$ )(4658)	$0.674 \pm 0.047$	...	...	$0.140 \pm 0.020$	$0.048 \pm 0.006$	$0.169 \pm 0.009$	$0.284 \pm 0.082$	$0.196 \pm 0.012$
$\text{Fe}^{++}/\text{H}^+$ ( $\times 10^6$ )(4988)	$0.646 \pm 0.043$	...	...	$0.245 \pm 0.022$	$0.120 \pm 0.005$	$0.223 \pm 0.010$	...	$0.189 \pm 0.010$
ICF	4.220	...	...	11.075	13.521	8.917	8.161	8.718
$\log(\text{Fe}/\text{O})$ (4658)	$-1.883 \pm 0.033$	...	...	$-1.699 \pm 0.063$	$-2.007 \pm 0.057$	$-1.828 \pm 0.025$	$-1.667 \pm 0.128$	$-1.822 \pm 0.029$
$\log(\text{Fe}/\text{O})$ (4988)	$-1.901 \pm 0.031$	...	...	$-1.456 \pm 0.040$	$-1.610 \pm 0.021$	$-1.707 \pm 0.021$	...	$-1.837 \pm 0.025$

TABLE 5  
EMISSION LINE INTENSITIES AND EQUIVALENT WIDTHS IN SPECTRA OBTAINED WITH OTHER TELESCOPES

Ion	GALAXY								
	J 0240-0828			J 0519+0007			HS 0837+4717		
	$F(\lambda)/F(H\beta)$	$I(\lambda)/I(H\beta)$	EW <sup>a</sup>	$F(\lambda)/F(H\beta)$	$I(\lambda)/I(H\beta)$	EW <sup>a</sup>	$F(\lambda)/F(H\beta)$	$I(\lambda)/I(H\beta)$	EW <sup>a</sup>
3727 [O II]	53.31 ± 1.31	55.53 ± 1.45	103.7	34.18 ± 0.76	42.19 ± 0.98	41.3	40.86 ± 0.91	51.12 ± 1.21	57.3
3750 H12	2.70 ± 0.26	3.08 ± 0.40	5.2	2.31 ± 0.36	3.33 ± 0.66	2.8	2.35 ± 0.26	3.46 ± 0.50	3.3
3771 H11	2.95 ± 0.25	3.32 ± 0.38	6.0	3.32 ± 0.35	4.55 ± 0.62	4.2	3.19 ± 0.24	4.49 ± 0.47	4.5
3798 H10	5.11 ± 0.33	5.56 ± 0.44	10.4	5.23 ± 0.35	6.82 ± 0.59	6.8	4.64 ± 0.29	6.25 ± 0.51	6.4
3820 He I	1.09 ± 0.20	1.13 ± 0.21	2.3	0.96 ± 0.22	1.16 ± 0.26	1.3	0.88 ± 0.24	1.08 ± 0.30	1.2
3835 H9	6.99 ± 0.36	7.52 ± 0.47	13.7	6.34 ± 0.31	8.09 ± 0.53	8.7	6.06 ± 0.31	7.92 ± 0.52	8.4
3868 [Ne III]	47.08 ± 1.20	48.75 ± 1.30	86.9	37.17 ± 0.66	44.54 ± 0.84	51.0	42.38 ± 0.91	51.36 ± 1.16	58.7
3889 He I + H8	18.08 ± 0.64	19.00 ± 0.74	32.6	17.29 ± 0.42	21.08 ± 0.63	22.9	15.79 ± 0.47	19.57 ± 0.68	21.9
3968 [Ne III] + H7	31.17 ± 0.89	32.41 ± 0.98	61.0	27.59 ± 0.54	32.80 ± 0.73	40.3	28.27 ± 0.72	34.03 ± 0.94	40.5
4026 He I	2.57 ± 0.28	2.65 ± 0.28	5.6	1.23 ± 0.22	1.42 ± 0.26	1.9	1.81 ± 0.28	2.12 ± 0.33	2.6
4068 [S II]	1.35 ± 0.33	1.39 ± 0.34	2.9	0.70 ± 0.23	0.81 ± 0.27	1.1	0.77 ± 0.24	0.90 ± 0.28	1.1
4101 Hδ	25.98 ± 0.77	26.89 ± 0.84	57.0	25.92 ± 0.50	30.00 ± 0.66	41.4	24.42 ± 0.65	28.62 ± 0.83	36.3
4227 [Fe V]	0.67 ± 0.24	0.69 ± 0.25	1.6	0.84 ± 0.21	0.94 ± 0.23	1.5	0.23 ± 0.23	0.26 ± 0.26	0.3
4340 Hγ	46.13 ± 1.18	47.12 ± 1.24	104.6	46.85 ± 0.75	51.49 ± 0.88	86.8	45.43 ± 1.01	50.29 ± 1.16	75.6
4363 [O III]	14.32 ± 0.55	14.54 ± 0.57	33.5	14.16 ± 0.33	15.41 ± 0.36	26.7	15.86 ± 0.49	17.35 ± 0.54	25.5
4387 He I	...	...	...	...	...	...	0.42 ± 0.40	0.46 ± 0.43	0.7
4471 He I	4.12 ± 0.30	4.17 ± 0.31	10.4	3.68 ± 0.22	3.93 ± 0.23	7.6	4.21 ± 0.29	4.50 ± 0.31	7.7
4658 [Fe III]	0.72 ± 0.27	0.73 ± 0.27	2.1	...	...	...	0.68 ± 0.19	0.70 ± 0.20	1.3
4686 He II	2.90 ± 0.32	2.91 ± 0.32	8.8	2.45 ± 0.20	2.52 ± 0.20	5.8	2.05 ± 0.29	2.11 ± 0.30	4.0
4711 [Ar IV] + He I	2.53 ± 0.28	2.54 ± 0.28	7.5	2.22 ± 0.18	2.27 ± 0.19	5.3	2.08 ± 0.25	2.13 ± 0.26	4.0
4740 [Ar IV]	1.67 ± 0.27	1.68 ± 0.27	4.8	1.44 ± 0.17	1.47 ± 0.17	3.4	1.33 ± 0.24	1.35 ± 0.25	2.7
4861 Hβ	100.00 ± 2.25	100.00 ± 2.26	299.3	100.00 ± 1.50	100.00 ± 1.52	242.5	100.00 ± 1.93	100.00 ± 1.96	212.3
4921 He I	1.18 ± 0.35	1.18 ± 0.35	3.5	0.92 ± 0.19	0.90 ± 0.18	2.2	1.19 ± 0.28	1.18 ± 0.28	2.6
4959 [O III]	235.64 ± 4.81	234.50 ± 4.80	680.3	145.09 ± 2.16	142.52 ± 2.13	375.0	189.98 ± 3.45	186.28 ± 3.41	407.0
4988 [Fe III]	0.58 ± 0.22	0.58 ± 0.22	1.7	...	...	...	0.83 ± 0.37	0.81 ± 0.36	1.8
5007 [O III]	698.63 ± 13.56	694.21 ± 13.51	2008.0	443.82 ± 6.51	432.67 ± 6.39	1154.0	569.02 ± 9.91	553.43 ± 9.73	1199.0
5199 [N I]	...	...	...	...	...	...	0.39 ± 0.26	0.37 ± 0.24	1.0
5271 [Fe III]	...	...	...	...	...	...	0.54 ± 0.50	0.50 ± 0.47	1.4
5755 [N II]	0.59 ± 0.61	0.58 ± 0.60	2.9	...	...	...	0.67 ± 0.33	0.58 ± 0.29	2.2
5876 He I	12.00 ± 0.57	11.63 ± 0.56	59.1	12.14 ± 0.26	10.46 ± 0.23	43.6	13.42 ± 0.49	11.44 ± 0.43	44.2
6300 [O I]	2.30 ± 0.31	2.21 ± 0.30	14.5	0.98 ± 0.12	0.80 ± 0.10	3.9	2.02 ± 0.28	1.63 ± 0.23	7.7
6312 [S III]	1.11 ± 0.24	1.07 ± 0.23	7.0	0.87 ± 0.11	0.71 ± 0.09	3.7	1.48 ± 0.27	1.19 ± 0.22	5.6
6363 [O I]	0.70 ± 0.36	0.67 ± 0.34	4.4	...	...	...	0.73 ± 0.25	0.59 ± 0.20	2.8
6548 [N II]	4.09 ± 0.54	3.90 ± 0.52	22.9	...	...	...	...	...	...
6563 Hα	292.35 ± 6.00	278.86 ± 6.23	1635.0	345.75 ± 5.08	274.41 ± 4.41	1450.0	353.47 ± 6.48	276.10 ± 5.53	1281.0
6583 [N II]	8.60 ± 0.54	8.20 ± 0.52	48.1	2.11 ± 0.20	1.67 ± 0.16	5.5	6.21 ± 0.51	4.83 ± 0.40	7.3
6678 He I	3.61 ± 0.35	3.44 ± 0.34	19.8	3.41 ± 0.20	2.67 ± 0.16	15.1	4.17 ± 0.34	3.21 ± 0.26	14.9
6717 [S II]	4.66 ± 0.37	4.43 ± 0.36	29.0	2.71 ± 0.19	2.12 ± 0.15	11.6	5.00 ± 0.36	3.84 ± 0.28	19.2
6731 [S II]	4.20 ± 0.38	3.99 ± 0.36	26.0	2.36 ± 0.18	1.84 ± 0.14	10.0	4.37 ± 0.37	3.35 ± 0.29	16.5
7065 He I	5.92 ± 0.44	5.58 ± 0.42	37.6	5.76 ± 0.31	4.34 ± 0.24	25.6	8.47 ± 0.42	6.25 ± 0.32	38.2
7136 [Ar III]	3.64 ± 0.37	3.43 ± 0.35	21.8	2.59 ± 0.31	1.94 ± 0.23	12.9	4.79 ± 0.36	3.51 ± 0.27	21.5
7281 He I	0.56 ± 0.22	0.53 ± 0.21	3.6	...	...	...	0.81 ± 0.29	0.58 ± 0.21	3.6
7320 [O II]	1.30 ± 0.30	1.22 ± 0.28	8.8	...	...	...	1.78 ± 0.27	1.28 ± 0.20	8.3
7330 [O II]	1.65 ± 0.35	1.55 ± 0.33	11.5	...	...	...	1.32 ± 0.26	0.95 ± 0.19	6.2
7751 [Ar III]	0.90 ± 0.22	0.84 ± 0.21	7.7	...	...	...	1.12 ± 0.26	0.77 ± 0.18	5.6
C(Hβ)	...	0.060	...	...	0.303	...	...	0.320	...
F(Hβ) <sup>b</sup>	...	1.84	...	...	1.51	...	...	2.66	...
EW(abs) Å	...	0.50	...	...	0.00	...	...	0.60	...

TABLE 5—Continued

Ion	GALAXY								
	I Zw 18NW			CGCG 007-025			HS 1028+3843		
	$F(\lambda)/F(H\beta)$	$I(\lambda)/I(H\beta)$	EW <sup>a</sup>	$F(\lambda)/F(H\beta)$	$I(\lambda)/I(H\beta)$	EW <sup>a</sup>	$F(\lambda)/F(H\beta)$	$I(\lambda)/I(H\beta)$	EW <sup>a</sup>
3727 [O II]	...	...	...	...	...	...	54.47 ± 0.86	54.16 ± 0.92	113.0
3750 H12	...	...	...	...	...	...	2.59 ± 0.19	3.75 ± 0.35	5.6
3771 H11	...	...	...	...	...	...	4.14 ± 0.18	5.29 ± 0.31	8.9
3798 H10	...	...	...	4.70 ± 0.21	7.91 ± 0.44	8.9	5.02 ± 0.19	6.16 ± 0.31	10.9
3820 He I	...	...	...	1.16 ± 0.16	1.17 ± 0.17	2.1	1.06 ± 0.14	1.05 ± 0.14	2.3
3835 H9	5.83 ± 0.61	6.69 ± 0.95	1.9	5.63 ± 0.22	9.18 ± 0.45	9.7	7.58 ± 0.19	8.70 ± 0.30	16.4
3868 [Ne III]	17.44 ± 0.77	18.49 ± 0.84	5.0	37.03 ± 0.72	37.34 ± 0.77	62.4	62.04 ± 0.95	61.69 ± 1.00	136.2
3889 He I + H8	19.13 ± 0.81	20.74 ± 1.09	6.3	17.22 ± 0.40	20.48 ± 0.55	33.1	18.12 ± 0.35	19.27 ± 0.44	36.7
3968 [Ne III] + H7	18.40 ± 0.83	19.84 ± 1.08	6.2	24.34 ± 0.53	27.67 ± 0.67	45.4	34.66 ± 0.56	35.57 ± 0.63	80.0
4026 He I	...	...	...	1.43 ± 0.14	1.43 ± 0.14	2.8	2.17 ± 0.15	2.16 ± 0.15	5.2
4068 [S II]	0.53 ± 1.06	0.56 ± 1.12	0.2	0.82 ± 0.16	0.82 ± 0.17	1.6	1.13 ± 0.14	1.13 ± 0.14	3.0
4101 Hδ	26.00 ± 0.93	27.53 ± 1.12	10.1	22.13 ± 0.50	25.10 ± 0.62	44.7	25.78 ± 0.42	26.53 ± 0.47	72.8
4227 [Fe V]	0.37 ± 0.73	0.38 ± 0.76	0.1	0.15 ± 0.14	0.15 ± 0.14	0.3	0.55 ± 0.12	0.55 ± 0.12	1.7
4340 Hγ	47.39 ± 1.27	49.07 ± 1.40	21.0	45.04 ± 0.86	47.54 ± 0.95	94.7	45.90 ± 0.69	46.38 ± 0.72	157.6
4363 [O III]	6.96 ± 0.60	7.14 ± 0.62	2.9	11.66 ± 0.31	11.58 ± 0.32	24.6	16.28 ± 0.28	16.19 ± 0.28	56.8
4387 He I	...	...	...	0.34 ± 0.15	0.33 ± 0.15	0.7	0.47 ± 0.08	0.46 ± 0.08	1.6
4471 He I	2.70 ± 0.49	2.75 ± 0.50	1.2	3.67 ± 0.19	3.63 ± 0.19	8.5	4.37 ± 0.13	4.34 ± 0.13	16.1
4658 [Fe III]	0.33 ± 0.66	0.33 ± 0.67	0.2	0.54 ± 0.14	0.53 ± 0.14	1.4	0.87 ± 0.12	0.87 ± 0.12	3.6
4686 He II	3.44 ± 0.52	3.47 ± 0.52	1.7	1.38 ± 0.16	1.35 ± 0.16	3.6	1.37 ± 0.12	1.36 ± 0.12	5.8
4711 [Ar IV] + He I	0.80 ± 0.87	0.81 ± 0.88	0.4	1.80 ± 0.15	1.77 ± 0.15	4.8	3.25 ± 0.12	3.23 ± 0.12	14.0
4740 [Ar IV]	...	...	...	1.01 ± 0.14	0.99 ± 0.14	2.7	2.15 ± 0.12	2.13 ± 0.12	9.4
4861 Hβ	100.00 ± 2.40	100.00 ± 2.43	57.4	100.00 ± 1.76	100.00 ± 1.80	267.6	100.00 ± 1.46	100.00 ± 1.48	451.0
4921 He I	0.62 ± 0.57	0.61 ± 0.57	0.4	0.99 ± 0.15	0.96 ± 0.15	2.7	1.08 ± 0.10	1.07 ± 0.10	4.9
4959 [O III]	68.45 ± 1.75	67.91 ± 1.75	40.2	192.35 ± 3.21	187.67 ± 3.21	523.0	247.30 ± 3.58	245.91 ± 3.58	1184.0
4988 [Fe III]	0.41 ± 0.81	0.40 ± 0.81	0.2	0.70 ± 0.16	0.68 ± 0.16	1.9	...	...	...
5007 [O III]	213.81 ± 4.67	211.60 ± 4.65	131.2	577.04 ± 9.32	562.29 ± 9.30	1569.0	752.05 ± 10.84	747.82 ± 10.85	3670.0
5015 He I	2.15 ± 0.58	2.13 ± 0.58	1.3	1.39 ± 0.17	1.35 ± 0.17	2.3	...	...	...
5199 [N I]	...	...	...	0.55 ± 0.17	0.54 ± 0.17	1.8	...	...	...
5271 [Fe III]	...	...	...	0.24 ± 0.30	0.24 ± 0.30	0.8	...	...	...
5518 [Cl III]	...	...	...	0.18 ± 0.17	0.18 ± 0.17	0.7	...	...	...
5538 [Cl III]	...	...	...	0.21 ± 0.17	0.21 ± 0.16	0.8	...	...	...
5755 [N II]	...	...	...	0.14 ± 0.22	0.13 ± 0.21	0.6	...	...	...
5876 He I	5.98 ± 0.54	5.67 ± 0.51	5.6	11.83 ± 0.37	11.29 ± 0.37	50.2	12.29 ± 0.21	12.22 ± 0.21	85.8
6300 [O I]	0.52 ± 0.76	0.49 ± 0.71	0.6	2.49 ± 0.20	2.36 ± 0.19	12.7	1.39 ± 0.08	1.38 ± 0.09	12.2
6312 [S III]	0.58 ± 0.64	0.54 ± 0.60	0.7	1.73 ± 0.18	1.64 ± 0.17	8.9	1.16 ± 0.08	1.16 ± 0.08	10.2
6363 [O I]	0.19 ± 0.38	0.18 ± 0.35	0.2	0.83 ± 0.17	0.79 ± 0.16	4.2	0.51 ± 0.09	0.50 ± 0.09	4.4
6548 [N II]	0.35 ± 0.70	0.32 ± 0.65	0.4	1.43 ± 0.19	1.35 ± 0.18	6.8	...	...	...
6563 Hα	296.22 ± 6.27	273.81 ± 6.32	369.7	198.45 ± 3.35	188.03 ± 3.52	944.5	279.46 ± 4.05	278.16 ± 4.40	2686.0
6583 [N II]	0.59 ± 0.89	0.54 ± 0.83	0.7	3.64 ± 0.23	3.43 ± 0.22	17.3	4.08 ± 0.12	4.06 ± 0.12	24.3
6678 He I	2.61 ± 0.55	2.40 ± 0.51	3.4	3.48 ± 0.24	3.27 ± 0.23	17.7	3.02 ± 0.11	3.01 ± 0.12	29.5
6717 [S II]	1.91 ± 0.45	1.76 ± 0.42	2.6	8.10 ± 0.31	7.61 ± 0.30	41.6	3.53 ± 0.12	3.51 ± 0.12	34.1
6731 [S II]	1.47 ± 0.59	1.35 ± 0.54	2.0	6.34 ± 0.28	5.95 ± 0.28	32.7	3.26 ± 0.12	3.24 ± 0.12	32.0
7065 He I	2.17 ± 0.45	1.97 ± 0.42	3.4	3.86 ± 0.23	3.61 ± 0.22	21.7	5.79 ± 0.17	5.76 ± 0.18	54.0
7136 [Ar III]	1.45 ± 0.47	1.31 ± 0.43	2.3	5.56 ± 0.26	5.18 ± 0.25	33.0	4.03 ± 0.16	4.01 ± 0.16	47.5
7281 He I	0.46 ± 0.53	0.42 ± 0.48	0.8	0.70 ± 0.16	0.65 ± 0.15	4.4	...	...	...
7320 [O II]	0.40 ± 0.80	0.36 ± 0.73	0.7	1.85 ± 0.19	1.72 ± 0.18	11.7	...	...	...
7330 [O II]	0.26 ± 0.53	0.24 ± 0.48	0.4	1.55 ± 0.17	1.44 ± 0.16	9.8	...	...	...
7751 [Ar III]	0.44 ± 0.87	0.39 ± 0.78	0.9	1.43 ± 0.18	1.32 ± 0.17	10.3	...	...	...
9069 [S II]	3.11 ± 0.46	2.68 ± 0.40	9.4	12.69 ± 0.46	11.54 ± 0.46	155.5	...	...	...
$C(H\beta)$	...	0.100	...	...	0.000	...	...	0.000	...
$F(H\beta)^b$	...	1.94	...	...	5.02	...	...	1.83	...
EW(abs) Å	...	0.15	...	...	0.00	...	...	2.60	...

TABLE 5—Continued

Ion	GALAXY								
	J 1253-0312			J 1323-0132			HS 2236+1344		
	$F(\lambda)/F(H\beta)$	$I(\lambda)/I(H\beta)$	EW <sup>a</sup>	$F(\lambda)/F(H\beta)$	$I(\lambda)/I(H\beta)$	EW <sup>a</sup>	$F(\lambda)/F(H\beta)$	$I(\lambda)/I(H\beta)$	EW <sup>a</sup>
3727 [O II]	78.42 ± 1.17	84.56 ± 1.40	105.9	...	...	...	54.67 ± 0.95	60.72 ± 1.12	92.5
3750 H12	2.42 ± 0.09	3.75 ± 0.17	3.3	1.33 ± 0.28	4.75 ± 1.31	2.2	2.94 ± 0.37	4.07 ± 0.69	5.1
3771 H11	3.01 ± 0.09	4.36 ± 0.17	4.2	2.79 ± 0.36	6.27 ± 1.00	4.6	3.96 ± 0.33	5.18 ± 0.62	6.9
3798 H10	4.60 ± 0.12	6.06 ± 0.18	6.3	4.10 ± 0.38	7.03 ± 0.76	8.0	5.42 ± 0.33	6.77 ± 0.61	9.4
3820 He I	1.01 ± 0.09	1.08 ± 0.09	1.4	1.08 ± 0.26	1.08 ± 0.26	2.0	1.42 ± 0.35	1.56 ± 0.38	2.6
3835 H9	6.08 ± 0.13	7.58 ± 0.19	8.8	6.14 ± 0.43	9.20 ± 0.74	11.4	6.12 ± 0.27	7.48 ± 0.54	11.1
3868 [Ne III]	45.92 ± 0.70	48.95 ± 0.81	68.7	46.84 ± 1.25	46.67 ± 1.33	87.1	35.43 ± 0.62	38.75 ± 0.72	64.9
3889 He I + H8	15.88 ± 0.27	17.93 ± 0.33	23.9	16.82 ± 0.66	19.83 ± 0.86	31.3	15.84 ± 0.36	17.97 ± 0.57	31.5
3968 [Ne III] + H7	27.63 ± 0.43	30.22 ± 0.51	43.0	28.62 ± 0.92	31.86 ± 1.12	48.0	24.61 ± 0.45	27.38 ± 0.67	44.8
4026 He I	1.45 ± 0.08	1.53 ± 0.09	2.2	1.56 ± 0.36	1.54 ± 0.37	3.0	1.81 ± 0.19	1.95 ± 0.20	3.3
4068 [S II]	1.35 ± 0.09	1.41 ± 0.10	2.1	...	...	...	...	...	...
4101 Hδ	23.79 ± 0.38	25.89 ± 0.44	36.8	23.58 ± 0.82	26.47 ± 0.99	43.6	22.42 ± 0.41	24.67 ± 0.62	41.1
4227 [Fe V]	0.23 ± 0.16	0.24 ± 0.17	0.4	0.64 ± 0.34	0.63 ± 0.34	1.2	1.36 ± 0.17	1.44 ± 0.18	2.6
4340 Hγ	44.94 ± 0.69	47.09 ± 0.75	79.0	45.15 ± 1.33	47.24 ± 1.45	96.3	46.01 ± 0.72	48.62 ± 0.85	94.7
4363 [O III]	10.07 ± 0.19	10.34 ± 0.20	18.2	19.32 ± 0.76	19.06 ± 0.77	41.5	16.96 ± 0.31	17.65 ± 0.32	35.0
4387 He I	0.48 ± 0.09	0.49 ± 0.09	0.9	0.89 ± 0.26	0.88 ± 0.26	2.2	0.44 ± 0.15	0.46 ± 0.16	0.9
4471 He I	3.91 ± 0.10	3.98 ± 0.11	8.0	3.71 ± 0.36	3.65 ± 0.36	8.8	3.55 ± 0.16	3.66 ± 0.17	7.4
4658 [Fe III]	1.02 ± 0.08	1.03 ± 0.08	2.2	...	...	...	...	...	...
4686 He II	1.17 ± 0.09	1.17 ± 0.10	2.5	1.70 ± 0.33	1.67 ± 0.33	4.1	1.05 ± 0.12	1.06 ± 0.13	2.6
4711 [Ar IV] + He I	1.86 ± 0.09	1.87 ± 0.09	4.1	4.75 ± 0.38	4.66 ± 0.38	12.9	3.25 ± 0.14	3.27 ± 0.14	8.1
4740 [Ar IV]	1.09 ± 0.08	1.09 ± 0.08	2.5	3.13 ± 0.36	3.07 ± 0.36	8.3	2.31 ± 0.12	2.32 ± 0.13	5.8
4861 Hβ	100.00 ± 1.48	100.00 ± 1.50	236.8	100.00 ± 2.34	100.00 ± 2.40	259.1	100.00 ± 1.48	100.00 ± 1.52	261.5
4921 He I	1.08 ± 0.08	1.07 ± 0.08	2.6	1.15 ± 0.28	1.13 ± 0.28	3.2	0.81 ± 0.10	0.80 ± 0.10	2.1
4959 [O III]	232.11 ± 3.41	229.30 ± 3.40	561.0	247.63 ± 5.25	241.87 ± 5.25	631.5	163.62 ± 2.40	161.52 ± 2.39	439.2
4988 [Fe III]	0.63 ± 0.09	0.63 ± 0.08	1.3	...	...	...	...	...	...
5007 [O III]	696.32 ± 10.10	685.90 ± 10.04	1683.0	735.27 ± 14.65	717.62 ± 14.64	1742.0	487.34 ± 7.08	479.20 ± 7.02	1350.0
5015 He I	...	...	...	2.20 ± 0.38	2.15 ± 0.38	5.4	...	...	...
5199 [N I]	0.43 ± 0.08	0.42 ± 0.08	1.2	...	...	...	...	...	...
5271 [Fe III]	0.52 ± 0.09	0.51 ± 0.09	1.5	...	...	...	...	...	...
5518 [Cl III]	0.43 ± 0.07	0.41 ± 0.07	1.4	...	...	...	...	...	...
5538 [Cl III]	0.21 ± 0.08	0.20 ± 0.08	0.7	...	...	...	...	...	...
5755 [N II]	0.31 ± 0.08	0.29 ± 0.07	1.1	...	...	...	...	...	...
5876 He I	13.00 ± 0.23	12.21 ± 0.23	49.5	10.26 ± 0.61	9.89 ± 0.60	44.8	11.05 ± 0.20	10.19 ± 0.19	44.1
6300 [O I]	2.74 ± 0.10	2.52 ± 0.09	11.9	0.53 ± 0.32	0.51 ± 0.32	2.6	1.23 ± 0.11	1.10 ± 0.10	5.3
6312 [S III]	1.92 ± 0.09	1.77 ± 0.08	8.3	0.92 ± 0.36	0.88 ± 0.35	4.4	0.96 ± 0.09	0.86 ± 0.08	4.2
6363 [O I]	0.92 ± 0.08	0.85 ± 0.07	4.0	...	...	...	0.42 ± 0.11	0.38 ± 0.10	1.8
6563 Hα	29.65 ± 0.50	27.33 ± 0.50	115.8	287.79 ± 6.23	276.23 ± 6.64	1482.0	308.65 ± 4.50	273.11 ± 4.35	1338.0
6583 [N II]	14.42 ± 0.28	13.12 ± 0.27	38.5	1.52 ± 0.44	1.45 ± 0.43	8.1	1.89 ± 0.12	1.67 ± 0.11	8.1
6678 He I	4.18 ± 0.13	3.79 ± 0.12	19.3	2.76 ± 0.43	2.64 ± 0.42	15.3	3.00 ± 0.13	2.63 ± 0.12	13.6
6717 [S II]	8.13 ± 0.18	7.35 ± 0.17	37.7	2.21 ± 0.37	2.11 ± 0.36	12.1	3.90 ± 0.15	3.42 ± 0.13	18.1
6731 [S II]	7.70 ± 0.17	6.96 ± 0.16	35.8	2.67 ± 0.46	2.55 ± 0.45	14.4	2.97 ± 0.15	2.60 ± 0.13	13.6
7065 He I	5.46 ± 0.14	4.87 ± 0.13	28.6	3.22 ± 0.42	3.06 ± 0.41	18.6	5.26 ± 0.20	4.53 ± 0.18	25.7
7136 [Ar III]	8.37 ± 0.18	7.45 ± 0.17	44.1	3.58 ± 0.45	3.41 ± 0.44	21.8	2.72 ± 0.19	2.33 ± 0.17	14.1
7281 He I	0.68 ± 0.08	0.61 ± 0.07	3.7	0.58 ± 0.29	0.55 ± 0.28	3.6	...	...	...
7320 [O II]	2.58 ± 0.10	2.28 ± 0.09	14.1	0.48 ± 0.27	0.45 ± 0.26	3.1	...	...	...
7330 [O II]	2.14 ± 0.10	1.89 ± 0.09	11.8	0.53 ± 0.36	0.51 ± 0.35	3.5	...	...	...
7751 [Ar III]	2.07 ± 0.09	1.80 ± 0.08	13.0	0.68 ± 0.27	0.65 ± 0.26	4.7	...	...	...
C(Hβ)	...	0.115	...	...	0.030	...	...	0.157	...
F(Hβ) <sup>b</sup>	...	23.41	...	...	1.35	...	...	2.62	...
EW(abs) Å	...	1.45	...	...	5.75	...	...	0.91	...

TABLE 6

IONIC AND TOTAL HEAVY ELEMENT ABUNDANCES IN GALAXIES OBSERVED WITH OTHER TELESCOPES

PROPERTY	GALAXY				
	J 0240-0828	J 0519+0007	HS 0837+4717	I Zw 18NW	CGCG 007-025
$T_e(\text{O III})$ (K)	15530 ± 310	20730 ± 340	19140 ± 380	20150 ± 1080	15440 ± 220
$T_e(\text{O II})$ (K)	14290 ± 260	15640 ± 240	15510 ± 290	15620 ± 780	14240 ± 190
$T_e(\text{S III})$ (K)	14280 ± 250	18940 ± 290	17880 ± 320	18850 ± 900	14400 ± 180
$N_e(\text{S II})$ ( $\text{cm}^{-3}$ )	400 ± 260	330 ± 210	350 ± 230	120 ± 220	150 ± 90
$\text{O}^+/\text{H}^+$ ( $\times 10^4$ )	0.061 ± 0.003	0.035 ± 0.002	0.043 ± 0.002	0.013 ± 0.002	0.106 ± 0.004
$\text{O}^{++}/\text{H}^+$ ( $\times 10^4$ )	0.702 ± 0.037	0.229 ± 0.009	0.347 ± 0.017	0.118 ± 0.014	0.576 ± 0.022
$\text{O}^{+++}/\text{H}^+$ ( $\times 10^6$ )	1.002 ± 0.282	0.373 ± 0.079	0.389 ± 0.128	0.285 ± 0.150	0.436 ± 0.119
$\text{O}/\text{H}$ ( $\times 10^4$ )	0.773 ± 0.037	0.268 ± 0.009	0.395 ± 0.017	0.134 ± 0.015	0.686 ± 0.023
$12 + \log(\text{O}/\text{H})$	7.888 ± 0.021	7.428 ± 0.015	7.596 ± 0.019	7.127 ± 0.047	7.836 ± 0.014
$\text{N}^+/\text{H}^+$ ( $\times 10^6$ )	0.668 ± 0.039	0.114 ± 0.009	0.334 ± 0.024	0.037 ± 0.044	0.280 ± 0.015
ICF	1.066	7.152	8.375	9.280	6.084
$\log(\text{N}/\text{O})$	-1.020 ± 0.036	-1.518 ± 0.040	-1.149 ± 0.038	-1.593 ± 0.562	-1.604 ± 0.029
$\text{Ne}^{++}/\text{H}^+$ ( $\times 10^5$ )	1.179 ± 0.068	0.520 ± 0.020	0.721 ± 0.035	0.230 ± 0.028	0.920 ± 0.039
ICF	1.023	1.061	1.049	1.051	1.071
$\log(\text{Ne}/\text{O})$	-0.807 ± 0.034	-0.686 ± 0.024	-0.717 ± 0.029	-0.743 ± 0.074	-0.843 ± 0.025
$\text{S}^+/\text{H}^+$ ( $\times 10^6$ )	0.092 ± 0.007	0.037 ± 0.002	0.068 ± 0.004	0.028 ± 0.008	0.145 ± 0.006
$\text{S}^{++}/\text{H}^+$ ( $\times 10^6$ )	0.640 ± 0.144	0.189 ± 0.025	0.371 ± 0.069	0.146 ± 0.163	0.957 ± 0.106
ICF	2.631	1.783	2.053	2.154	1.611
$\log(\text{S}/\text{O})$	-1.604 ± 0.088	-1.823 ± 0.050	-1.642 ± 0.071	-1.553 ± 0.409	-1.587 ± 0.044
$\text{Cl}^{++}/\text{H}^+$ ( $\times 10^8$ )	...	...	...	...	1.069 ± 0.655
ICF	...	...	...	...	1.469
$\log(\text{Cl}/\text{O})$	...	...	...	...	-3.640 ± 0.266
$\text{Ar}^{++}/\text{H}^+$ ( $\times 10^7$ )	1.511 ± 0.161	0.534 ± 0.065	1.059 ± 0.082	0.363 ± 0.120	2.237 ± 0.115
$\text{Ar}^{+++}/\text{H}^+$ ( $\times 10^7$ )	1.556 ± 0.259	0.696 ± 0.082	0.764 ± 0.142	...	0.932 ± 0.139
ICF	1.447	1.484	1.336	2.024	1.185
$\log(\text{Ar}/\text{O})$	-2.549 ± 0.090	-2.529 ± 0.086	-2.445 ± 0.070	-2.262 ± 0.152	-2.413 ± 0.038
$\text{Fe}^{++}/\text{H}^+$ ( $\times 10^6$ )(4658)	0.156 ± 0.058	...	0.122 ± 0.035	0.057 ± 0.115	0.115 ± 0.031
$\text{Fe}^{++}/\text{H}^+$ ( $\times 10^6$ )(4988)	0.124 ± 0.047	...	0.141 ± 0.063	0.069 ± 0.139	0.148 ± 0.035
ICF	6.292	...	2.216	3.901	8.538
$\log(\text{Fe}/\text{O})$ (4658)	-1.483 ± 0.163	...	-1.422 ± 0.124	-1.226 ± 0.875	-1.842 ± 0.119
$\log(\text{Fe}/\text{O})$ (4988)	-1.583 ± 0.167	...	-1.359 ± 0.195	-1.144 ± 0.875	-1.734 ± 0.104

TABLE 6—*Continued*

PROPERTY	GALAXY			
	HS 1028+3843	J 1253-0312	J 1323-0132	HS 2236+1344
$T_e(\text{O III})$ (K)	$15820 \pm 160$	$13480 \pm 120$	$17460 \pm 400$	$21110 \pm 290$
$T_e(\text{O II})$ (K)	$14440 \pm 140$	$13020 \pm 110$	$15100 \pm 320$	$15630 \pm 200$
$T_e(\text{S III})$ (K)	$14430 \pm 130$	$12560 \pm 100$	$16110 \pm 330$	$19030 \pm 240$
$N_e(\text{S II})$ ( $\text{cm}^{-3}$ )	$450 \pm 110$	$490 \pm 70$	$1310 \pm 470$	$110 \pm 100$
$\text{O}^+/\text{H}^+$ ( $\times 10^4$ )	$0.058 \pm 0.002$	$0.129 \pm 0.004$	$0.028 \pm 0.002$	$0.049 \pm 0.002$
$\text{O}^{++}/\text{H}^+$ ( $\times 10^4$ )	$0.718 \pm 0.020$	$0.998 \pm 0.028$	$0.551 \pm 0.032$	$0.246 \pm 0.008$
$\text{O}^{+++}/\text{H}^+$ ( $\times 10^6$ )	$0.544 \pm 0.103$	$0.549 \pm 0.099$	$0.560 \pm 0.258$	$0.179 \pm 0.046$
$\text{O}/\text{H}$ ( $\times 10^4$ )	$0.782 \pm 0.020$	$1.132 \pm 0.028$	$0.584 \pm 0.032$	$0.297 \pm 0.008$
$12 + \log(\text{O}/\text{H})$	$7.893 \pm 0.011$	$8.054 \pm 0.011$	$7.766 \pm 0.024$	$7.473 \pm 0.012$
$\text{N}^+/\text{H}^+$ ( $\times 10^6$ )	$0.324 \pm 0.009$	$1.301 \pm 0.030$	$0.107 \pm 0.025$	$0.113 \pm 0.006$
ICF	1.716	7.814	8.235	5.738
$\log(\text{N}/\text{O})$	$-1.314 \pm 0.018$	$-1.047 \pm 0.015$	$-1.477 \pm 0.119$	$-1.660 \pm 0.027$
$\text{Ne}^{++}/\text{H}^+$ ( $\times 10^5$ )	$1.417 \pm 0.043$	$1.812 \pm 0.057$	$0.823 \pm 0.050$	$0.434 \pm 0.015$
ICF	1.015	1.035	1.011	1.072
$\log(\text{Ne}/\text{O})$	$-0.735 \pm 0.018$	$-0.781 \pm 0.018$	$-0.846 \pm 0.036$	$-0.805 \pm 0.020$
$\text{S}^+/\text{H}^+$ ( $\times 10^6$ )	$0.073 \pm 0.002$	$0.190 \pm 0.004$	$0.051 \pm 0.010$	$0.054 \pm 0.002$
$\text{S}^{++}/\text{H}^+$ ( $\times 10^6$ )	$0.670 \pm 0.047$	$1.638 \pm 0.088$	$0.365 \pm 0.147$	$0.228 \pm 0.023$
ICF	2.766	1.985	4.088	1.520
$\log(\text{S}/\text{O})$	$-1.580 \pm 0.030$	$-1.494 \pm 0.023$	$-1.536 \pm 0.156$	$-1.840 \pm 0.037$
$\text{Cl}^{++}/\text{H}^+$ ( $\times 10^8$ )	...	$2.402 \pm 0.398$	...	...
ICF	...	1.519	...	...
$\log(\text{Cl}/\text{O})$	...	$-3.492 \pm 0.073$	...	...
$\text{Ar}^{++}/\text{H}^+$ ( $\times 10^7$ )	$1.735 \pm 0.073$	$4.191 \pm 0.112$	$1.236 \pm 0.164$	$0.636 \pm 0.046$
$\text{Ar}^{+++}/\text{H}^+$ ( $\times 10^7$ )	$1.889 \pm 0.110$	$1.477 \pm 0.115$	$2.138 \pm 0.263$	$1.059 \pm 0.061$
ICF	1.484	1.238	1.882	1.297
$\log(\text{Ar}/\text{O})$	$-2.482 \pm 0.035$	$-2.339 \pm 0.020$	$-2.400 \pm 0.112$	$-2.556 \pm 0.054$
$\text{Fe}^{++}/\text{H}^+$ ( $\times 10^6$ ) (4658)	$0.181 \pm 0.026$	$0.284 \pm 0.022$	...	...
$\text{Fe}^{++}/\text{H}^+$ ( $\times 10^6$ ) (4988)	...	$0.172 \pm 0.024$	...	...
ICF	7.308	1.077	...	...
$\log(\text{Fe}/\text{O})$ (4658)	$-1.397 \pm 0.064$	$-1.556 \pm 0.035$	...	...
$\log(\text{Fe}/\text{O})$ (4988)	...	$-1.773 \pm 0.060$	...	...

Table 7. Parameters of high ionization lines

Name	$12 + \log O/H$	$\frac{I(\text{He II } 4686)}{I(\text{He I } 4471)}$	$\frac{I([\text{Ne V}] 3426)}{I([\text{Ne III}] 3868)}$	$\frac{I([\text{Fe V}] 4227)}{I([\text{Fe III}] 4658)}$	$\frac{I([\text{Fe V}] 4227)}{I([\text{Fe III}] 4988)}$
I Zw 18NW (SDSS)	7.13	1.42	...	1.15	0.95
I Zw 18NW (MMT)	7.17	1.24	...	0.40	0.24
SBS 0335 – 052E (MMT)	7.31	0.75	0.031	0.68	0.41
J 0519 + 0007 (4m)	7.43	0.64	...	...	...
J 0519 + 0007 (MMT)	7.47	0.48	...	0.87	...
HS 2238 + 1344 (4m)	7.47	0.29	...	...	...
Tol 1214 – 277 (VLT)	7.55	1.46	...	1.74	1.48
Tol 1214 – 277 (3.6m)	7.56	1.67	0.085	...	...
HS 0837 + 4717 (SDSS)	7.60	0.47	...	0.37	0.32
HS 0837 + 4717 (MMT)	7.60	0.47	0.009	0.84	...
J 1323 – 0132 (SDSS)	7.77	0.46	...	...	...
Mrk 209 (MMT)	7.82	0.32	0.006	0.52	0.21
CGCG 007 – 025 (SDSS)	7.84	0.37	...	0.28	0.22
Mrk 71A (MMT)	7.87	0.09	...	0.40	...
HS 1028 + 3843 (4m)	7.89	0.31	...	0.63	...
J 0240 – 0828 (SDSS)	7.89	0.70	...	0.95	1.19
Mrk 71B (MMT)	7.91	0.64	...	1.32	...
J 1253 – 0312 (SDSS)	8.05	0.29	...	0.23	0.38
II Zw 40 (MMT)	8.12	0.14	...	0.42	...
mean [ $12+\log(O/H) \leq 7.6$ ]		0.89±0.49		0.86±0.44	0.68±0.47
mean [ $12+\log(O/H) > 7.6$ ]		0.37±0.19		0.59±0.35	0.50±0.40

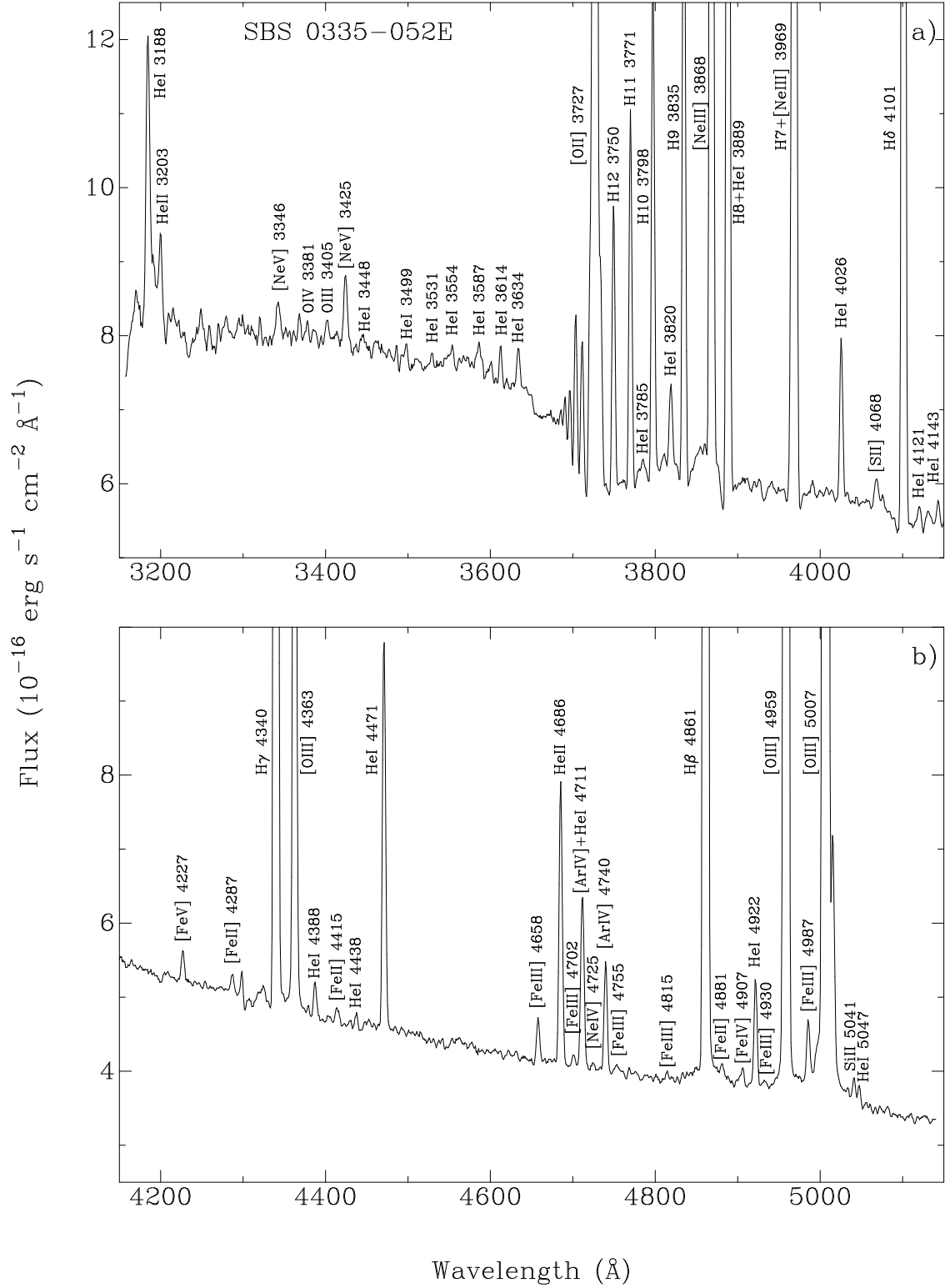


Fig. 1.— MMT spectrum of SBS 0335–052E with labeled emission lines and corrected to the rest frame.



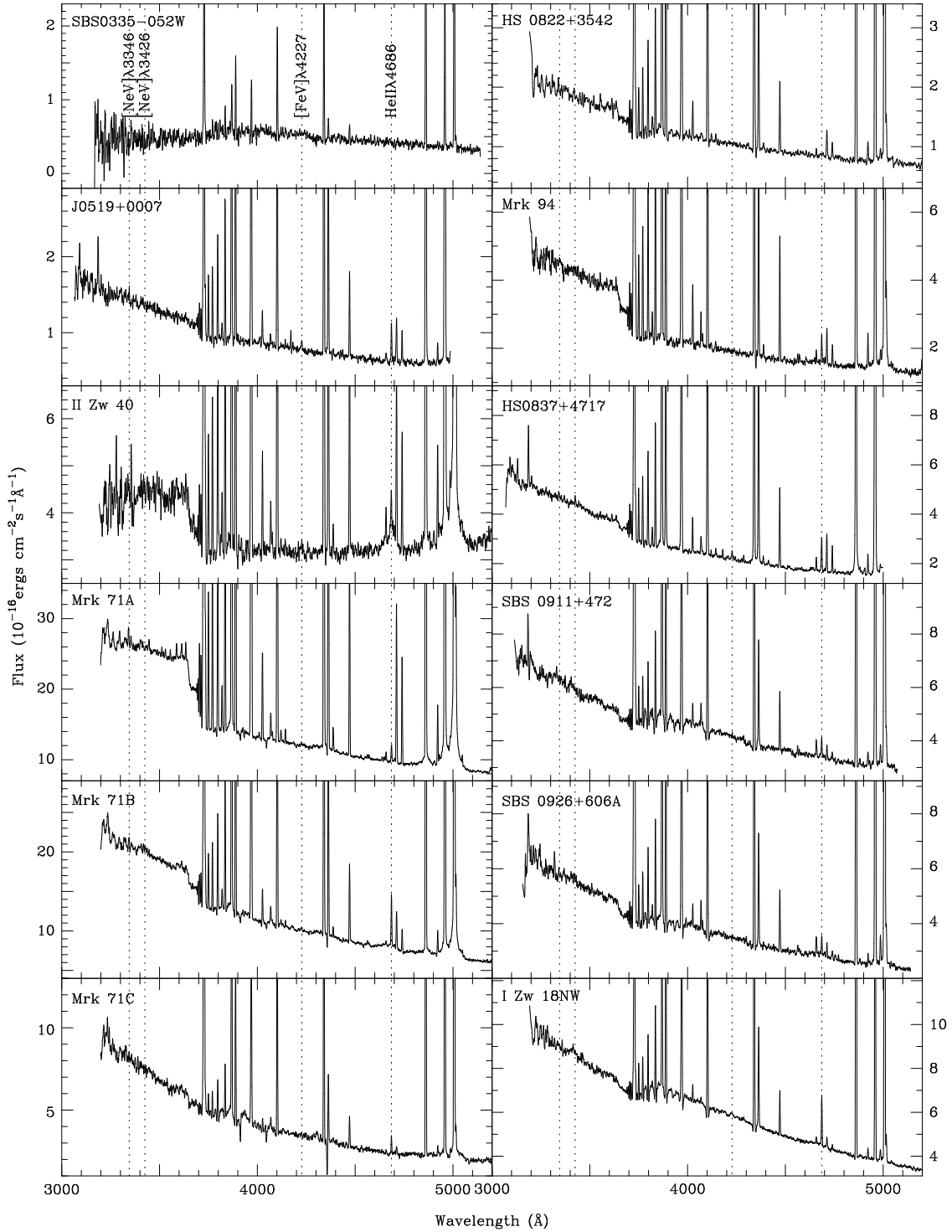


Fig. 2.— Spectra of other galaxies observed with the MMT corrected to the rest frame. The locations of the high-ionization  $[\text{Ne v}] \lambda 3346$ ,  $3426$ ,  $[\text{Fe v}] \lambda 4227$  and  $\text{He II } \lambda 4686$  emission lines are indicated by vertical dotted lines. The spectra are given from top to bottom and from left to right in order of increasing right ascension, as in Table 1.

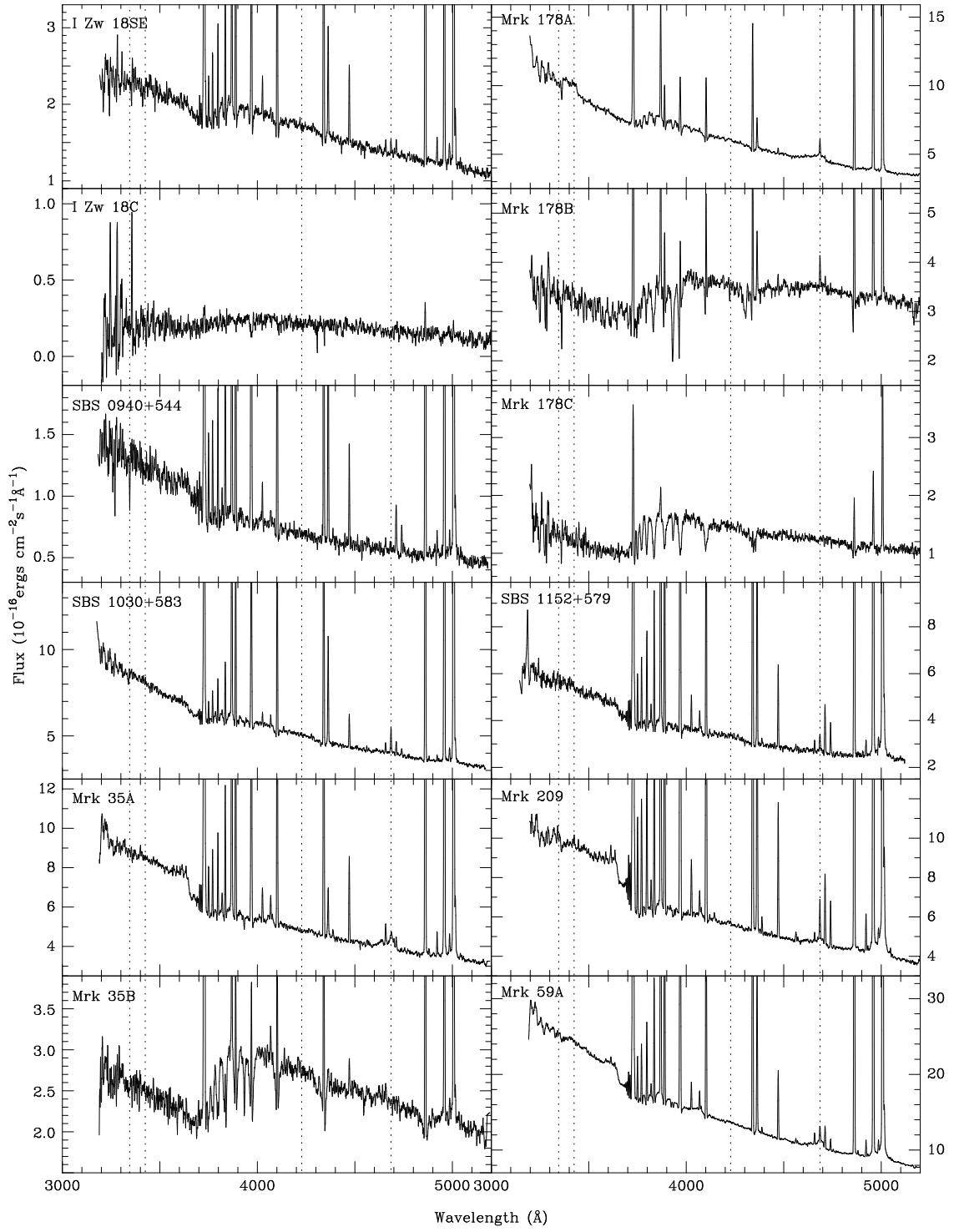


Fig. 2.— Continued.

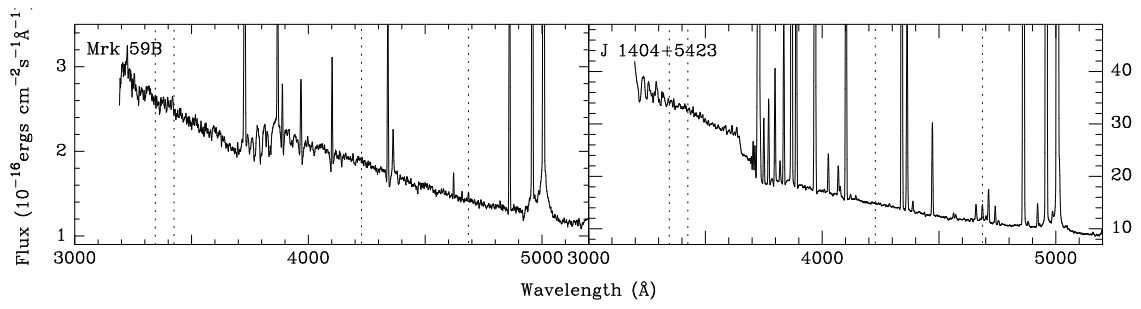


Fig. 2.— Continued.

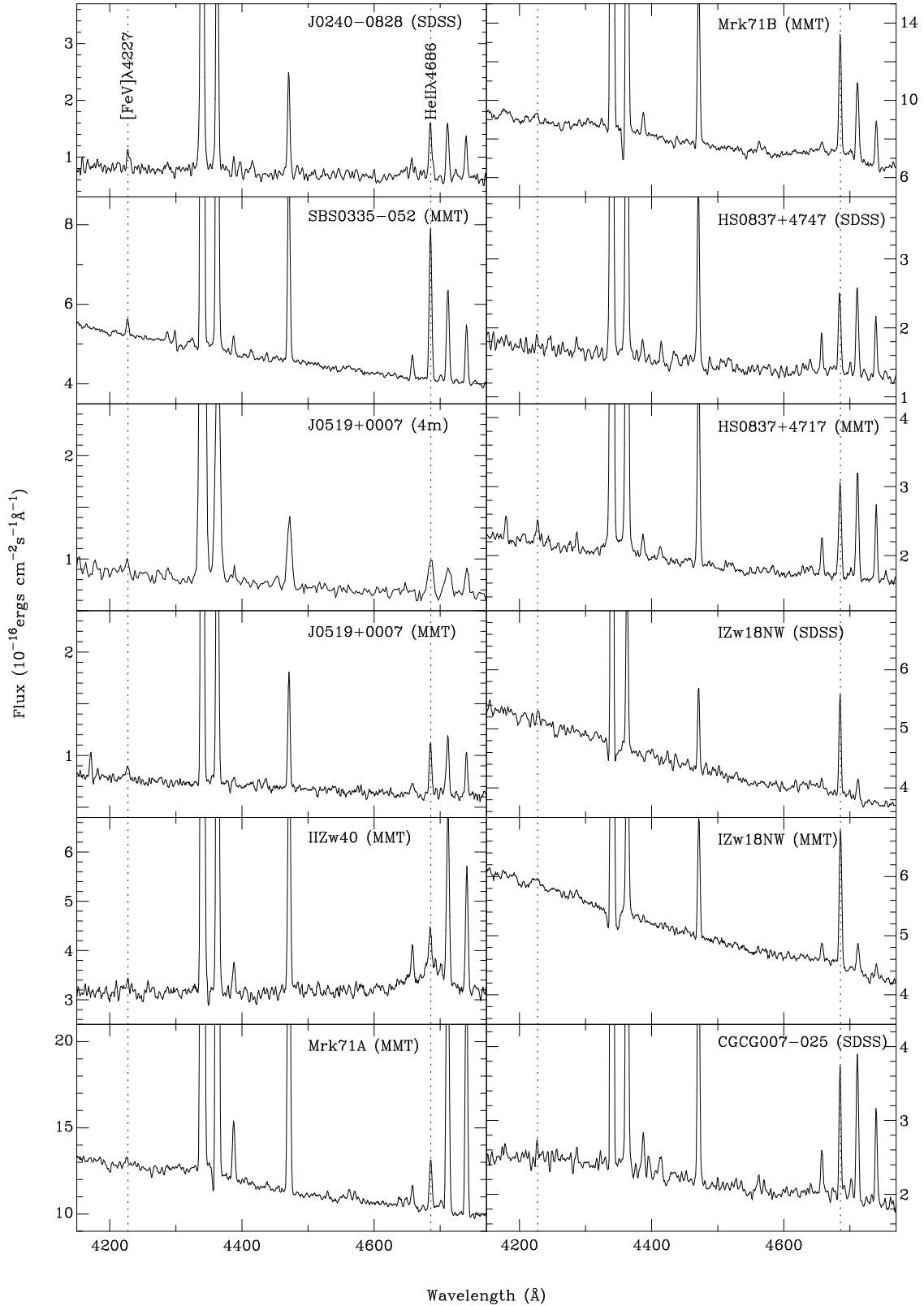


Fig. 3.— Spectra of galaxies with a detected [Fe v]  $\lambda 4227$  emission line. The vertical dotted lines show the location of the [Fe v]  $\lambda 4227$  and He II  $\lambda 4686$  emission lines.

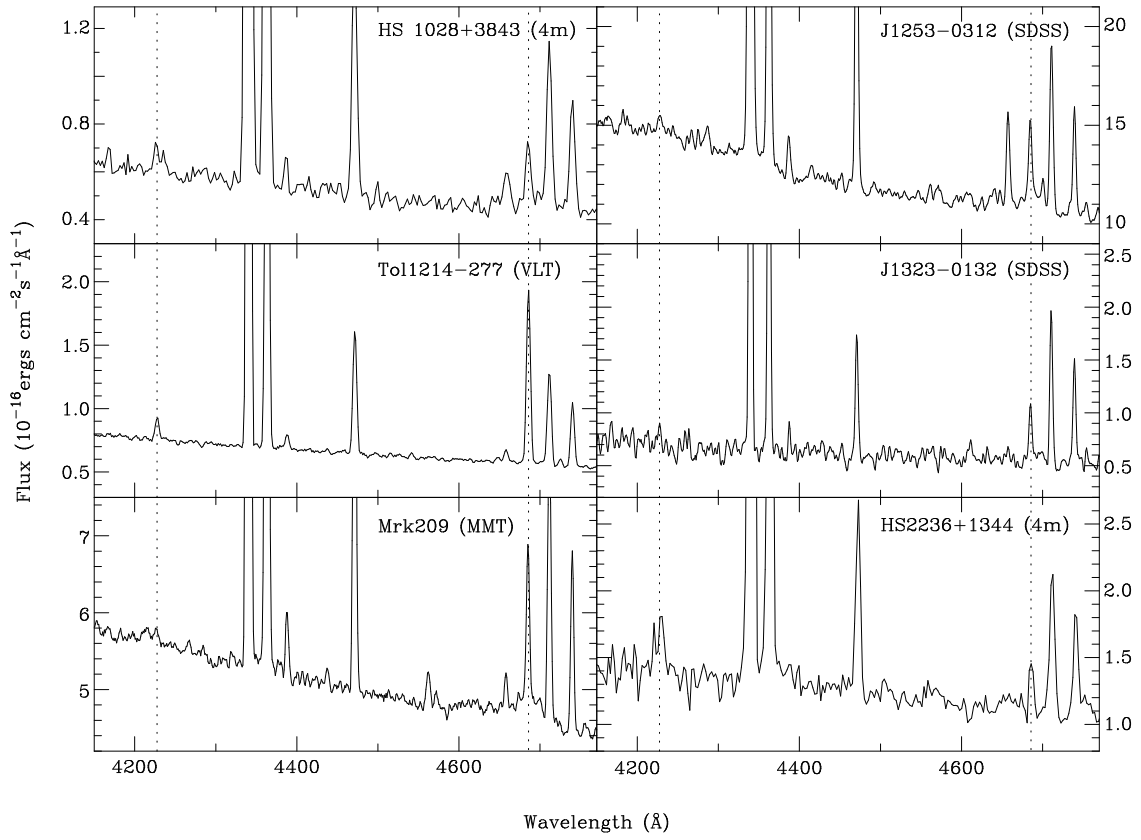


Fig. 3.— Continued.

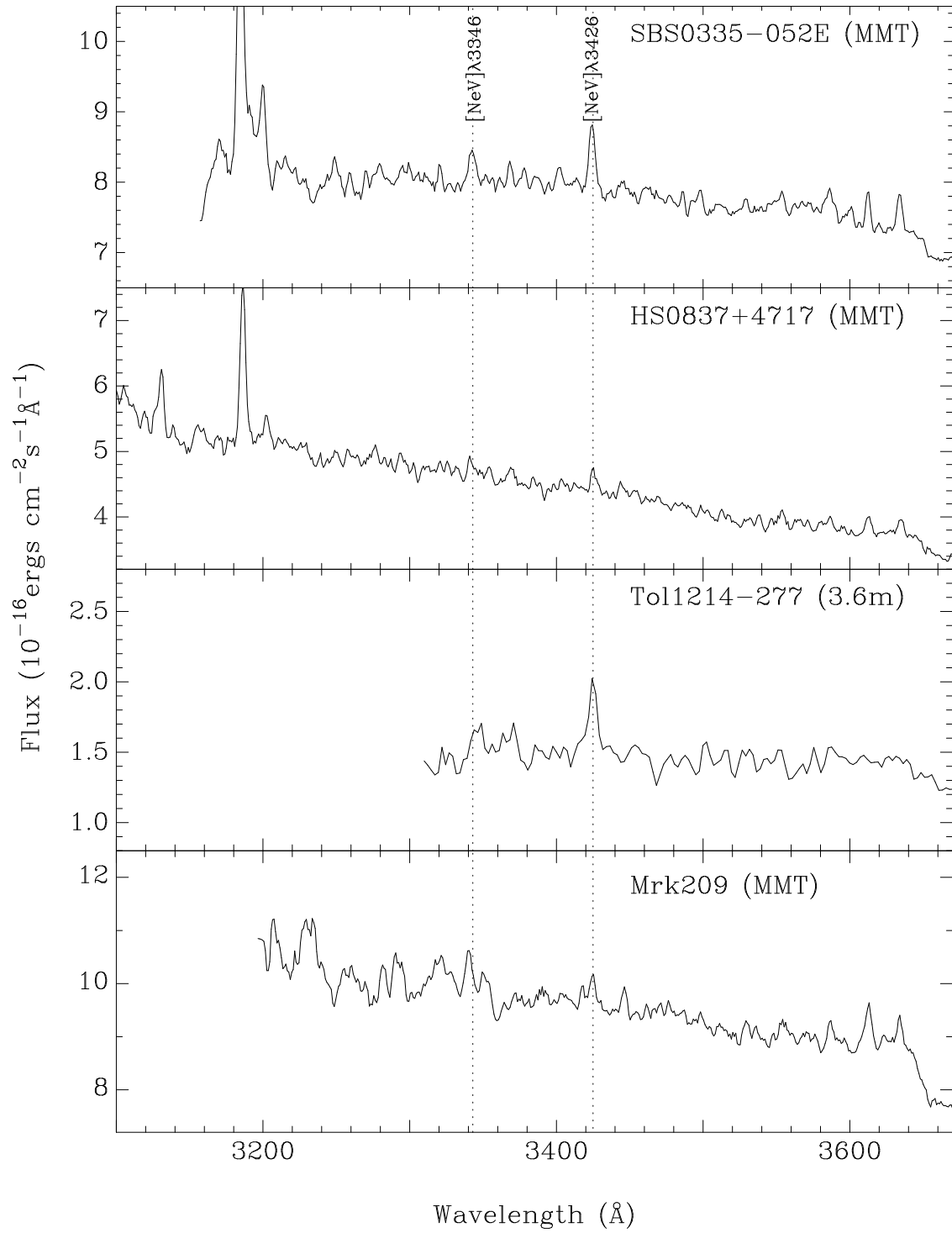


Fig. 4.— Spectra of galaxies with a detected [Ne v]  $\lambda 3426$  emission line. The locations of this line and of the [Ne v]  $\lambda 3346$  emission line are indicated by dotted vertical lines.

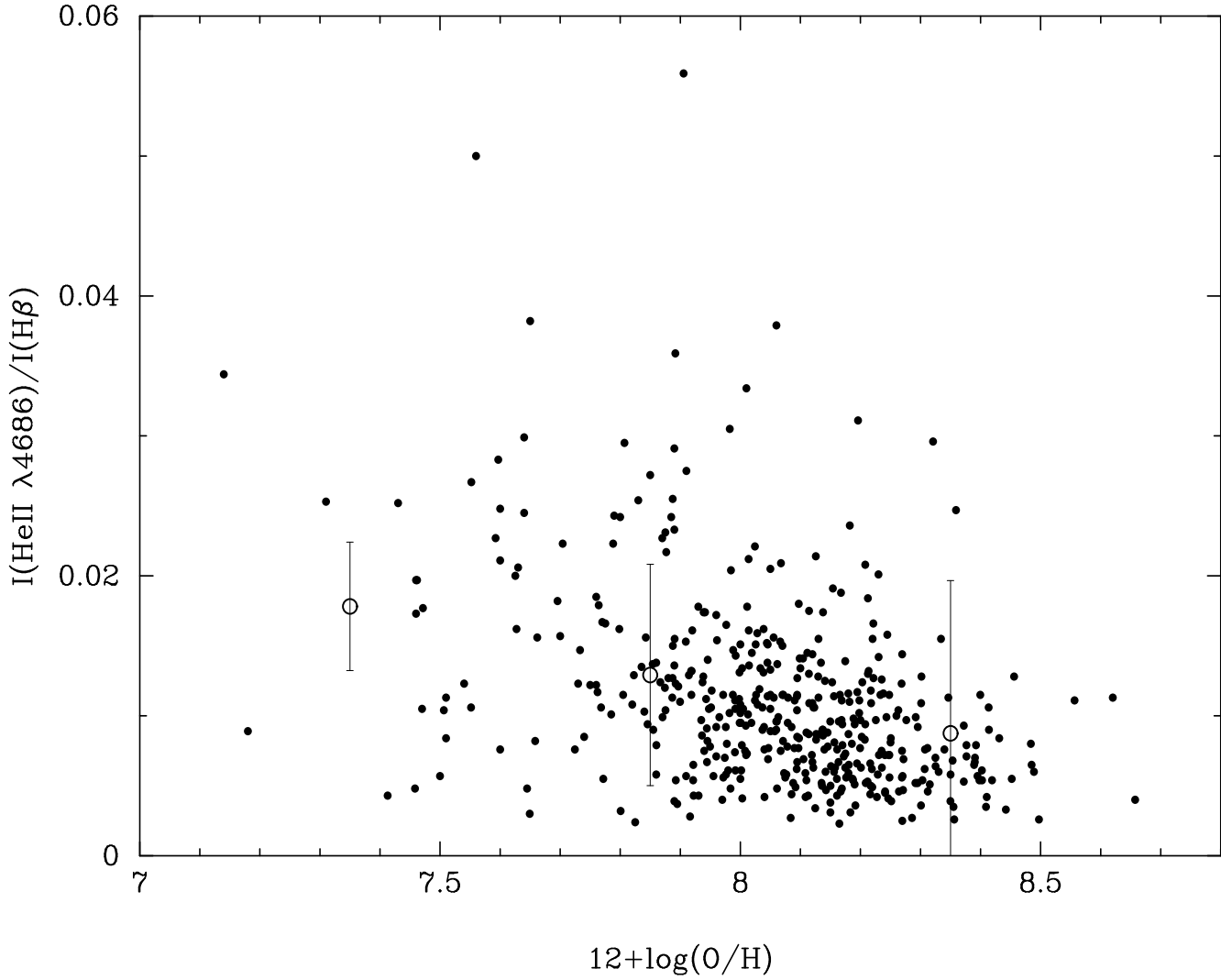


Fig. 5.— Intensity of the He II  $\lambda 4686$  emission line relative to  $\text{H}\beta$  as a function of oxygen abundance  $12 + \log(\text{O}/\text{H})$ . The dots show individual data points while the open circles show the means of the data points in the intervals 7.1 - 7.6, 7.6 - 8.1 and 8.1 - 8.6 of  $12 + \log \text{O}/\text{H}$ . The error bars show the mean error of the data points in each interval.

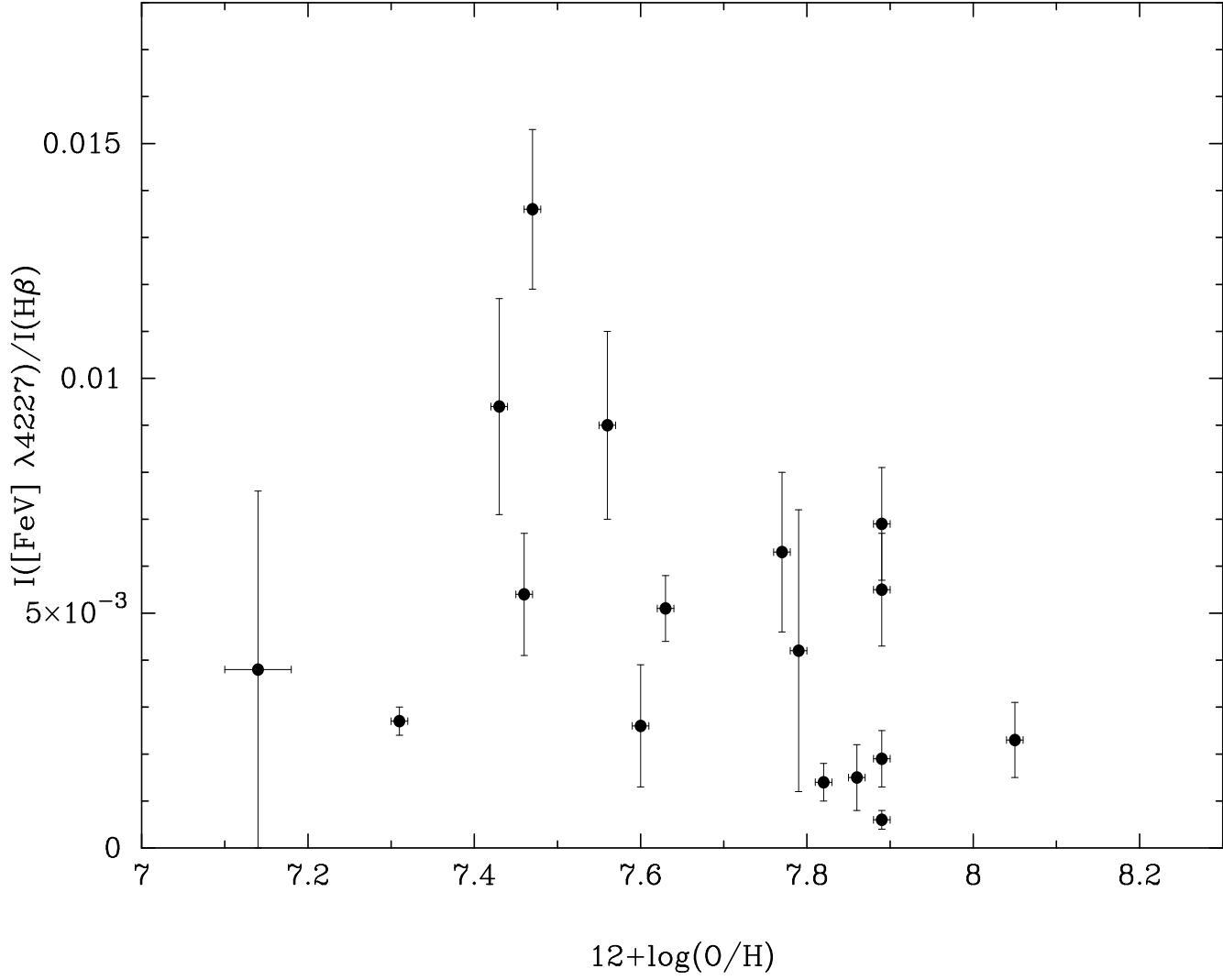


Fig. 6.— Intensity of the [Fe v]  $\lambda 4227$  emission line relative to  $\text{H}\beta$  as a function of oxygen abundance  $12 + \log(O/H)$ .



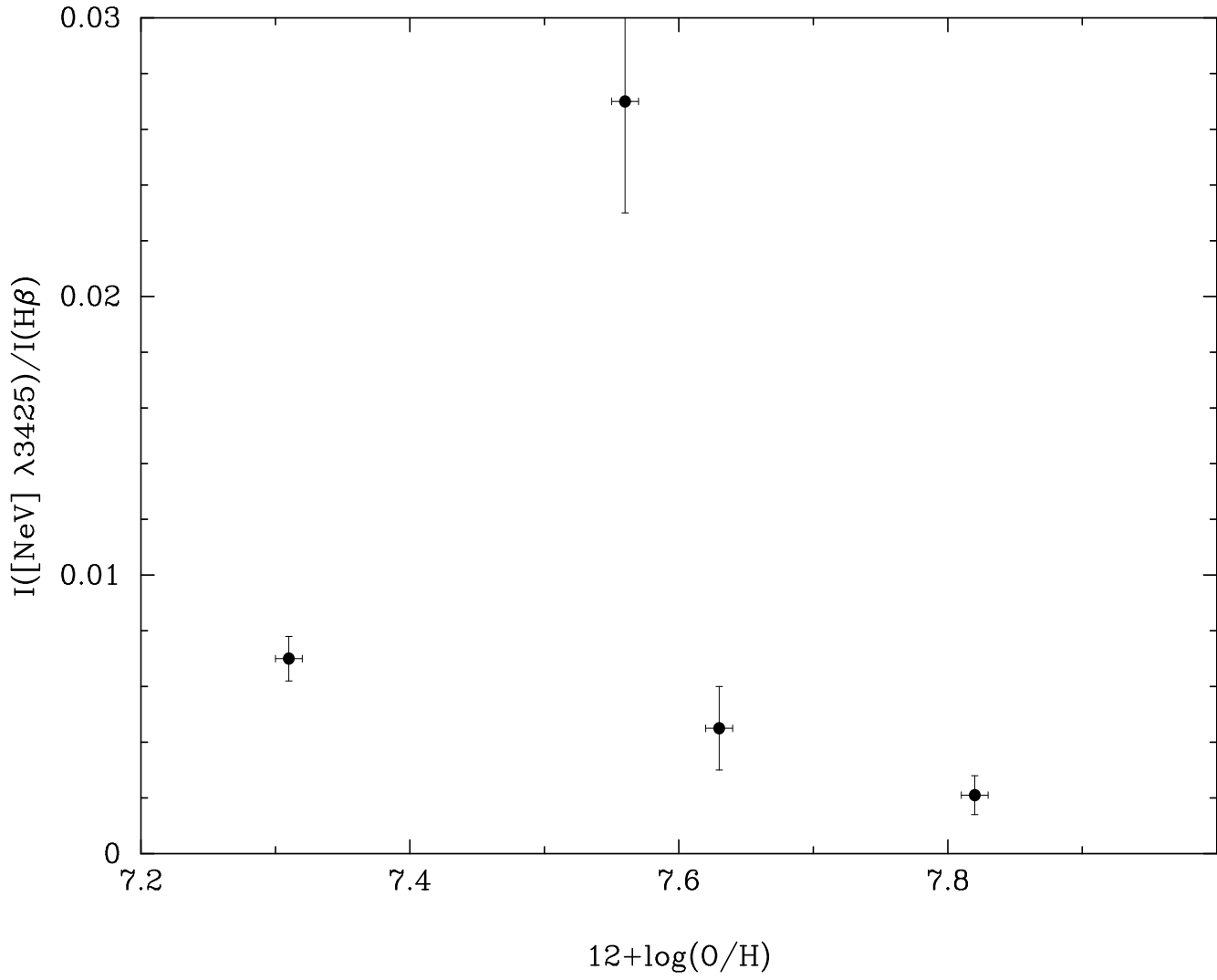


Fig. 7.— Intensity of the  $[\text{Ne V}] \lambda 3426$  emission line relative to  $\text{H}\beta$  as a function of oxygen abundance  $12 + \log(\text{O}/\text{H})$ .

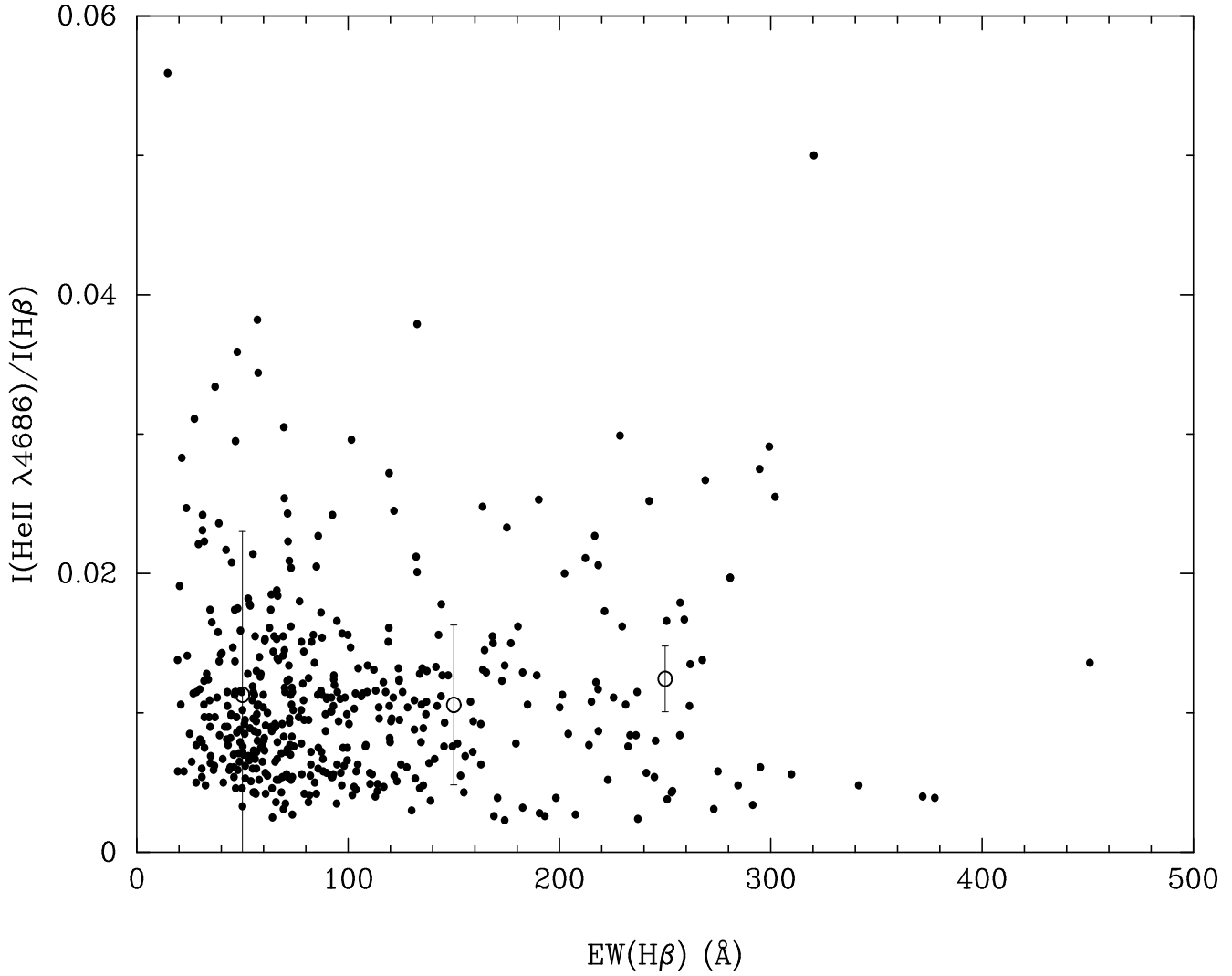


Fig. 8.— Intensity of the He II  $\lambda 4686$  emission line relative to  $\text{H}\beta$  as a function of the equivalent width of  $\text{H}\beta$ . The dots show individual data points while the open circles show the means of the data points in the intervals  $0 - 100$   $\text{\AA}$ ,  $100 - 200$   $\text{\AA}$  and  $200 - 300$   $\text{\AA}$  of  $\text{EW}(\text{H}\beta)$ . The error bars show the mean error of the data points in each interval.

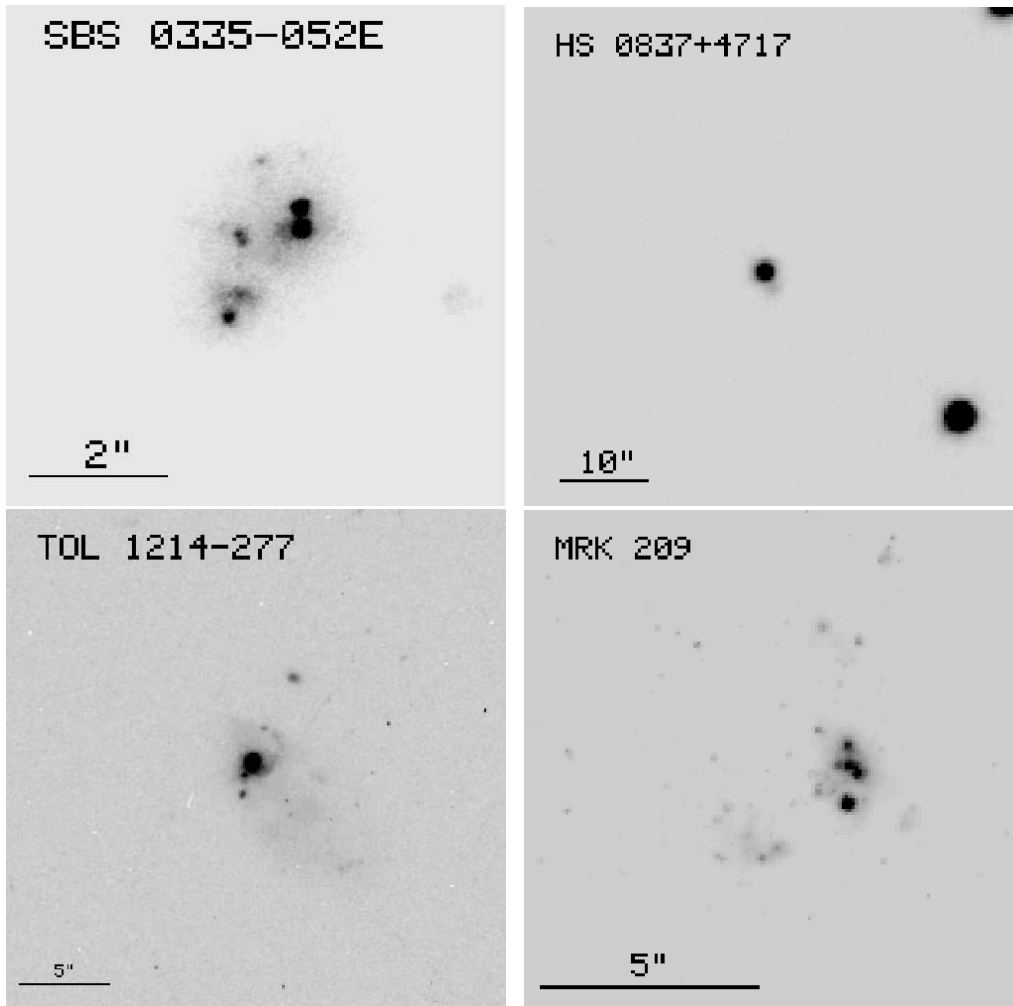


Fig. 9.— Images of known galaxies with detected [Ne v] emission (see their spectra in Fig. 4). North is at top and East to the left. The angular scales are given by horizontal bars. The pictures of SBS0335–052E, Tol 1214–277 and Mrk 209 are *HST* images taken respectively by the ACS camera with the F140LP filter, the WFPC2 camera with the F555W filter and the NICMOS camera with the F110W filter. The *g* - picture of HS 0837+4717 is a ground-based image from the Sloan Digital Sky Survey, hence its considerably worse angular resolution.

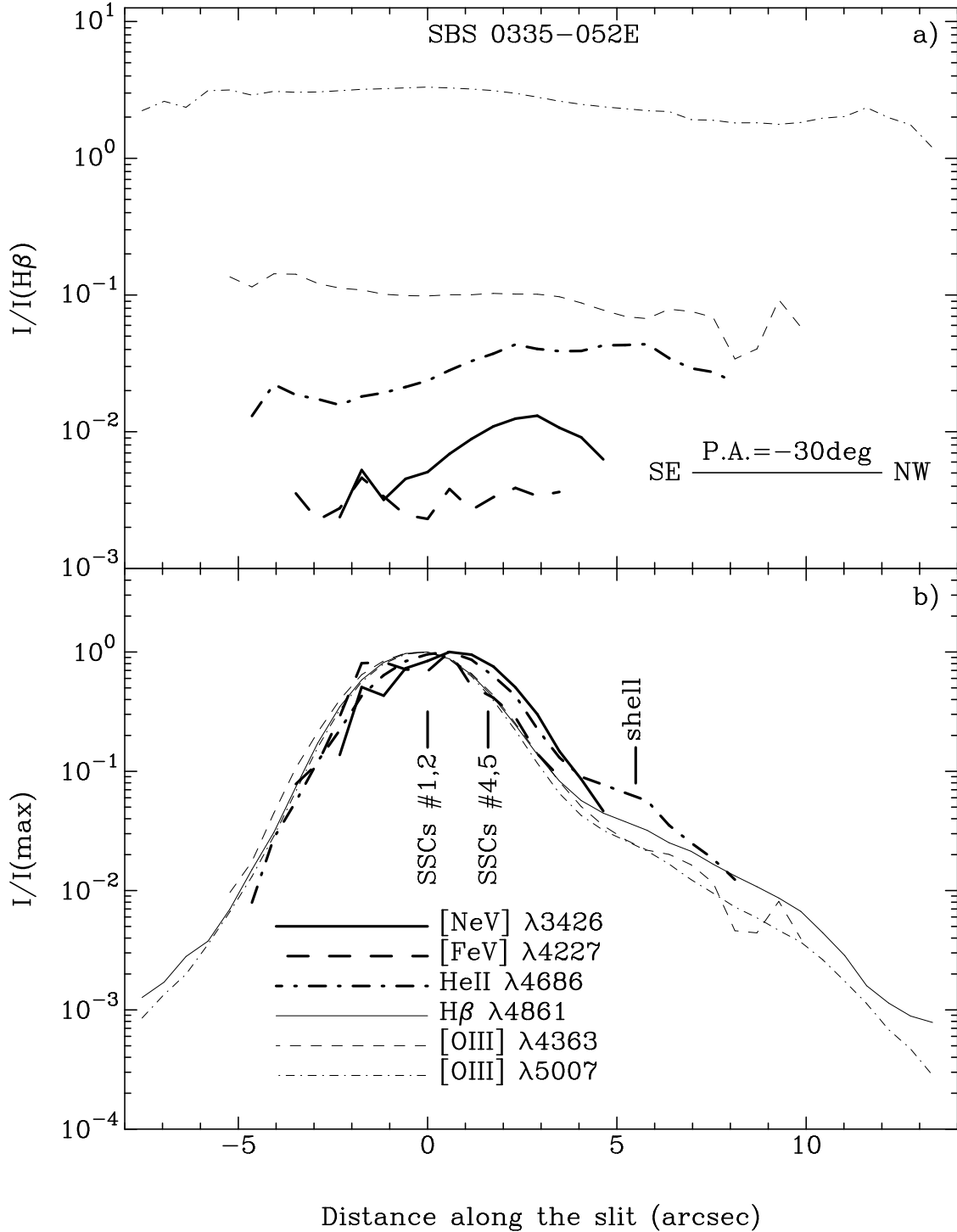


Fig. 10.— Comparison of the spatial distributions along the position angle of  $-30$  degrees of the intensities of various emission lines in SBS 0335-052E (a) relative to the intensity of  $H\beta$  and (b) relative to the maximum intensity of each line. The location of SSCs #1,2, SSCs #4,5 and the shell (Thuan et al. 1997) are indicated by short vertical lines. Note that the spatial distribution of the  $[Ne\ v]\ \lambda 3426$  emission line is considerably more compact than those of other emission lines with softer ionizing radiation, including  $He\ II\ \lambda 4686$ . The latter shows an excess emission at the shell location.